PROGRAMA DE DOCTORADO EN INGENIERÍA CIVIL

TESIS DOCTORAL

ANÁLISIS DE PUESTA EN OBRA Y ESFUERZOS CRÍTICOS A LARGO PLAZO DEL HORMIGÓN REFORZADO CON FIBRAS DE ACERO EN TORRES DE AEROGENERADORES

PhD THESIS

ANALYSIS OF IN-SITU AND LONG-TERM CRITICAL LOADS OF STEEL FIBRE-REINFORCED CONCRETE IN WIND TURBINE TOWERS

AUTORA

LAURA GONZÁLEZ SUÁREZ

DIRECTORES

CARLOS THOMAS GARCÍA

JOKIN RICO ARENAL

UNIVERSIDAD DE CANTABRIA

Escuela de Doctorado de la Universidad de Cantabria

Santander 2023

La mejor manera

de predecir el futuro

es crearlo.

AGRADECIMIENTOS

Para empezar, me gustaría agradecer a mis directores de Tesis, Carlos Thomas y Jokin Rico, por su paciencia, tiempo y consejos. A Carlos le tengo que agradecer el creer en mí desde el primer momento y darme esta oportunidad, animándome a escribir esta Tesis. Y por contagiarme esa pasión por investigar y transmitirme tantos conocimientos. A Jokin, le estoy agradecida por darme la oportunidad de seguir creciendo en el mundo laboral y por su ayuda y comprensión en la redacción de esta Tesis, así como por el apoyo técnico y disposición contante.

Al LADICIM, por dotarme de los medios para poder realizar las investigaciones necesarias. Por supuesto, a todos mis compañeros del laboratorio, que muchos se convirtieron en amigos, por ayudarme tanto en la ejecución de los ensayos y por el apoyo técnico. En especial, agradecer a Jose Sainz-Aja, sin él no hubiera sido posible llegar hasta aquí. Gracias por guiarme en tantas ocasiones, por tus consejos y tu paciencia.

Al equipo de INGECID, que me ha permitido crecer tanto profesional como personalmente. A Marina Llama, Francisco Ballester y Jokin Rico por darme la oportunidad de formar parte de este equipo, y a mis compañeros por su apoyo técnico y personal.

A la Universidad Politécnica de Barcelona, en especial a Albert de la Fuente, por la ayuda al colaborar en la realización de ensayos y al aportar sus conocimientos técnicos sobre el hormigón reforzado con fibras. Además, por su predisposición y ganas para la colaboración en futuras investigaciones y estudios.

Por último, al pilar más importante para mí, a mi familia.

A mis padres, mis mejores referentes, por estar a mi lado siempre. Sin todo su cariño, su esfuerzo y su apoyo no habría llegado hasta aquí. Agradecerles su comprensión y sus constantes palabras de aliento y motivación, que me han impulsado a avanzar, no solo durante el desarrollo de la Tesis, sino en todas las etapas de mi vida.

A María, por ser la mejor hermana pequeña que se puede tener y ejercer a veces de la mejor hermana mayor. Gracias por darme esa energía tan necesaria.

A Álvaro, por creer en mí en todo momento, por su paciencia, cariño y soporte incondicional. Gracias por animarme siempre a seguir.

Agradecer a todas las empresas que han hecho posible el desarrollo de esta Tesis, participando de una u otra forma en su desarrollo.

Al Ministerio de Economía, Industria y Competitividad, la financiación del proyecto S2C – "Desarrollo de un nuevo concepto de torre de hormigón in situ de gran altura para aerogeneradores de gran potencia", dentro de la convocatoria Retos-Colaboración 2017, del que ha partido inicialmente esta Tesis. De la misma forma, a las empresas que han colaborado en este proyecto.

De igual forma, gracias a las empresas colaboradoras, como BASF y Acelormittal, por proporcionar los recursos de manera desinteresada para la fabricación del material.

A la Universidad de Cantabria por la financiación a través de la Convocatoria de ayudas para el desarrollo del programa de doctorados industriales 2020 de la Universidad de Cantabria.

RESUMEN

El desarrollo de las energías renovables es esencial para combatir el cambio climático global, siendo una solución para la descarbonización económica, ya que gran parte de las emisiones de gases efecto invernadero son debidas al uso de energías fósiles. Entre estas energías limpias, la eólica es una de las que se contemplan a mayor gran escala y, en los últimos años, ha evolucionado notablemente. Gran parte de los esfuerzos realizados en su desarrollo se enfocan en obtener mayor potencia, para lo que es primordial conseguir torres más altas, con el objetivo de llegar a grandes alturas donde los vientos son mayores. Para lograr este objetivo, las torres requieren grandes prestaciones mecánicas, ya que mayores potencias implican mayores tamaños de rotor y, por tanto, diseños y materiales que soporten este incremento de peso.

Entre las tipologías existentes de torres de aerogeneradores, las de hormigón son las que mayor potencial tienen para alcanzar mayores alturas y capacidad portante de la torre. En este sentido, una alternativa al empleo hormigón armado convencional, para disminuir tiempos y costes, así como facilitar su construcción y disminuir el impacto medioambiental, es el empleo de hormigón reforzado con fibras como sustitución parcial del armado.

En los últimos años, las investigaciones sobre el hormigón reforzado con fibras han evolucionado notablemente, lo que ha ayudado a comprender mejor sus propiedades y optimizarlas. Gracias a los esfuerzos realizados, se ha permitido que este material adquiera cada vez más relevancia frente al hormigón armado

convencional, como reemplazo total o parcial de la armadura, haciendo su uso cada vez más común.

Las torres eólicas están sometidas a distintos esfuerzos críticos, entre los que destacan la flexión, fluencia y fatiga, por lo que es de vital importancia ahondar en el comportamiento del hormigón bajo estos esfuerzos, con el fin de que éste sea aceptado y empleado, además de ayudar a optimizar los diseños.

A pesar de que el conocimiento sobre el hormigón reforzado con fibras es cada vez mayor, siguen siendo necesarios estudios que aporten un mayor estado del arte que ayude a la mayor aceptación e implementación del mismo, especialmente estudios de sus propiedades a largo plazo, como la fatiga o la fluencia.

Por otro lado, la orientación y distribución de fibras en el hormigón tiene efectos sobre las capacidades mecánicas del material, por lo que es de gran utilidad el estudio de cómo afecta el método de vertido en la disposición de las fibras en el hormigón, con el objetivo de seleccionar la forma de puesta en obra para optimizar las propiedades del hormigón según la dirección de las fuerzas más críticas soportadas por la estructura en sí.

La presente Tesis tiene como objetivo generar conocimiento sobre estos aspectos asociados al hormigón reforzado con macrofibras metálicas. De cara a dar mayor relevancia a los estudios realizados y contribuir en mayor medida al estado del conocimiento científico actual en la materia, el documento de Tesis se plantea como un compendio de artículos publicados en revistas científicas, así como expuestos en congresos.

En primer lugar, se aborda la influencia que tiene el método de hormigonado en la disposición de las fibras dentro del hormigón y se relaciona a su vez esta última con su resistencia. En segundo lugar, se estudia el comportamiento del hormigón reforzado con fibras de acero bajo esfuerzos de fatiga a flexión. En la tercera y última línea de trabajo, se realiza un estudio sobre el comportamiento a fluencia del hormigón, estudiando su evolución dependiendo de la edad y magnitud de carga.

ABSTRACT

The development of renewable energies is essential to combat global climate change, and is a solution for economic decarbonization, since a large part of greenhouse gas emissions are due to the use of fossil fuels. Among these clean energies, wind power is one of those being considered on a larger scale and, in recent years, has evolved considerably. Much of the efforts made in its development are focused on obtaining greater power, for which it is essential to achieve higher towers, with the aim of reaching great heights where winds are higher. To achieve this goal, the towers require high mechanical performance, since higher powers imply larger rotor sizes and, therefore, designs and materials that support this increased weight.

Among the existing types of wind turbine towers, concrete towers have the greatest potential to reach greater heights and tower bearing capacity. In this sense, an alternative to the use of conventional reinforced concrete, in order to reduce time and costs, as well as to facilitate its construction and reduce the environmental impact, is the use of fiber-reinforced concrete as a partial replacement of the reinforced concrete.

In recent years, research on fiber-reinforced concrete has evolved significantly, which has helped to better understand and optimize its properties. Thanks to the efforts made, this material has become increasingly relevant compared to conventional reinforced concrete, as a total or partial replacement of the reinforcement, making its use more and more common.

Wind towers are subjected to different critical stresses, including bending, creep and fatigue, so it is of vital importance to delve into the behavior of concrete under these stresses, in order for it to be accepted and used, as well as to help optimize designs.

Although the knowledge about fiber-reinforced concrete is increasing, studies are still needed to provide a better state of the art to help its acceptance and implementation, especially studies of its long-term properties, such as fatigue or creep.

On the other hand, the orientation and distribution of fibers in concrete has effects on the mechanical capacities of the material, so it is very useful to study how the method of pouring affects the arrangement of the fibers in the concrete, with the objective of selecting the way of placement to optimize the properties of the concrete according to the direction of the most critical forces supported by the structure itself.

The present Thesis aims to generate knowledge on these aspects associated with concrete reinforced with metallic macrofibers. In order to give greater relevance to the studies carried out and to contribute to a greater extent to the current state of scientific knowledge on the subject, the Thesis document is presented as a compendium of articles published in scientific journals, as well as presented at conferences.

In the first place, the influence that the method of concreting has on the arrangement of the fibers within the concrete is addressed, and this in turn is related to its resistance. Secondly, the behavior of concrete reinforced with steel fibers under flexural fatigue stresses is studied. In the third and last line of work, a study is carried out on the creep behavior of concrete, studying its evolution depending on the age and magnitude of load.

ÍNDICE

CAPÍTULO I

Introducción

1.1. Contexto

Una de las mayores preocupaciones de la sociedad actual, que afecta a todos los continentes, es el cambio climático. Recientemente, se han alcanzado niveles récord mundiales de dióxido de carbono (CO_2), que han llegado a aumentar cerca de un 50% en los últimos 20 años [1], así como de otros gases de efecto invernadero (GEI) en la atmósfera.

El cambio climático es una realidad, donde los efectos más tangibles se han observado en eventos como la subida del nivel del mar y en los cambios de los fenómenos climáticos, cada vez más frecuentes y extremos. Un reflejo claro de ello es la subida de la temperatura media global, que ha aumentado casi el doble desde el periodo preindustrial, con la presencia de eventos meteorológicos tales como olas de calor, aumentos en la intensidad de la lluvia o sequías, cada vez más frecuentes y de mayor intensidad y duración. Como consecuencia de estos fenómenos, se han observado cambios negativos en especies de animales y plantas, que reflejan la magnitud del problema y la necesidad de actuación [1], [2].

Las actividades realizadas por el ser humano representan la mayor parte de las emisiones de GEI y cada vez más países toman conciencia de la problemática y establecen medidas que persigan la neutralidad de carbono. El Acuerdo de París, que entró en vigor el 4 de noviembre de 2016, es un tratado internacional jurídicamente vinculante sobre el cambio climático, que fue adoptado por 196 Partes en la Conferencia de las Naciones Unidas sobre el Cambio Climático (COP21) en París. El objetivo general de este Acuerdo es limitar el aumento de la temperatura media mundial, para lo cual se deben reducir las emisiones de GEI, disminuyendo un 43% en 2030. El objetivo 13 de la Agenda 2030 para el Desarrollo Sostenible de la ONU exige medidas urgentes para combatir el cambio climático. La reducción de las emisiones de CO_2 a través de la transformación energética es clave para cumplir con los objetivos climáticos establecidos.

En la actualidad, fruto de la necesidad de disminuir los GEI, el mercado energético está evolucionando hacia las energías que fomentan los desarrollos sostenibles, tales como la eólica o la solar. Para que las energías renovables adquieran cada vez más peso sobre las alternativas convencionales, se persigue conseguir mayores potencias y mejores rendimientos de las mismas.

Entre las energías renovables existentes, la eólica es la más consolidada a gran escala, la cual se caracteriza por ser una energía limpia, inagotable, de bajo impacto y bajo coste, comparada con otras alternativas. Por lo tanto, la evolución de la tecnología de la energía eólica resulta clave para la transición energética y la descarbonización económica.

Una reducción del coste de la electricidad obtenida a partir de la energía eólica se consigue gracias a emplear aerogeneradores más potentes, lo que genera una mayor competitividad frente a los combustibles fósiles.

Los aerogeneradores constan de una torre que eleva una góndola en cuyo extremo se encuentra un rotor compuesto por un buje donde se fijan las palas. El proceso de funcionamiento consiste en la activación por efecto del viento del rotor y se acciona el generador eléctrico que convierte la energía mecánica en eléctrica. Por último, un transformador transfiere la electricidad a la red.

Para cubrir con la demandada necesidad del sector eólico de fabricar aerogeneradores más potentes, se necesita mayor altura, donde los vientos son mayores. Por otro lado, un aumento de la potencia demanda mayores tamaños de rotor, lo que requiere a su vez un aumento de la capacidad portante de la torre para resistir el aumento de peso debido al aumento de tamaño de la turbina y el rotor. Por estos motivos, el diseño y los materiales de la torre en sí del aerogenerador son de es de vital importancia para conseguir mayores alturas y potencias asociadas.

En base al material empleado en las torres de los aerogeneradores, estas se clasifican en estructuras de acero, de hormigón o híbridas [3]:

- Torres metálicas: Son estructuras compuestas por acero, cuyo diseño está condicionado por factores tales como la complejidad del cimiento, las dificultades de transporte y suministro, los procesos de montaje o la sensibilidad de las juntas a fatiga, así como los elevados requerimientos de mantenimiento. El aumento de altura de las torres metálicas está condicionado a un aumento de su espesor. Las torres eólicas de acero tienen limitaciones de transporte, estructurales y económicas que hacen que la altura máxima que puedan alcanzar sea más limitada respecto a las otras opciones. A partir de cierta altura, se reduce notablemente la eficiencia económica. Además, los valores límite en la frecuencia natural de la torre incrementan los precios de los cimientos y los riesgos de deformabilidad del terreno.
- Torres de hormigón: estas torres se caracterizan tener una alta resistencia además de tener una larga vida útil y exentas prácticamente de necesidad mantenimiento respecto a las otras opciones. Debido a la libertad de geometrías que permiten estos diseños, se puede optimizar el comportamiento dinámico y estructural, permitiendo llegar a alturas superiores.
- Torres híbridas: son estructuras híbridas entre las dos tipologías previas. Se componen de un tramo superior de estructura metálica que es acoplado a un tramo inferior de hormigón. Estas torres tienen frecuentemente problemas de fatiga entre las uniones de ambos tramos, además de tener un alto coste inicial de inversión.

Entre las tipologías descritas previamente, la solución de mayor versatilidad, que responde mejor a la necesidad del incremento de la altura de las torres y, por tanto, al aumento de las potencias de los aerogeneradores, con la importancia que ello conlleva en el impulso de la energía eólica, es la de hormigón. Además, cabe destacar que el empleo de hormigón consiste en un proceso más sencillo, rápido y de menor coste, que le da una importante ventaja competitiva respecto al acero.

Dentro de los retos en el desarrollo de las torres de hormigón, se encuentra la velocidad y economía del montaje, para competir con las torres metálicas y poder replicar las torres a gran escala, de manera industrial. Dentro de las torres de hormigón, la **adición de fibras como solución** permitiría simplificar el proceso constructivo, al eliminar parcialmente el armado, y reducir notablemente los plazos del mismo, suponiendo una importante ventaja competitiva frente a otro tipo de torres. Además, el hormigón reforzado con fibras ha demostrado ser más sostenible y económico que el hormigón armado.

Por ello, su empleo en torres eólicas tiene un doble propósito ambiental: por un lado, disminuir el consumo de materias primas (mejora del impacto ambiental) al emplear fibras en sustitución parcial de la armadura; por otro lado, conseguir un aumento de la energía eólica, energía verde, gracias a la obtención de grandes alturas de torres, ligadas con un aumento de la potencia de los aerogeneradores.

El hormigón reforzado con fibras (HRF) es definido por el Código Estructural como aquel que "incorpora en su composición fibras cortas, discretas y aleatoriamente distribuidas en su masa". En los últimos años, el interés por este tipo de material ha ido creciendo, lo cual ha sido reflejado en el incremento de investigaciones y publicaciones científicas sobre este tema. A medida que avanza esta investigación, su uso en componentes estructurales se está aceptando en las directrices y recomendaciones de diseño nacionales e internacionales. De esta forma, el empleo del HRF para distintos usos es cada vez más común, ya que la adición de fibras al hormigón se ha demostrado que le confiere unas mejores prestaciones en cuanto a diferentes propiedades mecánicas y no mecánicas (resistencia al fuego). A continuación, se enumeran algunas de estas mejoras.

Probablemente, la propiedad más significativa del HRF, debido a sus implicaciones estructurales y de diseño, es el desarrollo de la capacidad de flexión/tracción post-fisuración, que permite controlar tanto la propagación como la abertura de grietas. La capacidad de absorción de la energía del hormigón aumenta de forma significante respecto al tradicional sin refuerzo, lo que evita una rotura instantánea del mismo. Esta propiedad hace que la rotura del hormigón pueda ser predicha ya que aparecen fisuras previas, mientras que en el convencional sin armado la rotura se produce de forma más violenta.

Se ha demostrado que las fibras de acero contribuyen a mejorar las propiedades mecánicas, como la resistencia a flexión, tracción, impacto y fatiga de las mezclas de hormigón. La mejora de estas propiedades depende tanto de las propiedades de las fibras (tamaño, material…), como del volumen de las mismas que es incorporado al hormigón.

En base a los beneficios que ofrece el hormigón con fibras, éste se puede emplear en diversas aplicaciones, consiguiendo mejorar tanto costes como plazos asociados a la colocación del hormigón armado tradicional, así como algunas de sus propiedades.

La adición de fibras debe conferir al hormigón unas características mecánicas tales que permitan prescindir de la armadura pasiva del hormigón. En esta línea, los esfuerzos críticos a considerar son, entre otros, la **flexión, el cortante, la resistencia residual a flexotracción y la resistencia mínima a compresión**.

Las torres eólicas están sometidas a cargas dinámicas provocadas por el viento y el movimiento de la turbina, por lo que uno de los procesos de deterioro estructural más importante de las torres eólicas es la **resistencia a fatiga**. Estudiar este fenómeno es importante para cualquier estructura móvil por lo que resulta fundamental un estudio de la fatiga para asegurar que el hormigón es capaz de mantener sus características funcionales durante el periodo de vida útil, el cual debe garantizar generalmente que sea superior a los 20-30 años en este tipo de estructuras.

Por otro lado, las torres de hormigón con fibras deben de ir postesadas por el interior, lo cual requiere una **alta resistencia a la fluencia**, con el objetivo de que resista los esfuerzos solicitados. La fluencia es de gran importancia ya que, además de afectar al hormigón en sí, puede afectar al pretensado generando deformaciones y pérdidas de carga.

Es importante destacar que los comportamientos por cargas tanto de fatiga como por fluencia no han seguido el ritmo de investigación de otras propiedades a corto plazo, por lo que existe una necesidad en los estudios de estos fenómenos en el HRF.

Esta Tesis ha considerado tres aspectos, ligados a la construcción y el diseño orientado a torres eólicas:

- La **disposición y orientación de las fibras** en el hormigón hace que algunas de las propiedades del hormigón mejoren o no, de forma que, si se conoce cómo se orientan las fibras en función del método de hormigonado y cómo influye esta disposición en las propiedades críticas del diseño, se podría planificar de forma que resistan mejor los esfuerzos solicitados.
- La **resistencia a fatiga** del hormigón es clave en el diseño de torres eólicas ya que soportan cargas cíclicas debidas al viento y al movimiento de la turbina.
- Las torres eólicas suelen requerir de algún tipo de pretensado, generalmente postesado interior, para minimizar la cantidad de armado; en el caso de las torres eólicas en hormigón con fibras, este pretensado es esencial por su menor capacidad frente a esfuerzos de tracción. Por ello, el **comportamiento a fluencia** del hormigón es clave en el diseño de la torre, ya que la fluencia puede conducir a la pérdida de capacidad mecánica del material, teniendo claras implicaciones estructurales y de diseño.

No obstante, pese a que se centra en esfuerzos críticos referidos a las torres de aerogeneradores, los resultados expuestos en la presente Tesis son extrapolables a cualquier diseño que requiera el estudio de estos esfuerzos y emplee este material. Además, las investigaciones realizadas contribuyen al estado del arte de este tipo de material en estudios a largo plazo, los cuales han sido investigados en general en menor medida respecto a otros esfuerzos.

Para la realización de las investigaciones, se ha empleado una dosificación de hormigón con árido calizo y la adición de macrofibras metálicas, siendo el mismo material para cada uno de los estudios.

Cabe mencionar que esta Tesis parte del proyecto S2C – "Desarrollo de un nuevo concepto de torre de hormigón in situ de gran altura para aerogeneradores de gran potencia", subvencionado por el Ministerio de Economía, Industria y Competitividad a partir de la convocatoria Retos-Colaboración 2017.

1.2. Objetivos

El *objetivo general* de esta Tesis es ampliar el estado de conocimiento actual del hormigón reforzado con fibras, en especial sobre algunos de los aspectos críticos para el diseño de las torres de hormigón para aerogeneradores, empleando este material.

Para conseguir el objetivo principal anteriormente descrito, se han planteado los siguientes *objetivos específicos*, que son abordados en cada uno de los capítulos posteriores del presente documento y que componen una colección de artículos que han sido publicados en revistas científicas:

1. Analizar cómo afecta el método de hormigonado en la disposición de las fibras y a su vez en la resistencia del hormigón.
2. Ampliar el conocimiento sobre el fenómeno de fatiga del HRF.
3. Estudiar el fenómeno de fluencia y el impacto que tiene la edad en carga del hormigón en el mismo.

Se busca que los resultados obtenidos y expuestos en la presente Tesis aporten conocimiento acerca del hormigón reforzado con fibras y sean de utilidad para motivar el empleo de dicho material en distintas estructuras, en especial en torres de aerogeneradores, así como para mejorar futuros diseños.

1.3. Organización de la Tesis

La presente Tesis Doctoral ha sido realizada por compendio de artículos, estructurada en capítulos (ver Fig. 1) que se corresponden con los distintos artículos publicados, fruto del trabajo desarrollado.

El cuerpo de la Tesis está compuesto por una introducción general, que se corresponde con el **Capítulo I**; el **Capítulo II** muestra los estudios sobre el efecto que tiene el hormigonado en la disposición de las fibras y cómo afecta esto a su resistencia; el **Capítulo III** presenta los estudios recogidos sobre la capacidad de resistencia a fatiga por flexión del hormigón; el **Capítulo IV** recoge las investigaciones acerca de la resistencia a la fluencia del hormigón con fibras; por último, en el **Capítulo V** se plasman las conclusiones finales sobre los trabajos realizados y las futuras líneas de investigación.

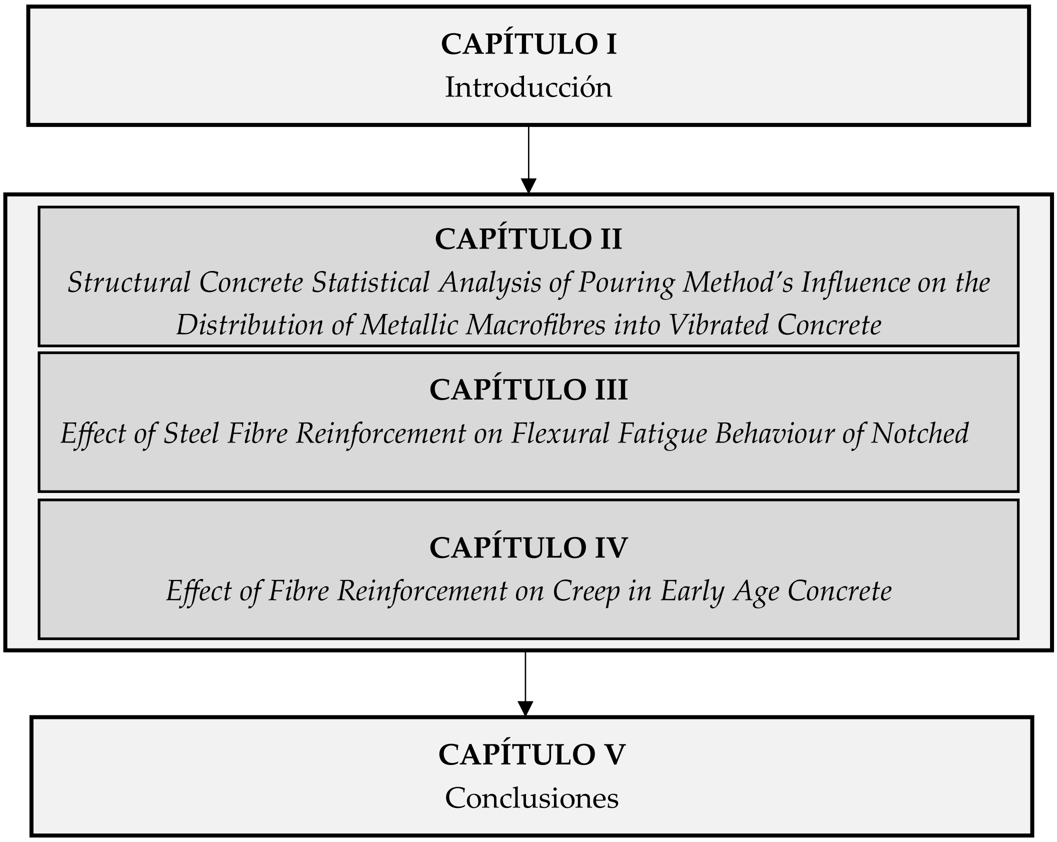

Fig. 1. Organización de la Tesis doctoral.

A Continuación, se describe el contenido de cada uno de los artículos publicados en revistas científicas que corresponden con los capítulos de la presente Tesis Doctoral.

1.3.1. *Artículo I*

El primer Artículo consiste en un artículo publicado en la revista Materials, cuya temática es el *análisis estadístico de la influencia del método de vertido en la distribución de macrofibras metálicas en hormigón vibrado*. Por otro lado, parte de los resultados de este estudio fueron expuestos en el VIII Congreso ACHE, celebrado en Santander en junio de 2022, bajo la ponencia de título “Influencia del método de hormigonado en la distribución de macro-fibras metálicas en el hormigón vibrado". El artículo, que corresponde con el Capítulo IV de la Tesis, está relacionado con la influencia que tiene la disposición de las fibras en la resistencia posterior del hormigón y cómo se distribuyen las mismas en función de la dirección de hormigonado y de la forma del encofrado. En concreto, se analizan las siguientes cuestiones:

- Evaluación de la disposición de las fibras según la dirección de hormigonado del encofrado, mediante la cuantificación de la cantidad y contenido de fibras por método inductivo.
- Influencia de la disposición de las fibras y relación con el hormigonado en la respuesta post y pre-fisuración del HRF.

1.3.2. Artículo II

El segundo Artículo consiste en un artículo publicado en la revista Materials, cuya temática es el *efecto del refuerzo de fibra de acero en el comportamiento a la fatiga por flexión del hormigón estructural entallado*. Por otro lado, parte de los resultados de este estudio fueron expuestos en el VIII Congreso ACHE, celebrado en Santander en junio de 2022, bajo la ponencia de título "Efecto del refuerzo de las fibras de acero en la evolución de la fatiga a flexión en hormigones estructurales". El artículo, que corresponde con el Capítulo II de la Tesis, se centra en los siguientes aspectos:

- Investigación sobre el efecto de distintos rangos tensionales para analizar el comportamiento a fatiga por flexión del hormigón reforzado con fibras.
- Análisis del comportamiento debido a la energía almacenada y disipada antes y después de la fisuración del hormigón.
- Análisis de la velocidad de apertura de fisura en función del tiempo y relación con el efecto del rango tensional aplicado.

Este artículo ha sido incluido en la presente Tesis Doctoral, ya que uno de los principales esfuerzos críticos que afecta a la durabilidad de las torres eólicas de hormigón es la fatiga del material.

1.3.3. Artículo III

El tercer y último Artículo consiste en un artículo publicado en la revista Applied Sciences, cuya temática es el *efecto del refuerzo de fibra en la fluencia del hormigón de edad temprana*. El alcance del artículo, que corresponde con el Capítulo III de la Tesis, consiste en cuantificar la influencia que tiene la edad de puesta en carga del hormigón con los resultados de fluencia. En concreto, se analiza lo siguiente:

- Efecto de la edad de puesta en carga en la evolución temporal de la deformación, con el objetivo de evaluar la deformación elástica diferida sufrida por las probetas tras el ensayo de fluencia.
- Propuesta de formulación para la fluencia en función de la edad de puesta en carga y la carga aplicada del HRF.
- Efecto de la edad de puesta en carga en la variación del módulo de elasticidad del HRF.

Este artículo tiene cabida en esta tesis ya que se trata de un condicionante clave a la hora de planificar los tiempos de las fases de la construcción de una torre eólica.

CAPÍTULO II

Statistical Analysis of Pouring Method's Influence on the Distribution of Metallic Macrofibres into Vibrated Concrete

- **Authors:** Laura Gonzalez, Jose A. Sainz-Aja, Álvaro Gaute, Jokin Rico, Albert de la Fuente, Ignacio Segura, Carlos Thomas
- **Published at**: Materials 2023 / Volume 16 / Issue 4
  10.3390/ma16041404
  7 February 2023
- **Impact factor:** 3.748

Abstract: The use of fibre-reinforced concrete (FRC) in structural applications is increasing significantly as a result of (1) the acceptance of this composite into design guidelines and (2) the improvement in terms of sustainability performance that has been reported for cases where FRC has been used. In this context, fibre orientation and distribution are factors that govern the post-cracking response of the FRC. Researchers have already dealt with the analysis of both variables from an experimental and numerical perspective, and design-oriented recommendations were included in existing design guidelines (i.e., fib Model Code 2020). Nonetheless, there are still technical aspects to be answered within a research framework before the influence of these variables on the mechanical response of FRC could be covered with sufficient reliability. In this regard, this research is aimed at shedding light on the influence of the mould geometry and concrete pouring/vibration procedures on the fibre orientation and distribution variables as well as on the post-cracking performance of the FRC. An extensive experimental programme aimed at characterising these variables using novel testing techniques (i.e., an inductive non-destructive approach for quantifying fibre amount and orientation and the BCN test for assessing the pre- and post-cracking responses of the FRC) was carried out for this purpose. A relationship has been found between the shape of the formwork and the direction of pouring, along with the direction and distribution of the fibres, both of which proved to have an influence on the residual tensile strength of the concrete. However, it has been confirmed that the first crack resistance depends on the concrete matrix, with the addition of fibres having no relevant influence on that mechanical parameter. The results and conclusions derived from this experimental programme can be extended to FRCs and boundary conditions similar to those established herein.

Keywords: fibre-reinforced concrete; fibre orientation; fibre distribution; inductive method; fibre content

2.1. Introduction

Fibre-reinforced concrete (FRC) is becoming increasingly important as research progresses, and its use in structural component is being accepted in national and international design guidelines and recommendations [4]. Structural macrofibres (steel or synthetic) used as unique reinforcement in some applications (i.e., pavements, tunnels, and column-supported flat-slabs for buildings, and others) or in combination with conventional reinforcement [5]–[12].

The addition of fibres allows improving several properties mechanical (i.e., post-cracking tensile strength and confinement level in compression) and non-mechanical (i.e., reduce spalling due to fire loads) of the concrete depending on the type and amount of fibres used [1], [8]–[10]. The most significant property of FRC, due to its structural and design implications, is the ability to develop post-cracking flexural/tensile capacity [13] which allows controlling both propagation and opening of cracks [13]–[15]. Other studies report that the addition of fibres increases Young's Modulus, especially at an early age [16] and improve the fatigue behaviour [4], [17]–[22]. In addition to the mechanical and geometrical properties of the fibres, it has been evidenced that the orientation and distribution of the fibres within the matrix have a major impact on the properties of the reinforced concrete. In this regard, the type and amount of fibres influence the fracture energy, which increases with increasing fibre dosage [18]. On the other hand, experimental results allow stating that there is a clear relationship between the orientation of the fibres and the mechanical, electrical and thermal properties of the composite materials [23]–[26]

The modulus of elasticity of reinforced concrete depends to a large extent on the orientation of the fibres, the more the fibres are aligned with the direction of stresses, the lower the tensile elastic limit [27]. The residual strength (strength once cracking occurs), that governs the bending strength capacity, also depends on the angle of inclination of the fibres, so that the smaller the angle, the higher the bending strength [28]. Preferential fibre orientation creates weaker planes, this favouring increased crack opening at lower load levels [29]. In addition, fibre orientation, in combination with fibre geometry, has an effect on thermal conductivity [30].

It has been shown that the change in fibre orientation and fibre distribution is highly dependent on the length and height of the formwork [27]. Studies conclude that fibres align as a result of the formwork wall effect [10]. The fibre distribution also has a significant influence on the ultimate flexural strength of the FRC, which increases with the increase in the number of fibres per unit area and the dispersion coefficient [28]. P. Martinelli et al. concluded that specimens in contact with the formwork have higher post-cracking stress than those closer to the surface, this influenced by fibre content (related to segregation) and fibre orientation [31].

Regarding the influence of the rheology of the fresh concrete on the fibre orientation, some authors affirm that the fluidity of the fresh concrete is the governing parameter [32]. This fluidity can be influenced by fibre typology [33] and the method and time of vibration of the concrete [34], between others. These vibrating characteristics are conditioning factors for the positioning and orientation of the fibres. Hence, the performance of the fibres in the residual strength capacity can be altered according to the vibration parameters.

In some studies, equations have been developed to help predict fibre orientation in concrete, as well as CFD-based methods to monitor fibre orientation and distribution [10], [27], [35], [36].

Knowledge of the variation in fibre orientation and distribution is of great importance for improving the mechanical properties of reinforced concrete. Some works such as [37]–[39] focus on quantifying the effect of concrete flowability/workability on fibre distribution and orientation. Since most of the existing works are based on empirical/analytical models, the need arises for this study, which aims to quantify the orientation/distribution based on non-destructive methods and within the reach of control laboratories to estimate fibre distribution and orientation in quality/production control.

In this paper, a complete characterization is performed on fibre distribution depending on the pouring method on concrete reinforced specimens with commercial hooked-end fibres HE++90/60. The characterization of this reinforced concrete is a continuation of other studies performed by some of the authors [17], [40].

2.2. Materials and methods

2.2.1. Materials

The concrete was manufactured using a CEM I 52.5N, according to EN 197-1:2011 [41], with a density of was 3.12 g/cm^3, obtained according to UNE 80103:2013 [42]. A superplasticizer additive, MasterEase 5025, was added at 1% wt. of cement to obtain the target fluidity of the concrete (17 cm of flowability measured with Abrams cone method).

Hooked-end type steel fibres were selected to manufacture the reinforced concrete. These fibres were HE 90/60 made by ArcelorMittal and its properties are shown in Tab. 1 and in Fig. 2, an image of these fibres can be seen.

Tab. 1. Steel fibre properties.

Parameter	Value
Fibre shape	Hooked end
Length (mm)	60
Diameter (mm)	0.90
Aspect ratio (l/d)	67
Tensile strength (MPa)	1200

Fig. 2. Hooked-end steel fibres used.

Limestone gravel and limestone sand used to produce the concrete. Its physical properties can be seen in Tab. 2 and Fig. 3 shows the grading of the aggregates obtained according to EN 933-1 [43].

Tab. 2. Aggregate physical properties.

Size [mm]	Sand equivalent	Absorption [%]	Density [g/cm³]
0/2	>75	0.49	2.69
0/4	>80	0.49	2.69
4/12	-	0.54	2.70
10/20	-	0.54	2.68

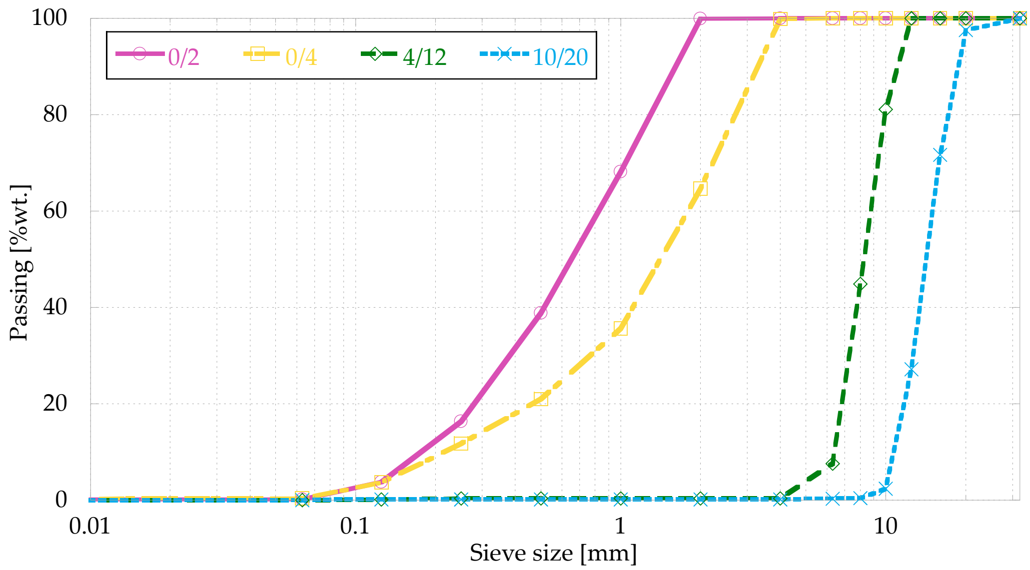

Fig. 3. Grading curve.

The concrete mix proportions were obtained by the Fuller method, adding a 0.44% by volume of steel fibres, and are shown in Tab. 3.

Tab. 3. Mix proportions.

Material	Mix [kg/m³]
Cement	390
0/4	480
4/12	480
10/20	480
Water	165
Additive	3.9 (1% wt. of cement)
Fibres	35

2.2.2. *Methods*

Conventional mechanical properties

Three different cubic specimens of 150x150x150 mm^3 were used to determine compressive strength at 28 days, according to EN 83507:2004 [44]. These specimens were vibrated with internal vibrator, according EN 12390-2:2020 [45] and cured in a humidity chamber under controlled conditions (20 ± 2 °C and 95 ± 5% humidity) up to the test moment.

Three different prismatic specimens of 600x150x150 mm^3 were used to determine the flexural tensile strength at 28 days, according to UNE-EN 14651:2007 [46]. These specimens were cured in a humidity chamber together with the cubes and vibrated in the same way that cubic specimens. The vertical displacement (δ) was recorded and used to calculate the Crack Mouth Opening displacement (CMOD), according to the standard (Equation 10).

$$CMOD = \frac{\delta - 0.04}{0.85}$$ **Equation 1**

Fig. 4. Flexural tensile strength test of the fibre reinforced concrete.

<u>*Pouring method*</u>

In order to quantify the fibre distribution and their influence on the behaviour of the concrete according to the direction of pouring, two blocks (initially without holes) of dimensions 1200x400x1200 mm were manufactured, simulating real dimensions. These blocks were arranged in two different ways, as shown in Fig. 6, and the concrete was vibrated with internal vibrator, according EN 12390-2:2020 [45].

In the first one, called "BH", the concrete was poured on the larger side of the cube (1200x1200 mm), while the one called "BV" was concreted on one of the small sides (1200x400 mm).

Fig. 5. Concrete pouring (left), BV (centre) and BH (right).

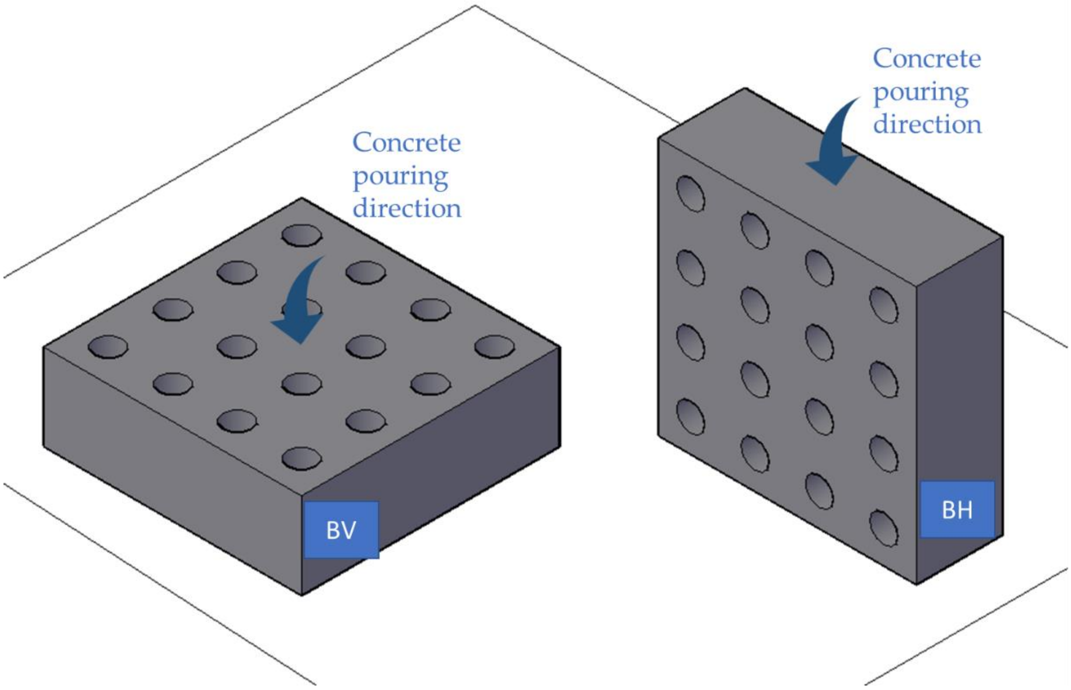

Fig. 6. Concrete pouring direction in each block.

<u>*Specimens production and nomenclature*</u>

From the previously described concrete blocks, cylindrical specimens with a diameter of 132 mm were extracted using a diamond drilling machine and cut to obtain 132 mm high specimens (l/d=1). These specimens were coded as follows:

- A letter and a number that indicate the position on the block (Fig. 7).
- A letter V or H, depending on the block from which they have been extracted.
- A letter I or S, in the case of BH block, which indicates whether the tested specimen comes from the top (pouring side) or the bottom (base) of the block.

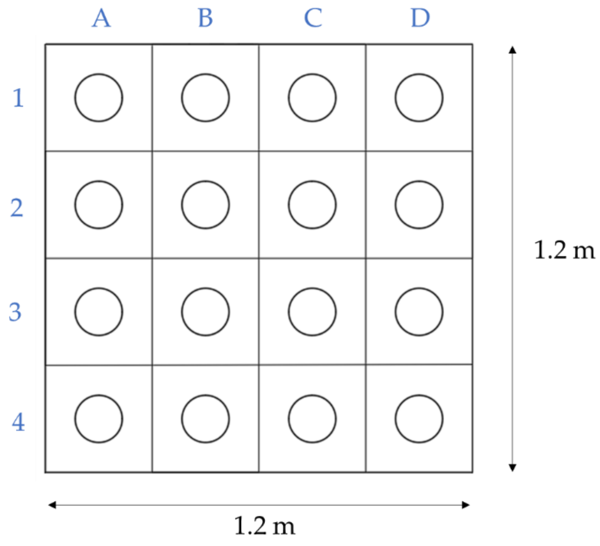

Fig. 7. Code of the extracted specimens.

Inductive characterisation

The inductive test is an application of Faraday's law of magnetism and takes advantage of the inductance variations produced by metallic elements when interacting with the magnetic field. For such a test, the specimens must be placed within a plastic container with an established cylindrical geometry. Copper or aluminium wire coils are placed around the container, constituting the sensor element of the system, which is shown in Fig. 8. An electrical current goes through the coil and produces a magnetic field around the device, interacting with the steel fibres inside the concrete.

Fig. 8. Inductive equipment SmartFibreC® for the quantification of the amount and orientation of steel fibres in hardened concrete.

The inductance variation measured when conducting the inductive test is essentially produced by the interaction between the fibres present in SFRC and the magnetic field. In this line, the results of the inductive test mainly depend on the type of fibre (content of steel in the fibres), the amount and the orientation [11], [36], [47], [48]. Additional parameters such as the type of concrete, the content of water or concrete age do not influence the magnetic permeability given that the influence of steel on the magnetic field is several orders of magnitudes higher than that of concrete. Accordingly, it is possible to simplify the inductance measurements by disregarding the contribution of concrete on the inductance variation. The physical parameter of the magnetic field induced is the magnetic inductance (in mmH), which magnitude is modified by the presence (type and orientation) of steel fibres.

Calibration must be done beforehand using samples with variable fibre content, that need to characterize by means of the inductive test and subsequently crushed and grinded to weigh the fibres inside the sample. The calibration curve is obtained considering a zero value of inductance for the zero-fibre content sample and the relation between inductance and weight of fibres of the samples analysed and crushed. Once this calibration is done, no further calibration must be done in case that the same type of fibre is used.

The test can be conducted in both cubic and cylindrical specimens [36] since these geometries allow the characterization of both moulded and core drilled test samples. Actually, it is possible to determine the fibre content with an error below 3% and with low scatter on the measurements.

<u>*Barcelona test*</u>

The Barcelona test (BCN) responds to a double punch test configuration applied to cylindrical (300xΦ150 mm) or cubic (150 mm) specimen. It is carried out by applying a vertical force above the specimen through cylindrical steel punches of 25 mm height and the diameter being ¼ of the cross-section minor dimension. The load is applied through the upper punch at 0.5 ± 0.05 mm/min. During the loading process, a triaxial compressive stress state occurs at both extreme faces and internal cones are generated (one per face). As the cones penetrate inside the specimen, vertical cracks -that open circumferentially- appear and fibres prevent these cracks to widen through a residual tensile concrete strength mechanism. A Load-Total Circumferential Opening Displacement (TCOD) curve or Load-Axial Displacement (vertical) can be derived from the test (Fig. 9).

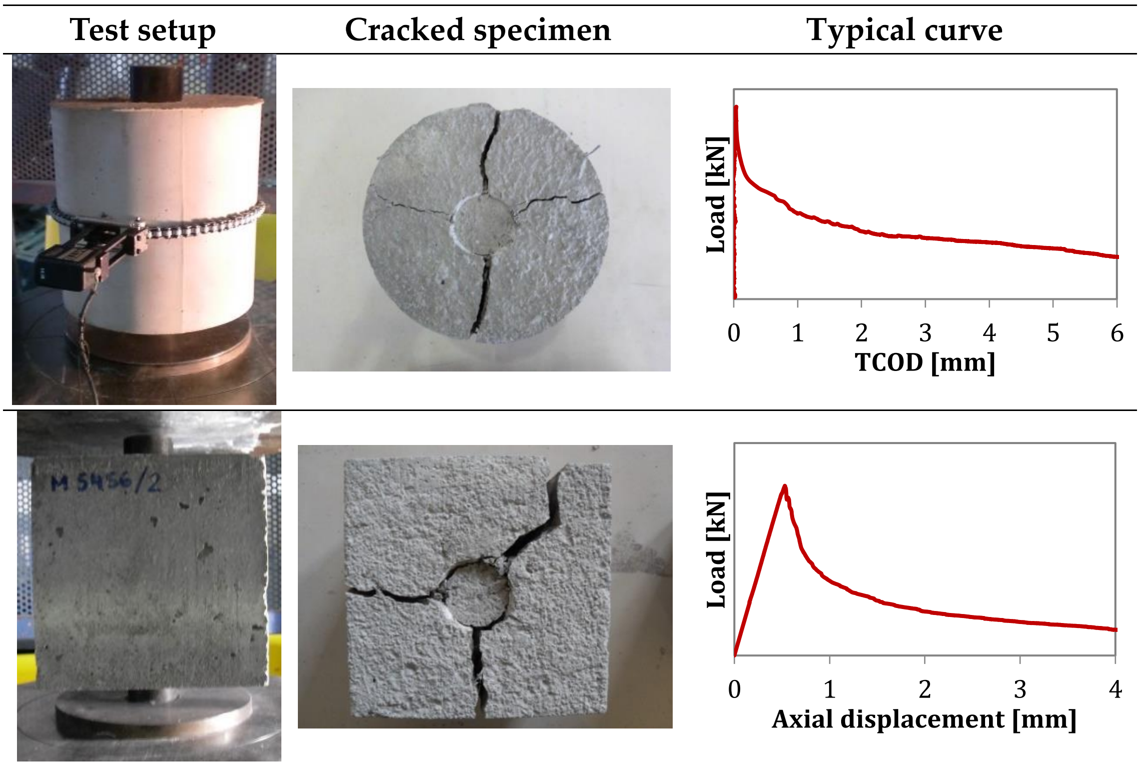

Fig. 9. Barcelona test in cylindrical and cubic specimens.

The BCN was originally developed to control the TCOD through a circumferential extensometer, as described in the standard UNE 83515. The test procedure was simplified through the definition of a correlation between the TCOD and the vertical displacement [36], [49], [50] to use the latter as the control variable. The analytical and theoretical description of such correlation is described in Fig. 10, showing how the *load-axial displacement* curve can be used to show the results of *load-TCOD*.

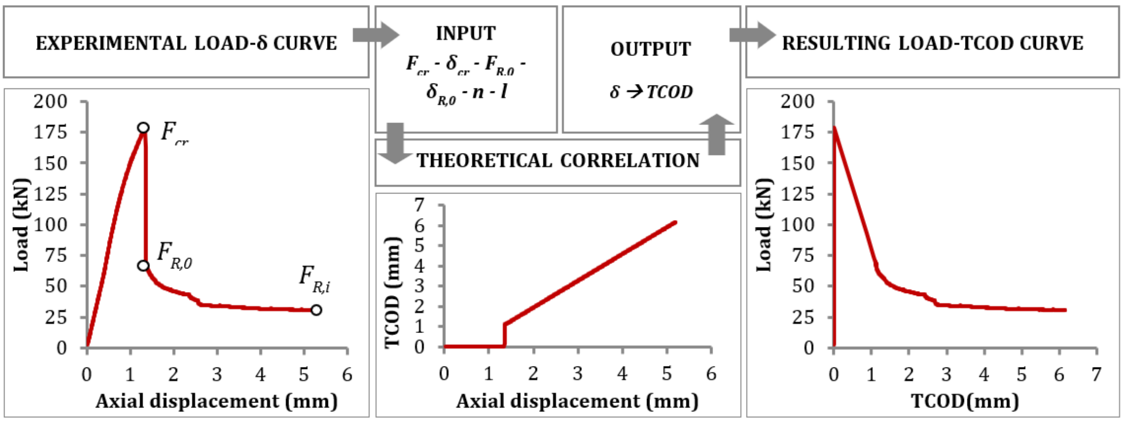

Fig. 10. Correlation between axial displacement and TCOD.

The correlation between the circumferential opening and the vertical displacement allows replacing cylindrical specimens for cubic samples. Even though the use of cylindrical specimens for testing is an advantage in case of extracting cores from existing structures, testing cubic specimens under the BCN and properly analysing the results could provide an evaluation of the fibres preferential orientation [49].

Cracks should propagate in the direction corresponding to the preferential orientation of the fibres, this meaning that the minimum orientation direction is perpendicular to the crack. For this, cubic specimens can be tested in different directions to take advantage of the relation between the post-cracking strength and fibre orientation. This provides an estimation of the orientation of fibres in % according to the contribution of the fibres in each direction to the residual strength [49].

Data curation

Statistical analysis:

Several statistical analyses were carried out using the Scipy Python library:

- T-Test: It is an analysis that allows the comparison of the mean value of two data distributions. In general, if a P-value of less than or equal to 0.05 is obtained, it is assumed that there is evidence of significant differences between the means of the distributions.
- Levene-Test: It is an analysis that allows the comparison of the standard deviation of two data distributions. In general, if a P-value of less than or equal to 0.05 is obtained, it is assumed that there is evidence of significant differences between the standard deviation of the distributions.
- Shapiro wilk: This is a test used to check the normality of a data set. In general, the test rejects the hypothesis of normality when the p-value is less than or equal to 0.05.

Correlation matrix:

The Python libraries Pandas and Matplotlib were used to generate the correlation matrix. The Pearson correlation coefficient (r) is visually represented in a correlation matrix. That is to say that these squared values will be the coefficient of determination (r^2), so that values close to -1 indicate a strong inversely proportional correlation. Values close to 1, a high correlation in a directly proportional way and those values close to 0 will imply a low correlation between the variables.

2.3. Results and discussion

2.3.1. Mechanical properties

The mean compressive strength –resulted from 3 specimens– was f_{cm} = 50 MPa (CoV=7.4%). The mean residual flexural strength for the 0.5 crack opening ($f_{Rm,1}$, CMOD=0.5 mm), was 3.5 MPa (CoV=7.1%) and for the 2.5 mm crack opening ($f_{Rm,3}$, CMOD=2.5 mm), was 6.3 MPa (CoV=8.3%). In Fig. 29 a compressive and a flexural tested specimen can be seen.

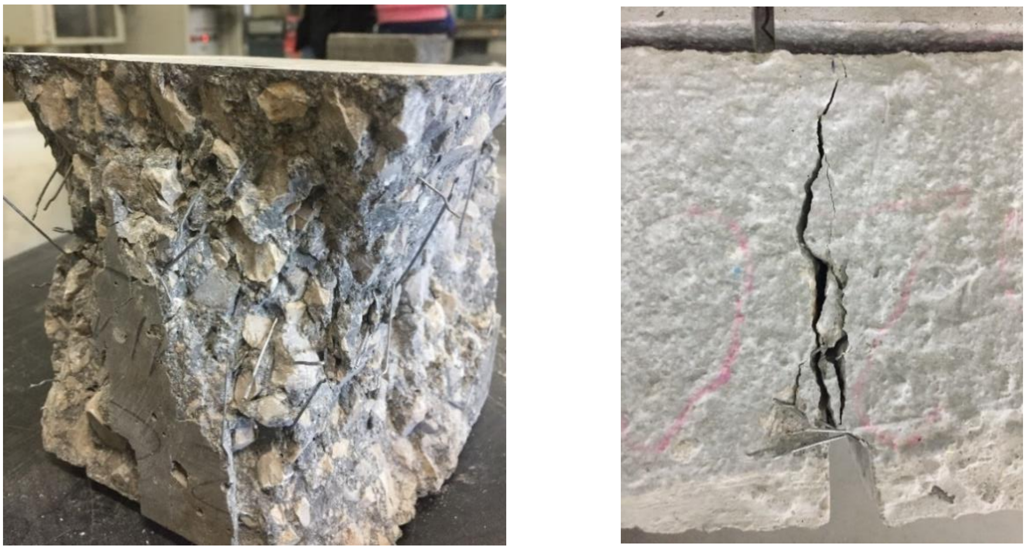

(a) **(b)**

Fig. 11. Specimens after compressive test (a) and flexural test (b).

2.3.2. *Inductive test*

Fig. 12 depicts the distribution of the amount of fibres as a function of the concrete pouring method (a) and as a function of height for BH (b). **Tab. 4** shows the results of the T-test and the Levene-test, which allow a comparison of the two distributions, and gathers the mean value, standard deviation and P-value of a T-test in the case of BH.

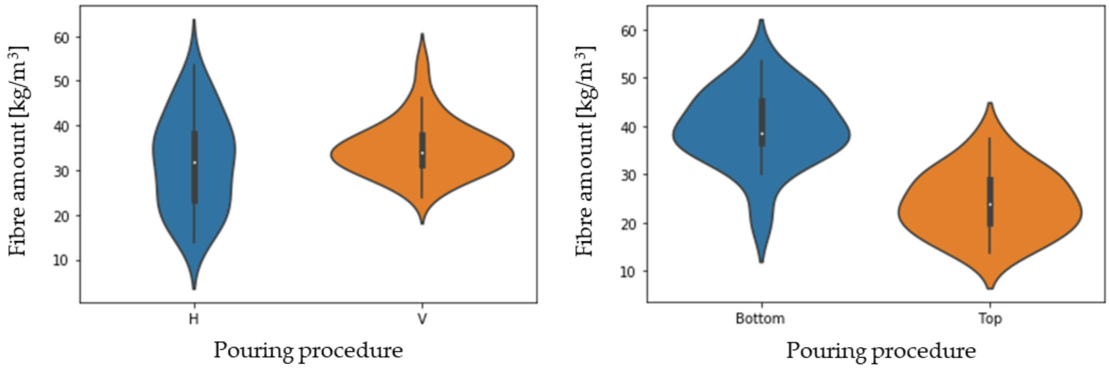

(a) (b)

Fig. 12. Fibre amount distributions as function of the pouring procedure (a) and as function of the height for BH (b).

Tab. 4. Statistical parameters on the influence of pouring procedure in the fibre amount distribution.

		MEAN	STD (CoV)	P_{value} (T-Test)	P_{value} (Levene-Test)
Influence in pouring procedure	BH	31.9	10.6 (33.2%)	1.0e-1	1.7e-4
	BV	35.0	6.3 (18.0%)		
Influence of height in BH	BH-Top	24.2	6.5 (26.9%)	4.6 e-7	-
	BH-Bottom	39.7	7.7 (19.4%)		

It is concluded that the amount of fibre is equivalent in both types of pouring, but that in the case of vertical pouring the results allowed proving that the distribution of the amount of fibres is more homogenous than in the case of horizontal concreting (notice the differences in CoVs). Thus, according to the results in Tab. 4, in BV (vertical concreting) the mean fibre distribution coincides with the theoretical distribution (35 kg/m^3) and with a significantly lower dispersion than that obtained for BH. A longer concrete face travel leads to a better fibre distribution (which is in line with other works [37]).

Concerning the effect of the height of the cross-section poured (BH top and bottom), the T-test provides a P_{value} of 4.6 e-7, this allowing stating that –with high probability– the height has a significant influence of the fibre amount distribution. In this regard, the average fibre amount at the top (24.2 kg/m^3) and bottom (39.7 kg/m^3) in the BH prism is 31% and 13% lower and greater, respectively, in comparison to the theoretical fibre amount (35 kg/m^3). This is due to a slight segregation effect [51], [52], with the fibres being denser than the concrete itself, and also due to the potential energy, that is bigger in BV, because the flow is higher.

Once it has been verified that in the case of BH there are significant differences depending on the position of the cores, it was then analysed whether these variations were also observed in the case of BV. Tab. 5 shows the results of mean value (each obtained from 12 values), standard deviation and Shapiro Wilk's P-Value according to the row and column for which it is computed, from which it can be concluded that in all cases the available data conform to a normal distribution.

Tab. 5. Statistical description of the fibre quantity depending on the position

Position	MEAN	STD (CoV)	Confidence interval 95%	Shapiro wilk (P_{value})
Row 1	36.0	8.3 (23.1%)	36.0 ± 5.3	0.45
Row 2	36.1	7.4 (20.5%)	36.1 ± 4.7	1.00

Position	MEAN	STD (CoV)	Confidence interval 95%	Shapiro wilk (P_{value})
Row 3	34.6	3.4 (9.8%)	34.6 ± 2.2	0.98
Row 4	32.1	3.0 (9.3%)	32.1 ± 1.9	0.54
Column A	31.5	4.3 (13.7%)	31.5 ± 2.7	0.89
Column B	37.4	4.8 (12.8%)	37.4 ± 3.0	0.94
Column C	34.5	3.5 (10.1%)	34.5 ± 2.2	0.36
Column D	35.8	9.4 (26.3%)	35.8 ± 6.0	0.07

It can be seen from the results obtained that there is more dispersion where there are greater fibres (more than 10% in values higher than the average of 35 kg/m^3 of fibres).

Tab. 6 presents the mean value and standard deviation values as a function of the exact position of the sample (for a given row and column condition). The results of hypothesis testing are shown in Tab. 7. The T-test results carried out on the sample means (of each zona) reveal the differences of the means are not significant and, with high probability, these belong to the same sample population. Consequently, it can be stated that the position is not an influencing variable for the fibre amount distribution.

Tab. 6. Statistical description of the fibre quantity depending on the position.

	Mean value [kg/m^3]				Standard deviation [kg/m^3]				CoV			
	A	B	C	D	A	B	C	D	A	B	C	D
1	30.57	39.13	34.45	40.07	3.86	6.84	3.58	14.72	12.6%	17.5%	10.4%	36.7%
2	28.52	40.30	37.77	37.98	4.24	4.55	1.82	11.74	14.9%	11.3%	4.8%	30.9%
3	36.04	36.19	35.23	30.77	4.29	2.46	2.16	2.53	11.9%	6.8%	6.1%	8.2%
4	30.87	34.04	30.49	33.67	2.32	4.29	2.48	0.92	7.5%	12.6%	8.1%	2.7%

Tab. 7. Analysis of significant differences between positions according to T-test.

	Columns						Rows					
	A-B	A-C	A-D	B-C	B-D	C-D	1-2	1-3	1-4	2-3	2-4	3-4
P_{value}	0.005	0.077	0.166	0.103	0.103	0.655	0.978	0.569	0.154	0.508	0.110	0.088

According to the results obtained and the statistical tests performed, it can be concluded that the fibre amount distribution tends to be more uniform in case of pouring the slabs from the vertical direction. According to the results obtained, the most suitable pouring method to achieve better homogeneity according to the number of fibres distributed in the slab, would be the BV.

Fig. 13 shows the fibre distribution in each plane, for each slab, differentiating top and bottom of the BH.

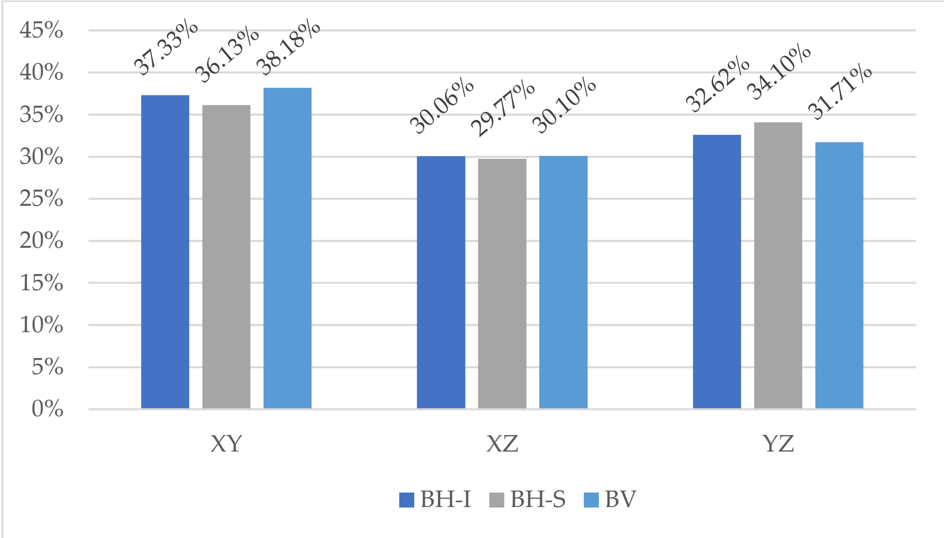

Fig. 13. Distribution of fibres in each plane.

It can be observed that in all cases the largest number of fibres (more than 36%) are oriented in the XY plane, which means that they are mostly aligned with the larger face of the formwork, both in the case of horizontal and vertical pouring direction.

Focusing the case on the horizontal concreting direction, it can be observed how in the upper part of the block this tendency is less clear, which may be due to the fact that the fibres have less time and space to align with the flow.

2.3.3. Barcelona test

Regarding the influence of pouring procedure in the Barcelona test results (pre- and residual strengths), Fig. 14 gathers the values of cracking (F_{ct}) and residual strengths (R_s) as a function of the type of concreting (a) and of the height in BH (b). The residual strengths (R_s) are given for crack openings of 0.5, 1.5, 2.5 and 3.5 mm. Tab. 8 shows the statistical results for these parameters.

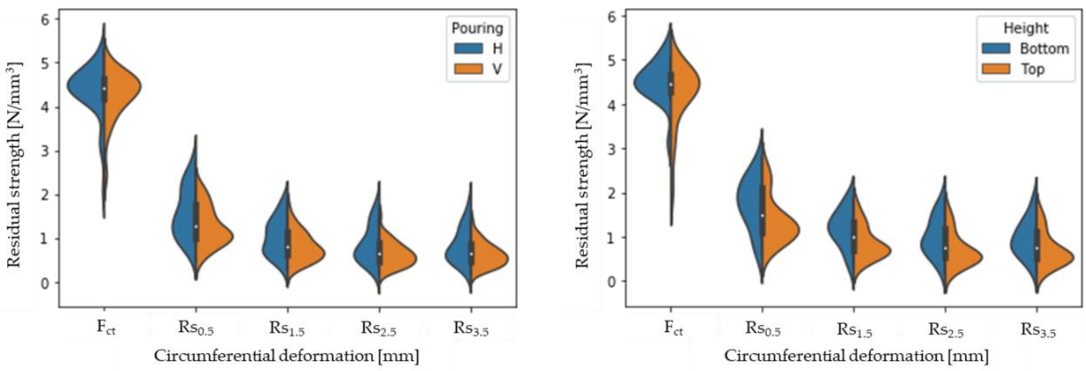

(a) (b)

Fig. 14. Distribution of the residual strength obtained by BCN Test as function of the pouring procedure (a) and as function of the height in BH (b).

Tab. 8. P_{value} of a T-test of the influence of pouring procedure in the resistance properties of concrete.

	F_{ct}	$Rs_{0.5}$	$Rs_{1.5}$	$Rs_{2.5}$	$Rs_{3.5}$
BH mean value	4.35	1.57	1.04	0.86	0.84
BH std value	0.62	0.58	0.43	0.43	0.41
BV mean value	4.26	1.26	0.81	0.64	0.63
BV std value	0.55	0.44	0.33	0.28	0.26
P_{value} (T-Test)	0.48	7e-3	8e-3	5e-3	6e-3
Top mean value	4.19	1.37	0.88	0.71	0.71
Top std value	0.71	0.51	0.36	0.37	0.37
Bottom mean value	4.51	1.77	1.19	1.01	0.97
Bottom std value	0.47	0.59	0.43	0.45	0.42
P_{value} (T-Test) in BH	0.14	0.04	0.03	0.04	0.06

Based on the results obtained, the method of pouring does not influence the cracking load, but it does influence the residual properties of the concrete. This is due to the influence of the concreting method on the fibre orientation, influence that other studies [37], [39] have affirmed. In all cases, in the case of BV, lower residual strength values are obtained.

Based on the results obtained in BH, it can be concluded that the position in height does have a certain influence on the post-cracking strength properties of the concrete, which makes sense considering that it has been found that there is a higher amount of fibres in the lower part of the concrete.

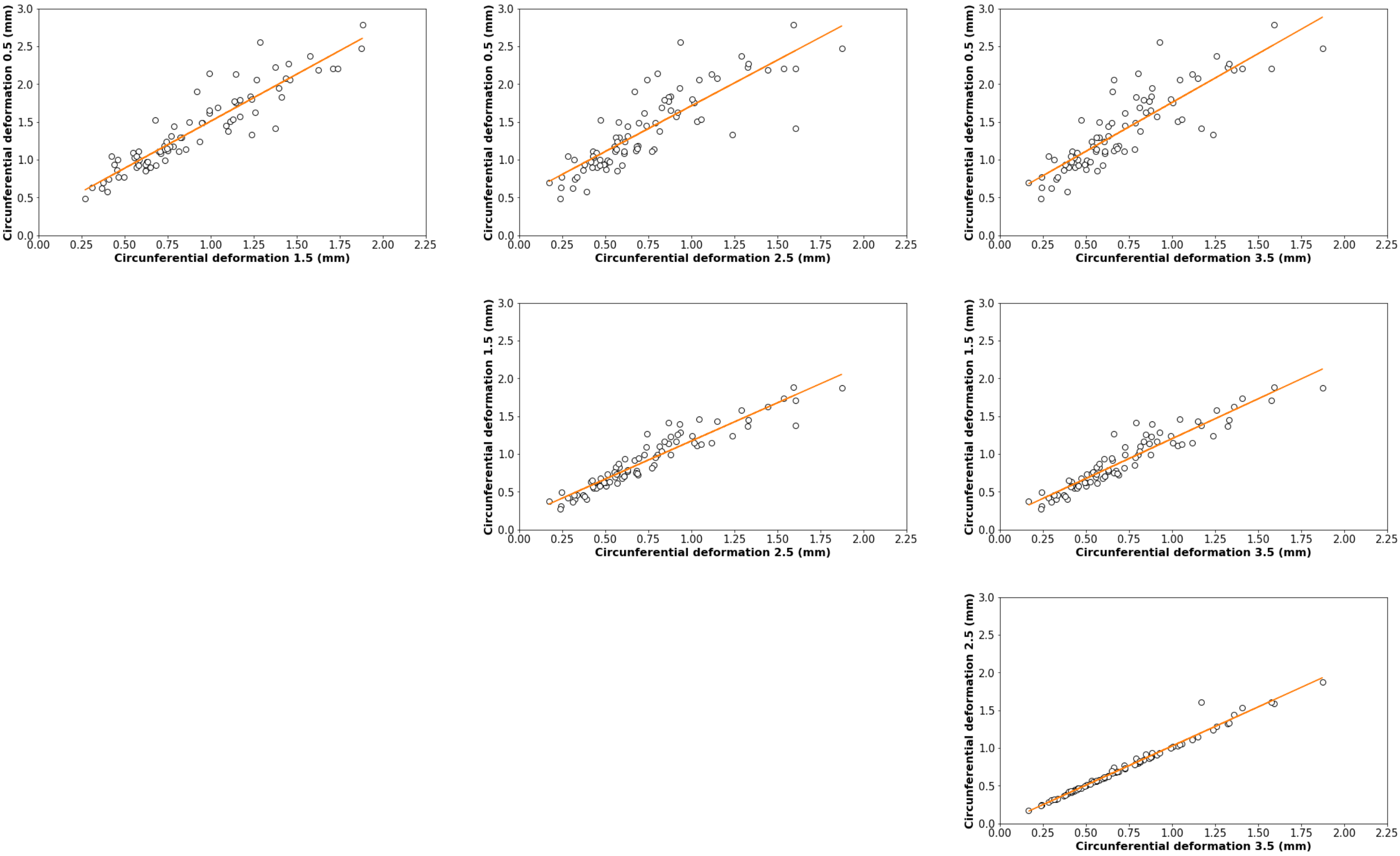

Fig. 15. Correlation between different values of circumferential deformation.

From Fig. 15 it can be seen that for large deformation values there is a very precise correlation between values, while for small values the distortion increases markedly. This is due to the fact that for larger deformations the fibres are the elements that are resisting the force almost completely, which, being metallic, have a more linear behaviour. At smaller deflections (crack openings), the fibre has more influence on the cracking load, as there is more fibre surface "gripping" both parts of the concrete.

2.3.4. Correlation between inductive test and BCN test

Fig. 16 shows the correlation matrix corresponding to the results of the inductive test (measures the amount and orientation of the fibres) and the Barcelona test.

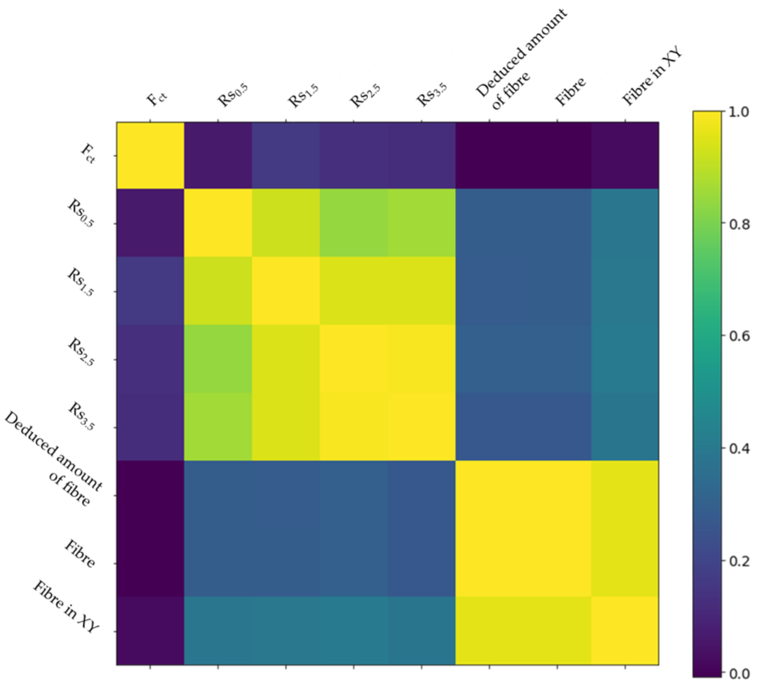

Fig. 16. Correlation plot.

From Fig. 16 it can be seen firstly that the parameter F_{ct} is not highly related to any other variable analysed. This is because it is a parameter depending on the concrete matrix, and throughout this study the concrete (without fibres) has been the same in all cases.

From Fig. 16, it can be seen that the circumferential deformation values are highly correlated with each other, especially in the case of $Rs_{2.5}$ and $Rs_{3.5}$. In particular, it can be seen that this correlation is higher the higher the circumferential deformation value. Fig. 15 shows the circumferential deformation values compared as a function of the deformation value.

Regarding the correlation between the results of the inductive test, a high linear correlation between all parameters is observed. Regarding the correlation between residual strength values and fibre quantity, it can be seen that the correlation is rather small, but that it correlates better with the projected fibre in the XY plane values than with total fibre values. This is because fibres oriented perpendicular to the direction of the force provide the most resistance.

In Fig. 17 it can be seen the amount of fibre in XY vs. circumferential deformations in BH, differentiating between top and bottom of the slab.

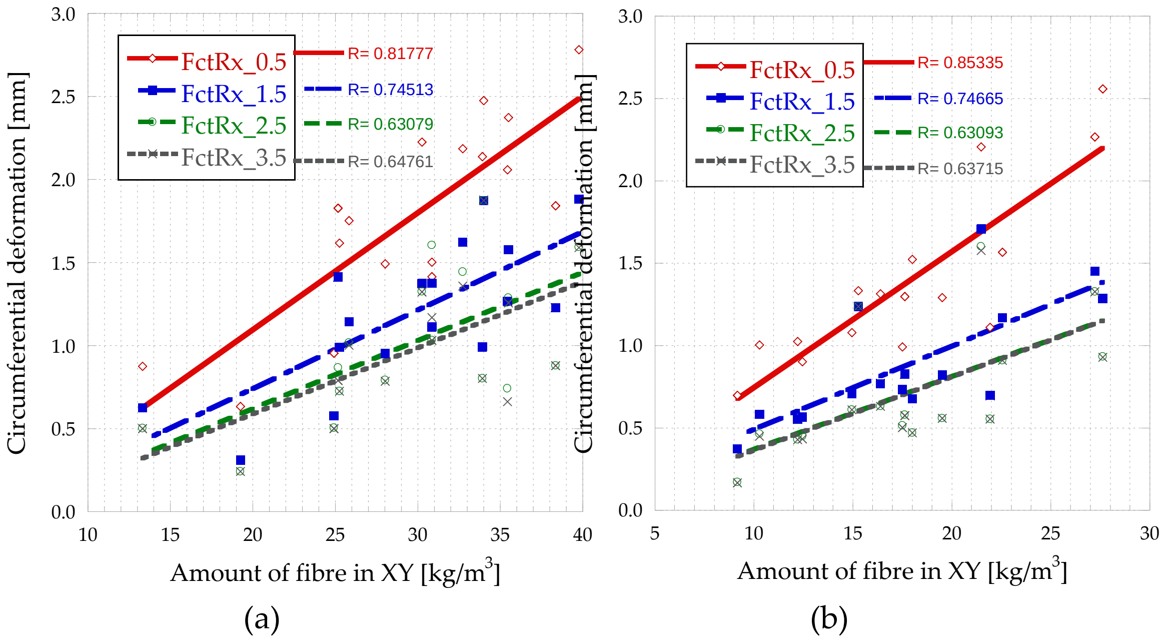

Fig. 17. Amount of fibre in XY vs. circumferential deformations in BH-bottom (a) and BH-top (b).

The circumferential deformation depends on the amount of fibre in the XY plane (parallel to the ground), so that the smaller the crack opening, the more dependent it is. Furthermore, it can be seen from Fig. 17 that the amount of fibre in this plane is higher in the lower part of the block, which results in higher resistances. Moreover, the results are more stable the smaller the crack opening (higher correlation coefficient), so that when the crack opening increases, the results are more heterogeneous. This is because the smaller the crack opening, the more fibre surface is in contact with the matrix on both sides of the crack.

This means that the fibres are oriented parallel to the direction of flow, so that they flow from the centre (where the concrete is poured) to the sides. The fibres are oriented preferentially in the direction of the larger faces of the formwork.

In Fig. 18 it can be seen the correlation between circumferential deformation for 0.5 mm of crack opening and the amount of fibre in XY plane.

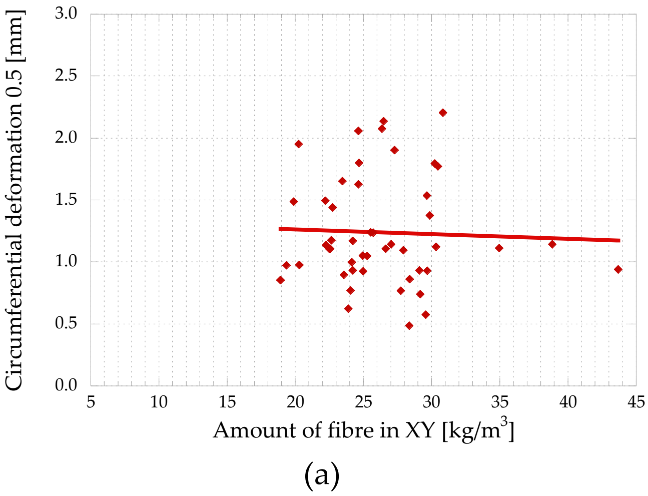

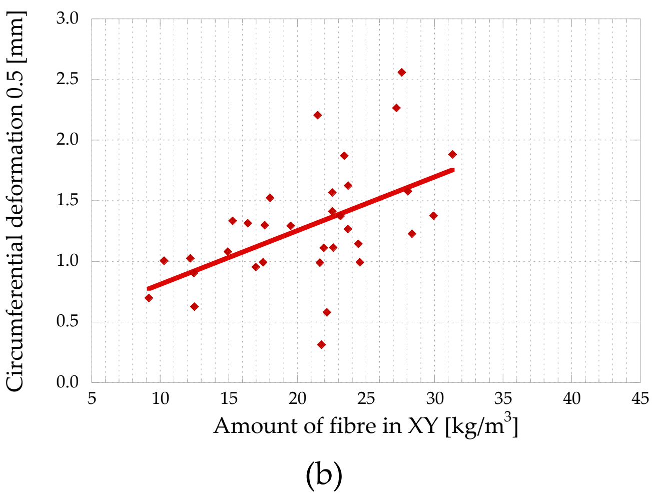

Fig. 18. Correlation between circumferential deformation vs. fibre quantity in XY plane for BV (a) and BH (b).

There is a trend between the number of fibres in the XY plane and the circumferential deformation in the BH. However, in the BV both parameters are not correlated.

Referring to the different parts of the BH, the Fig. 19 represents the quantity of fibres with respect to the circumferential deformation for a crack opening of 0.5 mm.

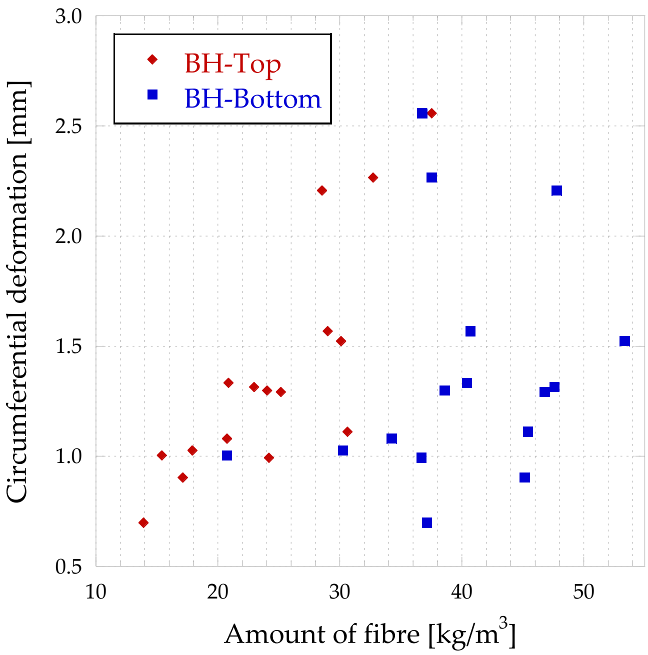

Fig. 19. Correlation between circumferential deformation vs. fibre quantity for BH as function of the height position.

As shown in Fig. 19, the lower part of the slab has a higher number of fibres. Furthermore, it can be seen from the previous figure that it is in this lower part where the greatest deformations are achieved, due to this fact.

2.4. Conclusions

For the specific case study of a reinforced and internal vibrated concrete with a fibre dosage of 35 kg/m^3, the main conclusion drawn from the analysis of the results is that the method of pouring has little influence on the cracking load and a great influence on the behaviour of the cracked concrete, with the following conclusions in particular:

- In horizontal pouring (BH) the preferential fibre direction is in the plane parallel to the bearing face on the ground (A mean of 38.18% of fibres are oriented in XY plane), while in vertical concreting, the preferred orientation is the face perpendicular to the ground. There is an influence of the formwork walls on the orientation of the fibres in the concrete, so that the fibres tend to align with the larger faces.
- The pouring method does not influence the cracking load (Fct), but does influence the residual strengths, which are higher the more fibres are perpendicular to the load (XY plane).
- In a vertical pouring, homogeneity according to the number of fibres distributed in the slab is achieved.
- There is a correlation between circumferential deformations, which is more accurate at high crack opening values.
- In the lower part of the BH there are more fibres than in the upper part (approximately twice the density), which in turn influences the residual strength, which is higher in the lower part.
- The results of the experimental program allow stating that both the BCN and inductive tests are suitable to quantify the amount of fibres within the concrete, their orientation and the post-cracking indirect strength

CAPÍTULO III

Effect of Steel Fibre Reinforcement on Flexural Fatigue Behaviour of Notched Structural Concrete

- **Authors:** Jose A. Sainz-Aja, Laura Gonzalez, Carlos Thomas, Jokin Rico, Juan A. Polanco, Isidro Carrascal and Jesús Setién
- **Published at**: Materials 2021 / Volume 14 / Issue 19
  10.3390/ma14195854
  6 October 2021
- **Impact factor:** 3.748

Abstract: One of the biggest challenges in facilitating the installation of concrete is the development of fibre-reinforced concrete. Although nowadays fibre reinforced concrete is relatively common, it is still necessary to deepen in the study on its behaviour, especially regarding its fatigue behaviour. This paper proposes a new methodology to analyse the bending fatigue behaviour of notched test specimens. From these tests, it was possible to verify that, despite carrying out the tests with load control, the presence of fibres extends the fatigue life of the concrete after cracking. This effect is of great importance since during the extra lifetime with the cracked concrete, the damage to the concrete will be evident and the corresponding maintenance measures can be carried out. Regarding the analysis of the results, in addition to obtaining a traditional S-N curve, two new criteria have been applied, namely energy and notch growth. From these two new approaches, it was possible to determine critical energy values that can be used as predictive indicators of the collapse of the element. Moreover, from the notch growth analysis, it was possible to determine crack growth rate as a function of the stress conditions for the concrete and the specific geometry. From the comparison among the results obtained from the different tests, a limit cracking index of 0.05 mm can be defined.

Keywords: Bending fatigue; fibre-reinforced concrete; S-N curve; Wöhler curve; Concrete damage.

2.1. Introduction

Concrete combined with other materials to create hybrid structures has been shown to have given good results in the behaviour of concrete, like the concrete-filled fibre-reinforced polymer, steel composite tube column or filled glass-fibre-reinforced polymer [53]–[55]. Fibre-reinforced concrete includes short, discrete fibres in its composition, randomly and homogeneously distributed in its mass [56]. This concrete constitutes one of the most relevant innovations in the field of special concretes [57]. The use of fibres has increased in the last 40 years, many types of fibres having been successfully adapted to different concrete applications, due to their ability to improve the capabilities of concrete, increasing its use in certain industries [58]. One of the advantages of the incorporation of fibres is in the control of cracking [8-10], providing a significant increase in the energy absorption capacity of concrete, even doubling it compared to traditional concrete, and preventing fragmentation at breakage, unlike concrete without fibres [59], [60]. In addition, various authors have quantified the improvements that fibres contribute to residual flexural strength [60]–[68]. On the other hand, fibres not only improve the mechanical properties, but they can also contribute to lowering thermal conductivity of concrete too. Several authors have studied this effect, showing that that addition of Polypropylene fibres reduce it for densities lower than 1800 kg/m^3, having the opposite effect with bigger densities [69][70].

There are different types of fibres according to the material used, but the most usual ones are steel fibres. Regarding the different shapes that these fibres can take, numerous studies have recommended hooked-end ones, since the adhesion between the cement matrix and the fibre is improved, compared to straight or corrugated fibres [68], [71].

Although concrete is one of the most commonly used materials in construction, it is not usual to analyse the effect of applying cyclical loading to it. Historically, concrete structures are not commonly subjected to these fatigue loads [72]–[76]. However, due to the great evolution that the construction sector has undergone in recent decades, which enables the optimization of the designs of structures, the exposure of an element to cyclical loads must be taken into account as it is the most critical efforts for the concrete [73]–[75], [77], [78], for example in airports pavements or bridge decks. Currently there are several studies that analyse the effect of fatigue on plain concrete using different methodologies including S-N curves, Staircase or Locati methods among others to analyse the fatigue behaviour under compression or bending fatigue of concrete. There are also studies that analyse the effect of fatigue on more special concretes such as recycled concretes. For reinforced concrete, for example Eurocode 2 [79], the design of the concrete structure for fatigue is mainly based on the design of the steel reinforcements for fatigue. On the other hand, there are just a few studies that analyse the effect of fatigue on other fibre-reinforced concrete.

It has been demonstrated that steel fibres contribute to the improvement in flexural, tensile, impact and fatigue strength of concrete mixtures [61], [64], [80], [81]. Specifically, there is a recognized improvement provided by the incorporation of short-range reinforcements such as steel fibres [82] or polypropylene fibres [83], [84]. The use of this kind of fibres has been shown to improve bending strength by up to between 25% and 50%. Moreover, the increase in the volume of fibres improves the mechanical properties [80] and increases the number of cycles that the concrete resists [85], [86]. The fatigue damage is 1-2 times higher than the damage obtained in a static test in concrete with fibres [87].

Fibres give to the concrete better behaviour under fatigue. It has been verified that the benefit of the addition of fibres to concrete is more pronounced at higher fatigue loading levels and is insignificant at lower levers [87], [88]. The number and the presence of fibres influence the load at which the first cracking appears. It has been demonstrated that the fatigue damage is influenced by the type and dimensions of the fibres [89]. Hooked-end fibres display poorer ductility than corrugated ones and the load after breaking decreases faster with corrugated fibres [81]. Some authors [22], [90] concluded that the predominant mode of failure is by pulling out of the fibres from the concrete matrix, when the contact between matrix and fibre is reduced. Z. Jun at al. [91] have concluded that there is a relation between the fatigue behaviour and the cyclic relation stress-crack width and that an optimum performance of the fatigue can be achieved optimizing the cyclic stress-crack width relationship. D. Caresso et al. have suggested that the reduction of the ductility is due to lower load fatigue levels [22].It has been demonstrated too that there is a critical CMOD point that is larger at higher fatigue loads due to the larger amount of energy accumulated in a short period of time in concrete with fibres [88] and the applied load influences the CMOD development, growing as it is increased [22].

Currently, knowledge about the fatigue process and damage mechanisms that occur in concrete is very scarce and even more so in the case of concrete with fibres, due probably to the time consuming for the fatigue tests. In addition, the relation between the cracking and the energy has not been practically studied and parameters that indicates premature failure and of fibre reinforced concrete are needed. In this paper, a complete characterization is done of notched-concrete specimens with commercial hooked-end fibres HE++90/60 under bending fatigue. During this characterization, consisting of 12 tests, the load evolution, actuator displacement and notch opening were recorded continuously throughout the test. From these data, it was possible to determine the fatigue life of the concrete as a function of the stress range applied. Moreover, two new analysis procedures were applied. From one of them, it was possible to determine an energy threshold after which concrete cracking occurs.

2.2. Materials and methods

2.2.1. Materials

For the manufacture of the concrete, a CEM I 52.5N type cement was used, according to EN 197-1:2011 [41], with a w/c ratio of 0.42. The density of the cement, obtained according to UNE 80103:2013 [42], was 3.12 g/cm^3.

The aggregates used to produce the concrete were limestone gravel (min/max of 4/12 and 10/20 mm) and limestone sand (min/max of 0/2 and 0/4 mm). The aggregates' physical properties can be seen in Tab. 9 and Fig. 20 shows the grading of the aggregates, obtained according to EN 933-1 [43].

Tab. 9. Aggregate physical properties.

Size [mm]	Sand equivalent	Absorption [%]	Density[g/cm^3]
0/2	>75	0.49	2.69
0/4	>80	0.49	2.69
4/12	-	0.54	2.70
10/20	-	0.54	2.68

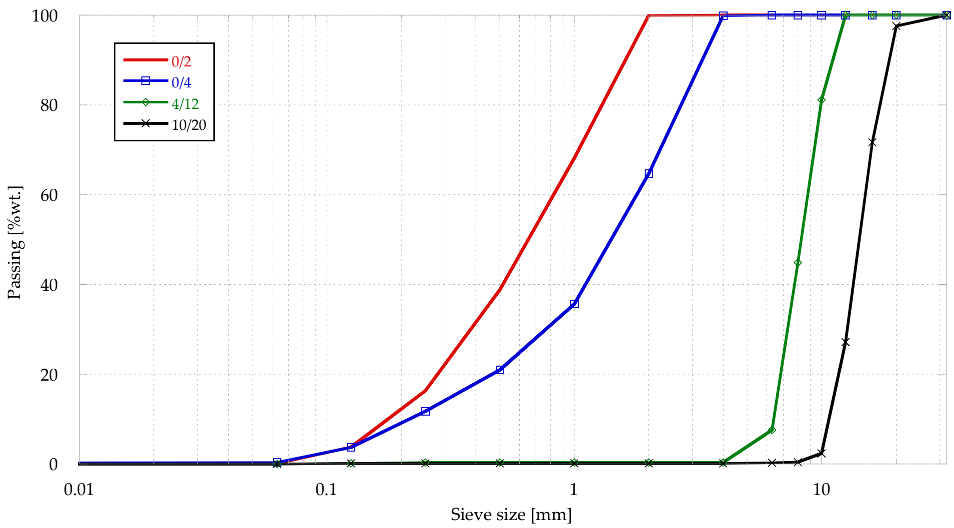

Fig. 20. Grading curve.

The selected steel fibres were hooked-end type, HE 90/60 made by ArcelorMittal, with a length (lf) of 60 mm, a diameter (df) of 0.90 mm and an aspect ratio (λ=lf/df) of 67 and a tensile strength of approximately 1200 N/mm^2.

Fig. 21. Hooked-end steel fibres used.

The concrete mix proportions were obtained by the Fuller method, adding a 0.44% by volume of steel fibres, and are shown in Tab. 10. The w/c ratio was 0.42 and the superplasticizer additive, MasterEase 5025, was 1% wt. of cement.

Tab. 10. Mix proportions.

Material	Mix [kg/m^3]
0/2	480
0/4	480
4/12	480
10/20	480
Cement	390
Water	165
Additive	3.9
Fibres	35

2.2.2. Methods

<u>*Conventional mechanical properties*</u>

Compressive strength was determinate, according to EN 83507:2004 [44]. Three different specimens were tested at 28 days. The specimens were cubic of 150x150x150 mm^3. All the compressive-tested specimens were cured in a humidity chamber under controlled conditions (20 ± 2 °C and 95 ± 5% humidity).

Flexural tensile strength was determined according to UNE-EN 14651:2007 [46]. Three different specimens were tested at 28 days. The specimens were prismatic of 600x150x150 mm³ and they were cured in a humidity chamber like the compressive ones. The Crack Mouth Opening displacement (CMOD) was calculated from the recorded vertical displacement (ρ), according to the standard (Equation 1).

$$CMOD = \frac{\rho - 0.04}{0.85} \qquad \textbf{Equation 2}$$

Fig. 22. Flexural tensile strength test (left) and measurement of vertical displacement with a LVDT (right).

<u>*Fatigue tests*</u>

The fatigue tests were performed at 90 days, using the Staircase method [92], [93]. Twelve specimens of 600x150x150 mm³ were tested. All the fatigue-tested specimens were cured in a humidity chamber under controlled conditions (20 ± 2 °C and 95 ± 5% humidity).

To prepare the specimens for the test, a crack was made, based on the standard EN 14651:2007 [94]. The cracks were cut with a wet disc saw and had a width of 5 mm and a height of 25 ± 2 mm, traversing the width of the specimen, as is shown at Fig. 23.

Fig. 23. Fatigue specimen.

To measure the CMOD a COD extensometer was used. Two metal pieces were fixed to the two sides of the crack, in the centre of it, and an extensometer was fitted, taking the specimens to breakage and recording the Load-COD data.

The specimen was placed on a cylinder of 30 mm diameter, on the opposite side to the cracked face. On the cracked face, two cylinders were place at a 500 mm separation, with the same dimensions as the first one. The test assembly of the specimen can be seen in Fig. 24.

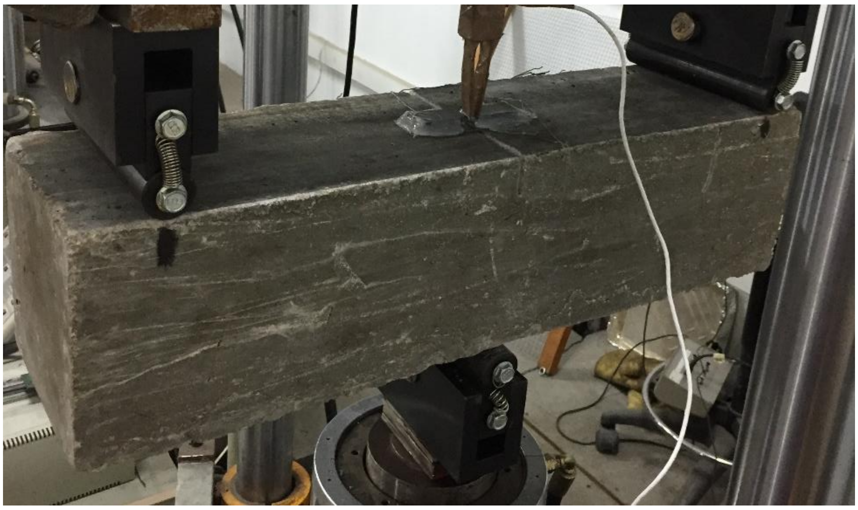

Fig. 24. Fatigue test.

Fatigue testing begins by loading the specimen to the medium load level at a speed of 0.5 MPa/s. When this mean load value has been reached, sinusoidal loads are applied between the maximum and minimum load values indicated in σ=stress; F=load applied; L= distance between the two lower cylinders; b= specimen width; h= distance from the base to the beginning of the notch.

at a frequency of 15 Hz. Different load scenarios were used to analyse the fatigue behaviour of fibre-reinforced concrete. The minimum load applied in all the tests was 2 kN and the maximum was varied to compare different states. In this **Tab. 11** the values of stress range (Δσ) and stress ratio (R) for each test are also indicated. The stress range corresponding to the applied load were obtained using Equation 3 taken from EN-14651 which considers the geometry of each of the specimens.

$$\sigma = \frac{3 * F * L}{2 * b * h^2}$$ **Equation 3**

σ=stress; F=load applied; L= distance between the two lower cylinders; b= specimen width; h= distance from the base to the beginning of the notch.

Tab. 11. Test parameters.

Specimen	Fmin [kN]	Fmax [kN]	R	b [mm]	h [mm]	Δσ [MPa]
F-01	2	8	0.25	153.6	124.8	1.881
F-02	2	9	0.22	154.6	126.2	2.132
F-03	2	8	0.25	153.0	127.6	1.806
F-04	2	9	0.22	156.4	123.0	2.219
F-05	2	10	0.20	162.0	124.0	2.109
F-06	2	15	0.13	159.0	130.0	3.628
F-07	2	8.5	0.24	163.5	125.8	1.884
F-08	2	11	0.18	157.0	125.0	2.752
F-09	2	10	0.20	160.0	123.0	2.479
F-10	2	9.5	0.21	157.0	126.0	2.257
F-11	2	9.8	0.20	153.0	125.0	2.447
F-12	2	12	0.17	160.0	124.0	3.049

During all the fatigue tests, the testing time, load, actuator displacement (ACT) and COD aperture of two cycles of every 100 were registered during the whole test. To analyse these data, and due to the waveform, a regression to a sinusoidal wave was done by mean of a one degree Fourier regression, see Equation 4, which was transformed into Equation 5 by means of Equation 6 [95]. This one-degree Fourier regression was applied using Matlab software [96]. In Fig. 25 an example of the comparison of the raw data and the regression can be seen. After this regression, the time variation of all the parameters which define a sinusoidal wave could be analysed, such as mean value or amplitude.

$$y(t) = a_0 + a_1 * \cos(w * t) + b_1 * \sin(w * t) \qquad \textbf{Equation 4}$$

$$y_t = y_0 + A * sen(w * t + \varphi_0) \qquad \textbf{Equation 5}$$

$$y_0 = a_0 \;\; ; \;\; A = \sqrt{a_1^2 + b_1^2} \;\; ; \;\; \varphi_0 = \arctan\left(\frac{a_1}{b_1}\right) \qquad \textbf{Equation 6}$$

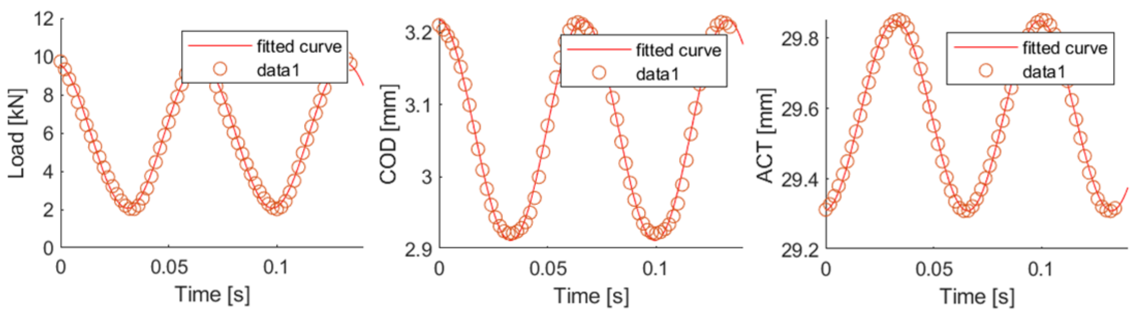

Fig. 25. Data fitting.

In addition to analysing the effect of the cycle concatenation on the mean value and amplitude, the effect on the area of the loop generated by drawing the COD opening versus the load was also analysed. Two different types of area were analysed, on the one hand, the area representing the energy provided Fig. 26 (a) and, on the other, the stored energy Fig. 26 (b).

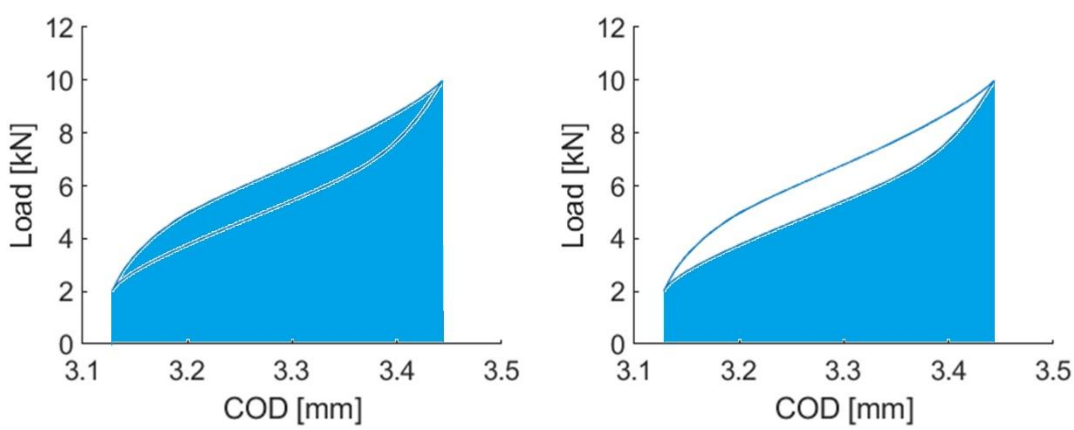

(a) **(b)**

Fig. 26. Determining the energy provided (a) and stored (b).

The total energy (stored+dissipated) represents the energy provided to the system to produce the deflection of the specimen. This total energy is divided into two types of energy, stored energy, and dissipated energy. The dissipated energy is the energy released by the specimen during the cycle. On the other hand, the stored energy is the energy that the material return/restore cycle by cycle.

During the analysis of the data, it was found that in all cases there were two clearly differentiated behavioural zones, before and after the cracking of the concrete. Fig. 27 shows the evolution of each of the parameters analysed throughout the test. The applied load wave is constant throughout the test, before and after the cracking. This is because the test is performed under load control. In the case of the evolution of the ACT and the COD, it is possible to clearly identify the moment of concrete cracking. From that point onwards, it can be seen how the values of both parameters begin to evolve rapidly, especially in the case of COD. In the case of the evolution of the curve load Vs. COD, the moment of the cracking can also be easily appreciated. From the cracking onward the area begins to grow rapidly and the curve slopes to the right. Once the results of the different tests were compared, it was concluded that until the cracking of the concrete the results were quite homogenous but, when the concrete cracks and the fibres are responsible for the specimen behaviour, the results become heterogeneous due to the random distribution of the fibres [52] and because fatigue is a phenomenon that focuses on a specific point of the sample, the crack. For this reason, the analysis was focused on the behaviour before cracking.

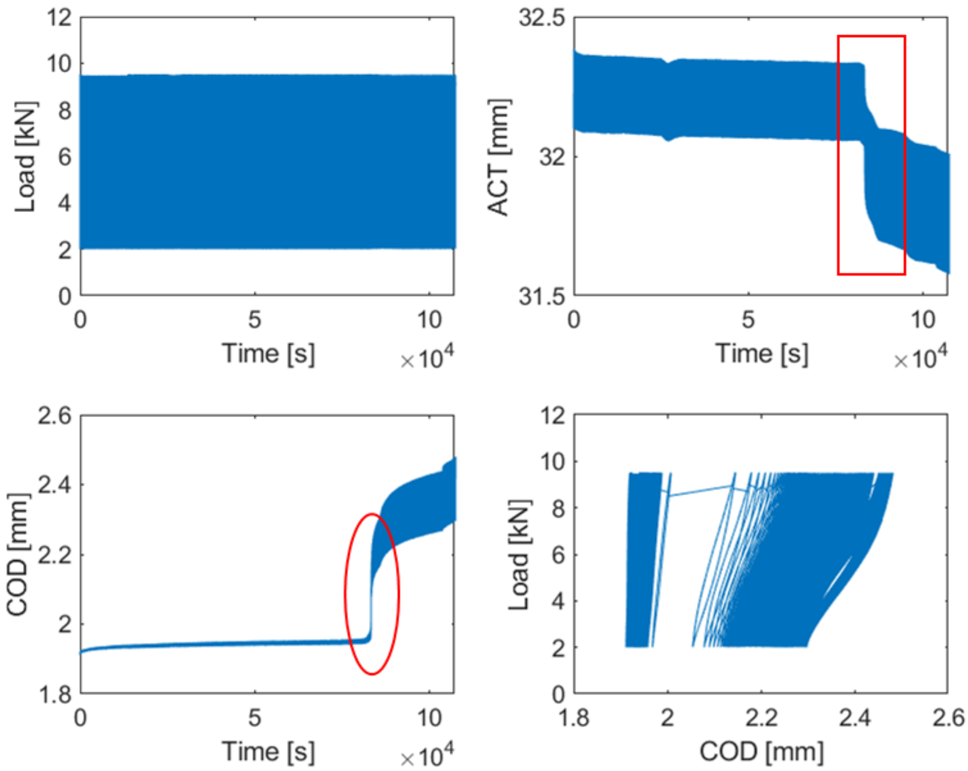

Fig. 27. Identification of two clearly differentiated phases within the test, before and after cracking (figure corresponding to test 10).

Another additional parameter was analysed during the fatigue tests, the COD opening velocity. This velocity was obtained as the derivative of the COD opening as a function of time. This curve has a U shape, see Fig. 28, since the initial part and the final part are phenomena of the beginning of the test or near to the crack. To compare the effect of the stress range of the test on the growth velocity of the COD opening, a value in the central zone of the stationary part was averaged, see Fig. 28.

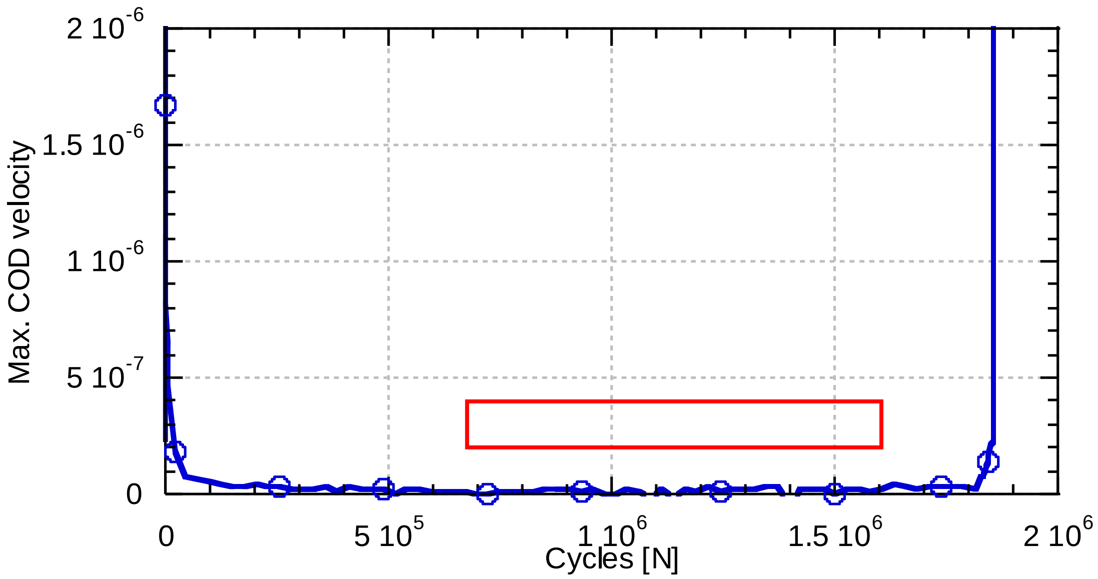

Fig. 28. Evolution of the velocity of the parameters analysed (example corresponding to test 2).

2.3. Results and discussion

2.3.1. Mechanical properties

The average compressive strength at 28 days is 50 MPa. In **Tab. 12**, the results of the compressive strength test in the 3 specimens can be seen.

Tab. 12. Compressive strength results at 28 days.

Specimen code	Compressive strength [MPa]
Specimen C1	53.80
Specimen C2	51.28
Specimen C3	46.48

Tab. 13 shows the residual flexural strength for the 2.5 mm crack opening ($f_{R,3}$, COD=2.5 mm). The average of these values is $f_{R,3}$=6.27 MPa. In Fig. 29 a compressive and a flexural specimen can be seen.

Tab. 13. Flexural tensile strength results at 28 days.

Specimen code	$f_{R,3}$ [MPa]
Specimen F1	5.80
Specimen F2	6.83
Specimen F3	6.17

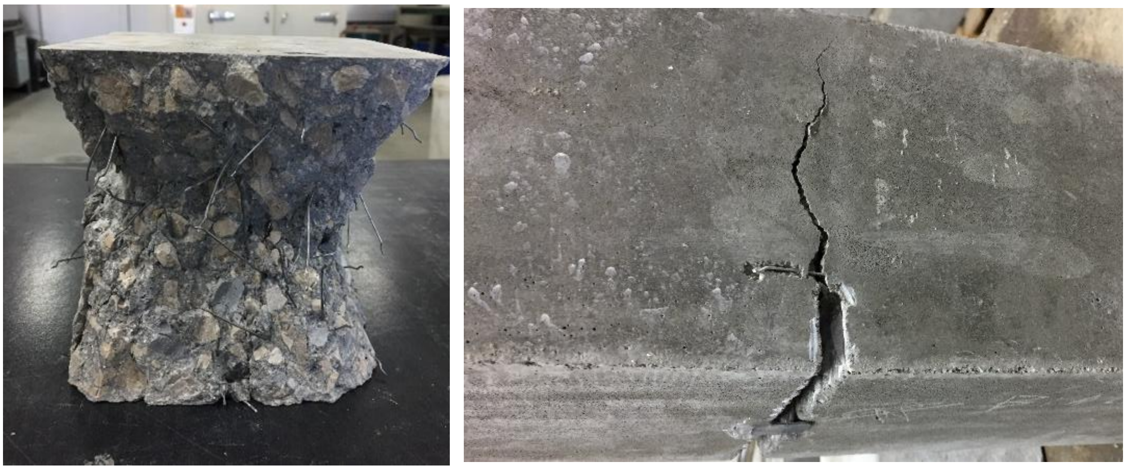

(a) (b)

Fig. 29. Specimens after compressive test (a) and flexural test (b).

2.3.2. S-N curve

Fig. 30 shows the number of cycles to either cracking (red circles) or breakage (blue squares) depending on the stress range of the test.

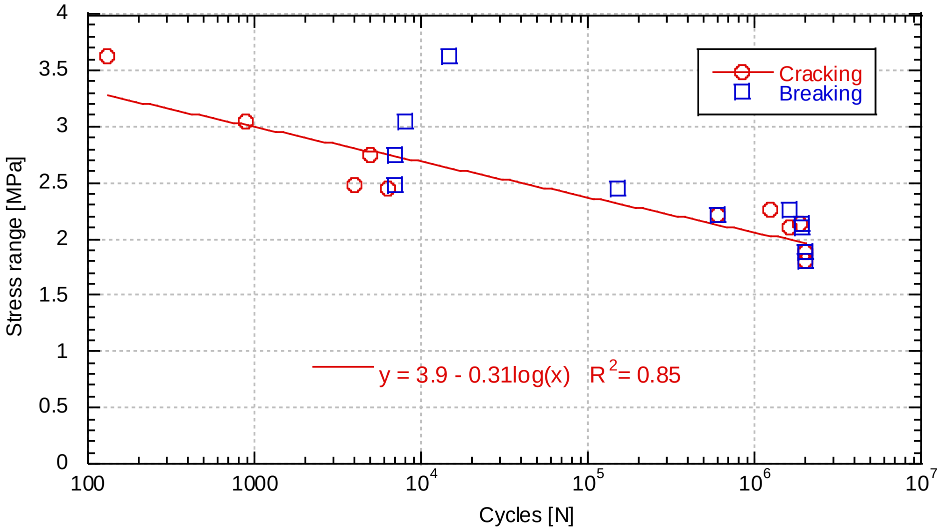

Fig. 30. S-N curve.

The cycles to cracking of the specimens fit very well with an S-N curve. On the other hand, the number of cycles until specimen breakage does not fit so well. This is because, after cracking of the concrete, the fibres are the ones that manage the fatigue process. For this reason, the orientation and number of fibres holding the crack will define the behaviour of the concrete. This result is in agreement with the results obtained by Jose Rios and Héctor Cifuentes [97], who concluded that the presence of fibres increased the scatter of the results during the flexural fatigue of fibre-reinforced concretes. Fig. 31 shows examples of cracking during the fatigue tests.

Fig. 31. Cracking of concrete in the fatigue test.

The fatigue life after cracking is very variable and does not seem to follow a clear trend. In all cases where component failure is reached, the presence of fibres has increased the life of the component to some extent. This does not have to happen because it is a concrete with fibres, since, the tests generally done on concrete with fibres are carried out under machine displacement control, while in this case they were done under load control.

The additional cycles provided by the presence of fibres, although generally not many, make the difference between having a fragile break. A fragile break means no apparent signs that the break will occur and having clear signals that the break is nearby. This, in a real situation, will enable measures to be taken after breakage becomes evident.

2.3.3. Crack opening during the fatigue tests

Fig. 32 shows the parameters recorded during the test, specifically a sample of the results of test 9. Fig. 32 (a) shows the appearance of these parameters at the beginning of the test, while Fig. 32 (b) shows the appearance of these parameters at the end of the test. The load values remain constant, which is because these tests were carried out under load control. About the displacement of the ACT, it increased from a displacement of 0.3 mm to 0.6 mm. The opening of the COD is the parameter whose behaviour varies most. At the beginning of the test the crack barely opened 8 microns, while in the final part of the test, with the specimen already cracked, the crack opened more than 0.3 mm.

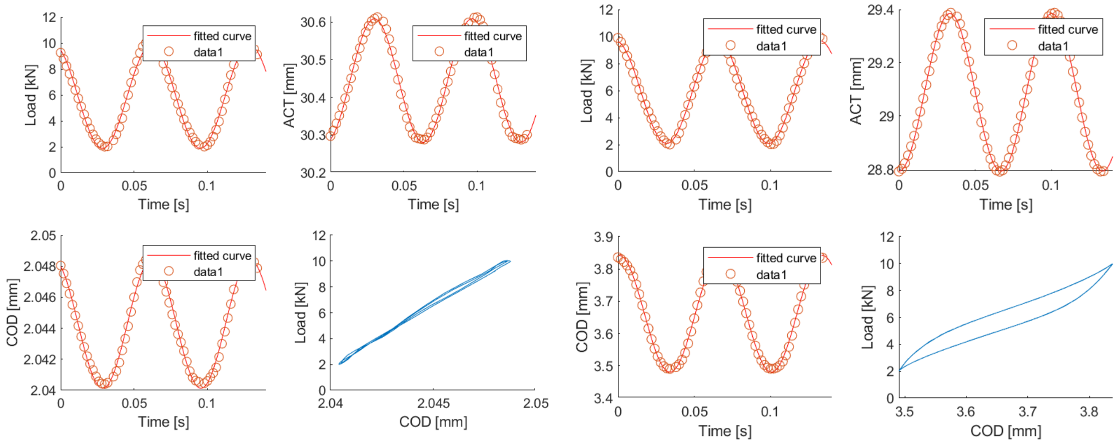

(a) (b)

Fig. 32. Comparison of the specimen response during the fatigue test.

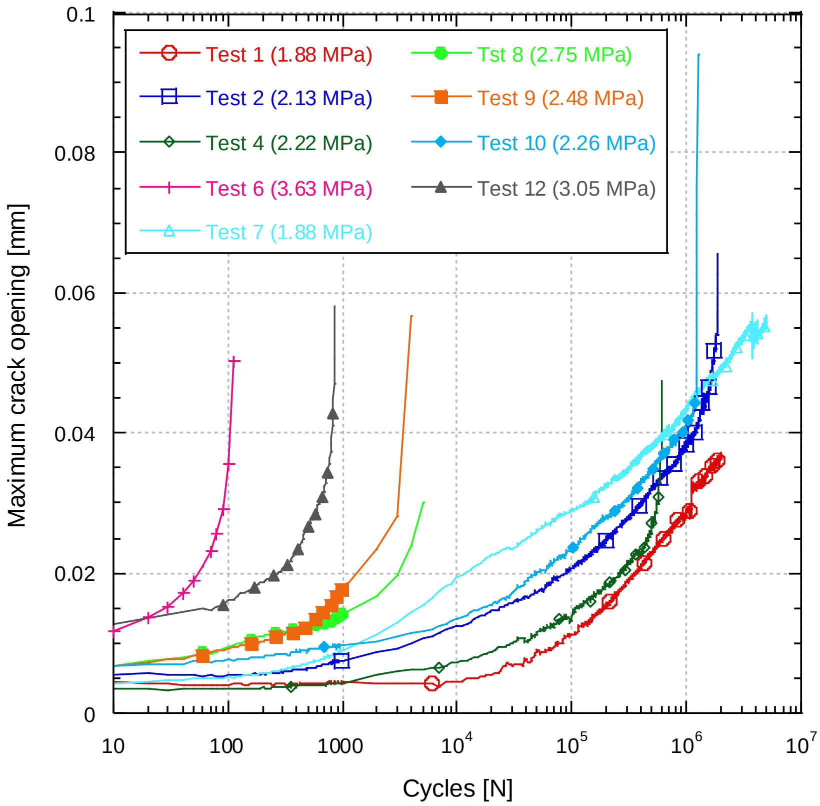

Fig. 33. Evolution of the crack maximum opening as a function of the number of cycles.

Fig. 33 shows the evolution of the maximal crack opening during the fatigue tests. Fig. 33 shows different curves, representing different test specimens with different stress range values. These curves all have a similar shape. They are initially approximately linear and stable but then in all cases increase approximately exponentially. It can also be seen that the higher the stress ratio applied during the fatigue test, the higher the curves are and the further to the left. This means that the larger the crack opening, the shorter the duration of the test. From the comparison among the results obtained from the different tests, a limit cracking index of 0.05 mm can be defined. From this observation it could be assumed that when the crack opening increases beyond this value of 0.05 mm, concrete cracking occurs.

As the specimen is subjected to a fatigue test based on the application of sinusoidal loads, the specimen is simultaneously subjected to two types of load. On the one hand, a constant load equivalent to the average value of the wave applied and, on the other hand, a sinusoidal load ranging from a maximum load *F* to a minimum of -*F*. Each of these two loads will have a different impact on the damage caused to the concrete. The constant applied load will accumulate creep damage, while in the case of cyclic loading, it will accumulate fatigue damage. Fig. 34 analyses each of these effects separately. Fig. 34 (a) shows the evolution of the average crack opening value over the course of the test. Fig. 34 (b) shows the evolution of the crack opening amplitude as a function of the number of cycles.

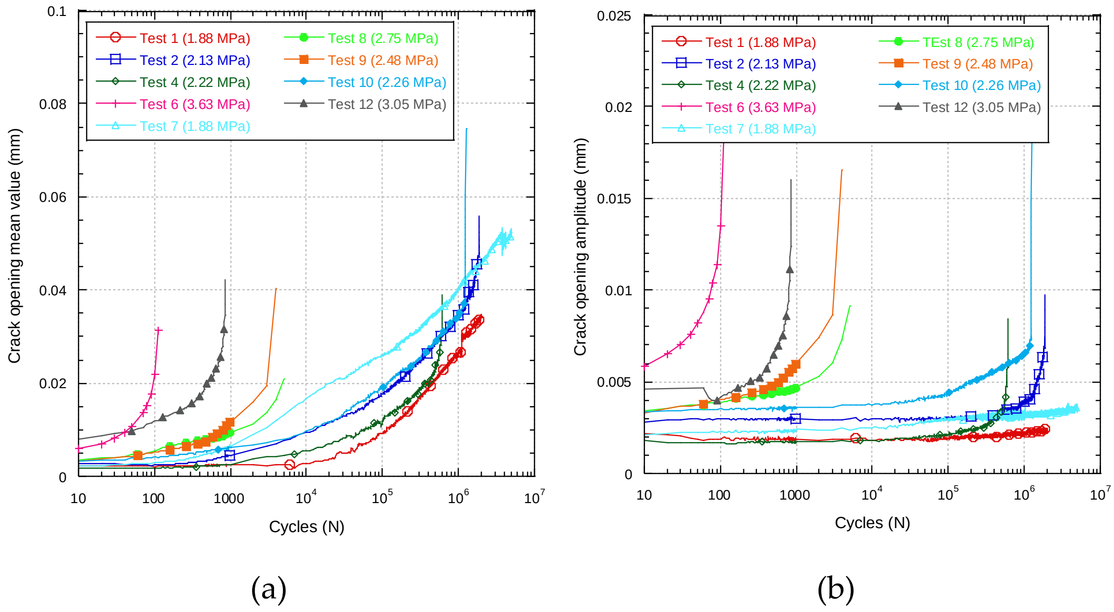

Fig. 34. Evolution of the mean crack opening value (a) and amplitude (b) as a function of the number of cycles.

It can be seen that Fig. 34 (a) has a very similar shape to Fig. 33, while in the case of Fig. 34 (b), an appreciable difference can be observed in the shape of the curves. In the case of the evolution of the mean value, an evolution can be seen from the first cycles in practically all cases. In the case of the amplitude, this is a much more stable parameter which is practically only appreciable in the last cycles before cracking occurs. From these results, it can be assumed that in tests where the load values are sufficiently low, the damage is predominantly creep damage, until a limit is reached that allows fatigue damage to begin to increase.

Fig. 35 shows the opening velocity of COD in the stationary section as a function of the stress range. It should be remembered that the cases were analysed only before the concrete cracking occurred. For this reason, for example Test 6 could not be included since the cracking occurs so early that a stationary crack growth rate is not reached before cracking.

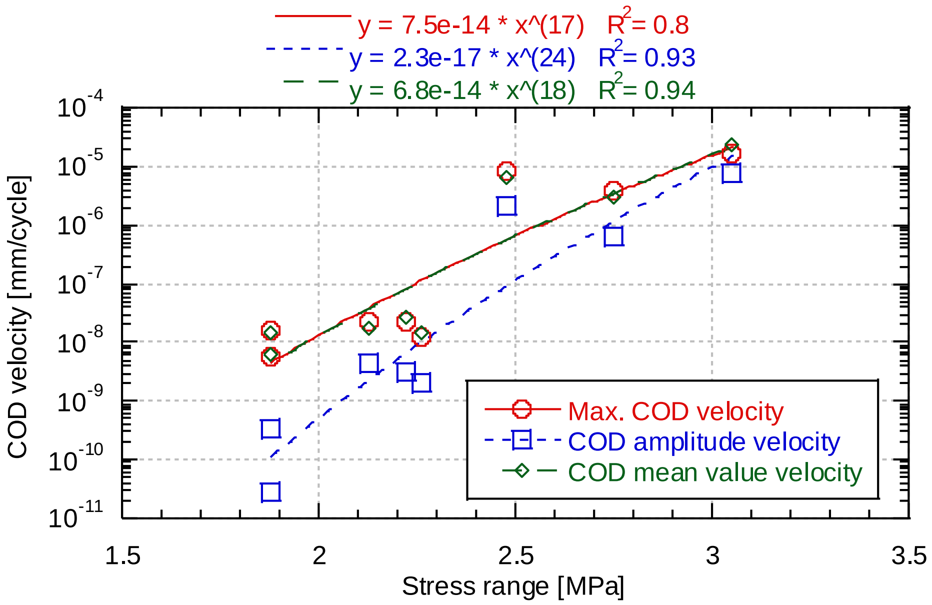

Fig. 35. COD velocity as a function of the test stress range.

Increasing the stress range value increases the growth rate of the maximum opening value, the average value, and the amplitude. Based on the analysis of the evolution of the growth of the notches throughout the test, it could be deduced that, in the case that the stress range is small, the evolution of the opening is practically that of the medium level. In the case of a test with high tensional range values, the values of crack opening amplitude and the mean value of it can become similar.

2.3.4. Energy evolution during the fatigue tests

Fig. 36 shows the evolution of the provided and stored energy during each fatigue test.

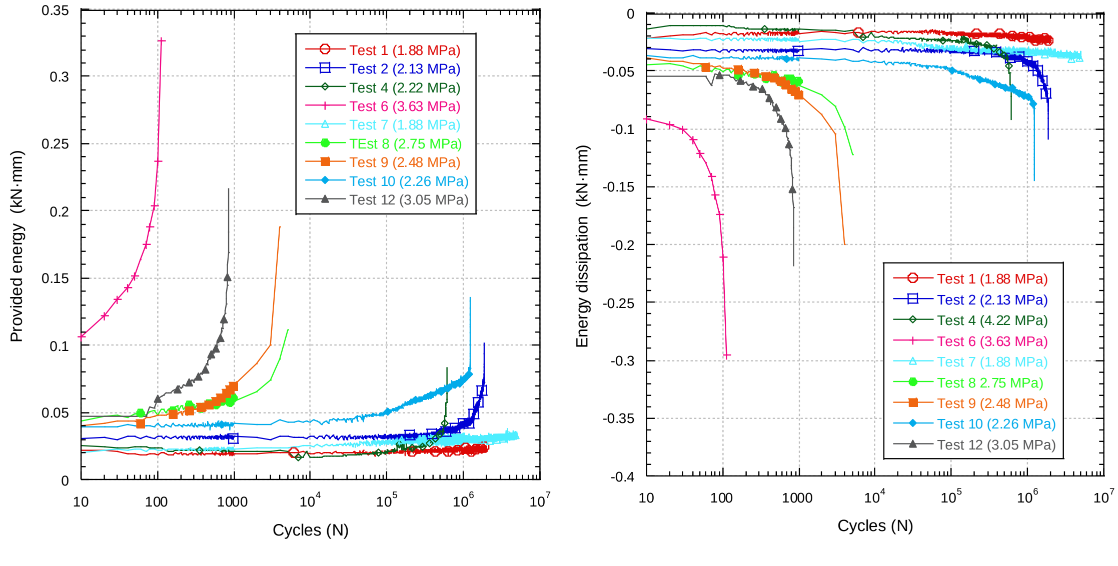

Fig. 36. Evolution of the provided (a) and stored (b) energy during the fatigue test.

In Fig. 36, for higher stress values greater energy is required to apply the load and greater energy is stored by the sample.

Fig. 37 shows the growth rate of the energy supplied in the stationary zone as a function of the stress range of the test.

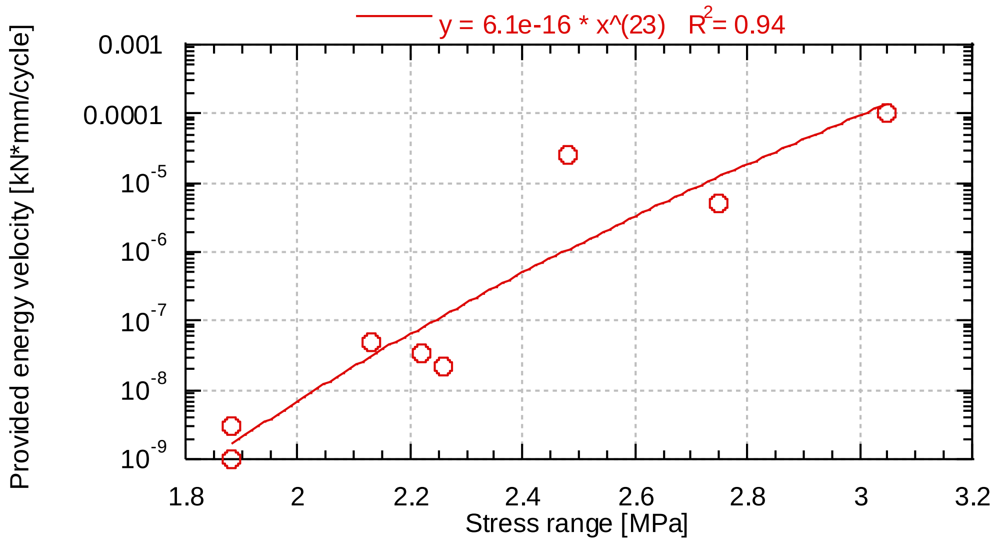

Fig. 37. Provided energy velocity as a function of the test stress range.

From Fig. 37, there is a relationship between the velocity of provision of energy of provided energy and the stress range of the test. In addition, as previously indicated, there is a critical energy value that indicates that the test specimen will break, so it could be used as a parameter to determine the remaining life of the concrete. However, it should be noted that since it is an energy parameter, it is specific to each geometry.

2.4. Conclusions

The following conclusions can be drawn from the work:

- An S-N curve of the material was obtained before it was cracked. Once the concrete has cracked, the quantity and orientation of the fibres is so important in the response of the concrete to cyclic loads that it leads to extremely heterogeneous behaviour.
- The presence of fibres was proven to increases the fatigue life of concrete, even in tests carried out under load control. This provides a time between the concrete breakage and the structural breakage, which can be used to take appropriate corrective measures.
- A critical crack opening was detected after which concrete cracking occurs, which could be used as an indicator the premature failure of the specimen.
- A critical energy value was observed that indicates that the test specimen will break, so it could be used as a parameter to determine the remaining life of the concrete. However, it should be noted that since it is an energy parameter, it is specific to each geometry.
- It was verified that the mechanism producing failure of the concrete is caused by microcracks inherent to concrete in the notch beginning to grow due to the loads applied. The velocity of growth of the cracks depends on the range of stress applied in the test, a correlation existing between them. However, geometry probably also has an influence.

There are not many research on the fatigue behaviour of fibre reinforced. However, the importance that this material may have soon, thanks to its better performance and savings in execution, necessary to investigate on it. Hence the importance of the results presented and the obtained results, opening the door to a new type of analysis regarding behaviour of concrete under bending fatigue. Although it is important to emphasize that this study has to be complemented with future studies in which not only different specimen geometries are analysed, but also different notch sizes.

CAPÍTULO IV

Effect of Fibre Reinforcement on Creep in Early Age Concrete

- **Authors:** Laura González, Jose A. Sainz-Aja, Álvaro Gaute, Jokin Rico, Carlos Thomas
- **Published at**: Applied sciences 2022 / Volume 12 / Issue 1
  10.3390/app12010257
  28 December 2021
- **Impact factor:** 2.838

Abstract: This research analyses the strain behaviour of fibre-reinforced concrete (FRC) in the event of a creep episode. The analysis of creep experienced by FRC specimens during the test reflects better performance than that predicted by the EHE-08 standard. The authors propose a formulation for the evaluation of creep strain undergone by FRC. During the research, the evolution of the modulus of elasticity of FRC after a creep episode is analysed. After the test campaign, it can be concluded that FRC loaded at an earlier age stiffens after a creep episode. After the creep test is completed, the delayed elastic strain undergone by FRC is analysed and it is observed that FRC loaded at an earlier age undergoes less deformation. The authors propose a formulation for the evaluation of the delayed elastic strain undergone by FRC after a creep episode.

Keywords: Fibre-reinforced concrete; steel fibres; creep strain; delayed elastic strain.

3.1. Introduction

Fibre-reinforced concrete (FRC) is being used more and more in structural applications due to the benefits it provides [4]. The addition of fibres to concrete improves the endurance limit, flexural strength, Young's modulus and the compressive strength. These improvements depend on the characteristics of the fibres, their material, and their dimensions. In addition, fibres or microfibres provide concrete with better behaviour after cracking [17], [80], [98]–[101].

The study of creep undergone by structural concretes has a great influence on the design of large structures, as well as on the definition of their construction process. Creep undergone by concrete at early ages influences the design of evolutionary construction processes such as the construction of bridge decks using the successive cantilever technique [102], while the study of creep at infinite time influences the analysis of the countershafts used in the construction of boards with large spans [103]–[105].

Some authors have studied the influence of fibres on creep in concrete, finding that fibres have a positive influence, as they improve creep behaviour compared with plain concrete [16], [104]–[106]. Steel fibres are especially efficient for creep deformation, compared to other types of fibres [4]. J. Blyszko [16] compared the influence of polypropylene fibres, time of load and applied load in creep measurement, reporting that the use of fibres improves creep behaviour of concrete loaded at early-ages, finding that Young's Modulus increases at the age of 24 h and that its influence in later stages is insignificant. He also found differences between the creep calculated based on the Code and the measured creep. Qingxin Zhao et al. [107] concluded that it is possible to predict the creep behaviour of FRC by comparing its elasticity modulus at 28 days with that of plain concrete. That is, the modulus of FRC at 28 days is inversely proportional to its long-term specific creep. They also concluded that fibres with elastic modulus lower than concrete can increase creep and the addition of steel fibres at less than 2% can reduce creep. In addition, it was shown that temperature influences creep in concrete; the higher the temperature, the greater the creep displacement [108].

Several authors have formulated different models for prediction of creep in non-reinforced concrete [109]–[112]. In addition, different models can be found in the literature, including the AASHTO (American Association of State Highway and Transportation Officials) model [113], the ACI (American Concrete Institute) model [114] or the EHE-08 model [115]. However, despite great progress in studying the short-term properties of fibre-reinforced concrete, research on the creep behaviour of FRC has not kept up [4].

In this paper, the influence of loading age of the specimens on creep evolution at early age and long-term was analysed using a reinforced concrete with hooked-end steel fibres. In addition, after performing creep analysis, the instantaneous and delayed deformation was measured. With the results obtained, the authors proposed a formulation for the calculation of the creep evolution and for the delayed elastic strain, depending on loading age. The characterization of this reinforced concrete is a continuation of another study performed by some of the authors [17].

3.2. Materials and methods

3.2.1. Materials

Four different fractions of limestone aggregates, two fine aggregates (0/2 mm and 0/4 mm), coded FA0-2 and FA0-4 respectively, and two coarse aggregates (10/20 mm and 4/12 mm), coded CA4-12 and CA10-20 respectively, were selected to manufacture the concrete. Physical properties and grading of these aggregates, obtained according to EN 933-1 [116], are shown in Tab. 14 and Fig. 38 respectively. Cement CEM I 52.5N type was used, according to EN 197-1:2011 [41], with a density of 3120 kg/m^3, obtained according to UNE 80103:2013 [42]. The quantity of cement used was 390 kg/m^3 and its composition can be seen in Tab. 15. A superplasticizer additive, Master Ease 5025, was added, in the proportion of 1% wt. of cement.

Tab. 14. Physical properties of the limestone aggregates.

Fraction of aggregate	Absorption [wt.%]	Density [kg/m^3]	Sand equivalent
FA0-2	0.49	2690	>75
FA0-4	0.49	2690	>80
CA4-12	0.54	2700	-
CA10-20	0.54	2680	-

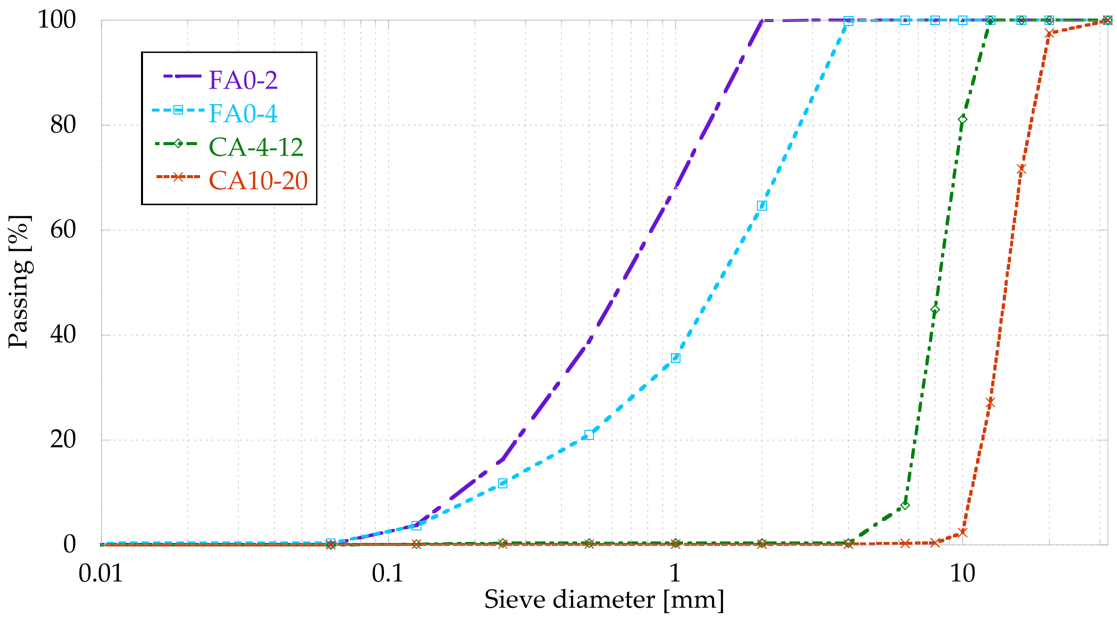

Fig. 38. Grading curve of the aggregates used.

Tab. 15. Chemical composition of the cement used.

	Fe_2O_3	CaO	SiO_2	Al_2O_3	MgO	TiO_2	SO_3	K_2O	Others
Compound [wt.%]	3.38	66.60	17.81	4.79	1.30	0.20	4.49	0.78	<0.5

A quantity of 35 kg/m³ of the selected Hooked-end steel fibres was added, with a tensile strength of 1200 MPa, a length of 60 mm and a diameter of 0.9 mm (Fig. 39). The concrete mix proportions obtained according to the Fuller method are shown in Tab. 16.

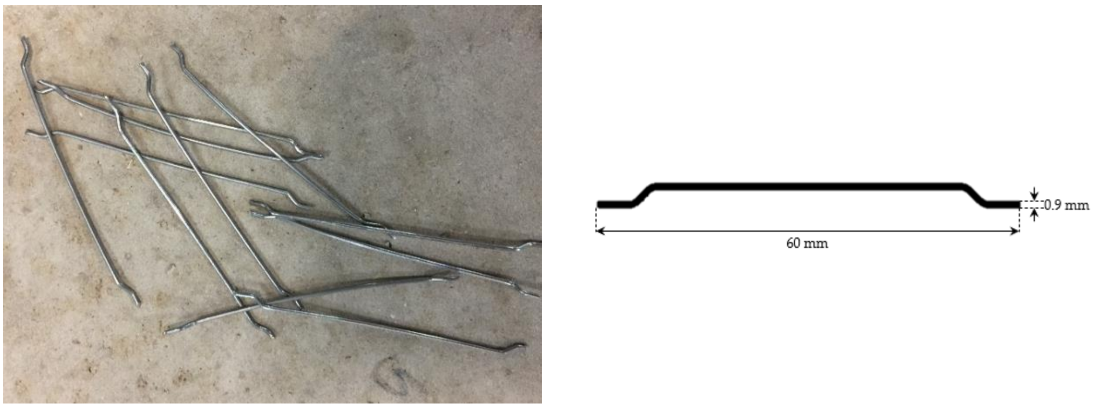

(**a**) (**b**)

Fig. 39. Hooked-end fibres used. (a) photograph; (b) schematic diagram.

Tab. 16. Concrete mix proportions.

Material	**Mix [kg/m^3]**
FA0-2	480
FA0-4	480
CA4-12	480
CA10-20	480
Cement	390
Water	165
Additive Master Ease 5025	3.9 (1% wt. cement)
Fibres	35
w/c	0.45

3.2.2. Methods

Compressive strength

EN 83507:2004 [44] was followed to determine the compressive strength at 24h, 3, 7 and 28 days. The tested specimens were cubic of 150x150x150 mm^3, cured in a humidity chamber under controlled conditions (20 ± 2 °C and 95 ± 5% humidity).

Creep test

The specimens manufactured for this test were cylinders with a diameter of 15 cm and a height of 30 cm. Until the time of the test, the specimens were cured in a humidity chamber under controlled conditions (20 ± 2 °C and 95 ± 5% humidity). To determine the creep deformation of the concrete, three strain gauges were installed on each specimen to measure the deformation due to applied load.

For the loading of the specimens, the authors designed a loading gantry that enabled the analysis of the evolution of creep deformation of several specimens simultaneously. In this investigation, four concrete specimens with fibres were loaded in each load frame. These frames were composed of 2 reaction beams, 4 Dywidag bars that perform the loading of the specimens, and a spherical hinge that enabled the specimen to be axially loaded, avoiding the introduction of bending stresses, as shown in the Fig. 40.

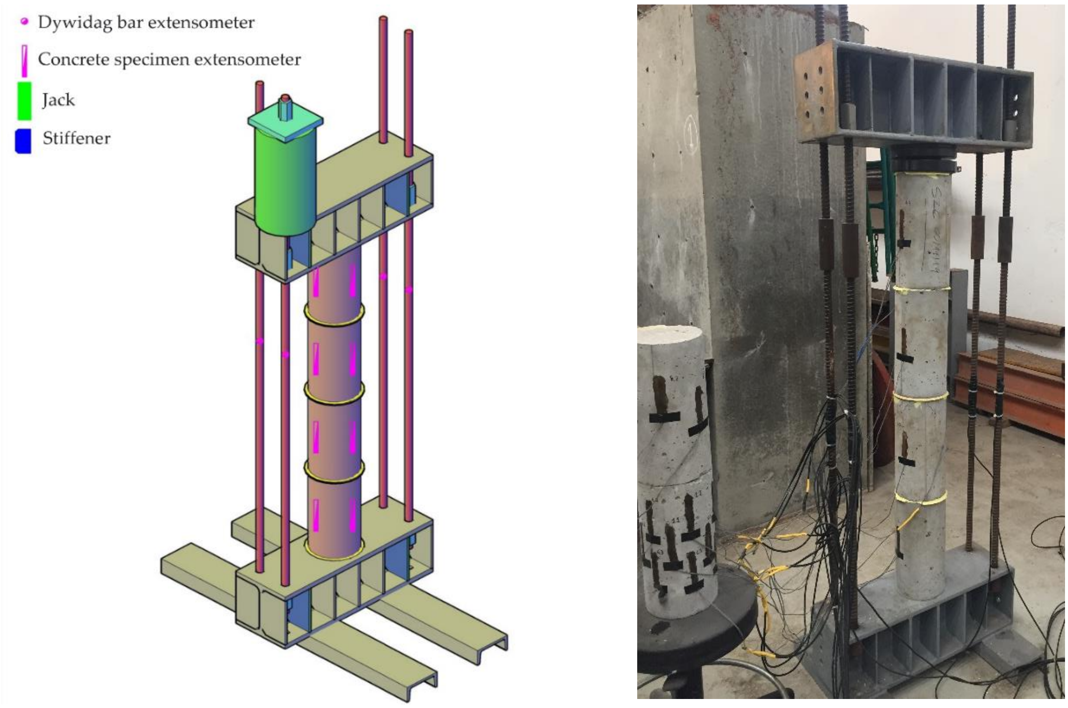

(**a**) (**b**)

Fig. 40. Test gantry configuration. (a) schematic drawing; (b) photograph.

The Dywidag bars load the specimens, which are tensed using a 60-ton hollow jack in 4 load steps, corresponding to 25, 50, 75 and 100% of the stressing strength. To control the stress in the Dywidag bars, it was decided to fit these structural elements by installing 2 bidirectional extensometers per bar, connected to each other by means of an electronic assembly in a complete Wheatstone bridge [117]. The deformation experienced by the fibre-reinforced concrete specimens is experimentally measured by installing 3 unidirectional strain gauges in 3 generatrices at 120º in each specimen. These bands are individually connected with control strain gauges that enable compensation for thermal effects during the test. The connection of the bands is made by means of an electronic mounting in a half Wheatstone bridge [117].

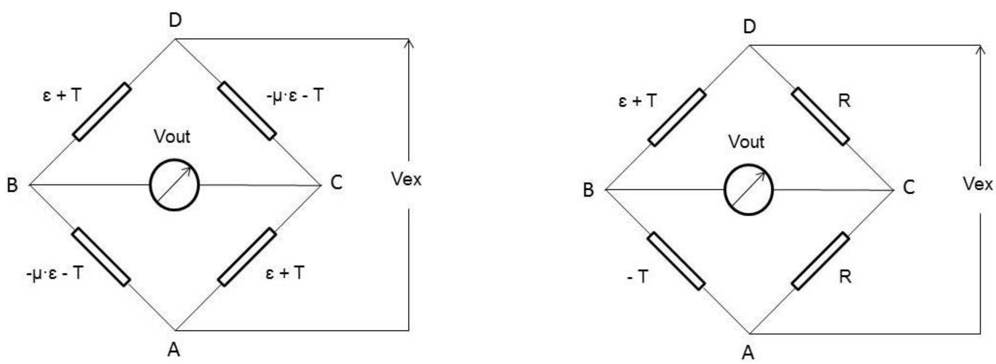

(**a**) (**b**)

Fig. 41. Electronic assembly of sensors: (a) full Wheatstone bridge; (b) half Wheatstone bridge.

In order to analyse the creep evolution of the concrete specimens with fibres and obtain the creep curves associated with this type of concrete at different loading ages, the specimens were divided into 4 groups and each group tested at 4 different loading ages. The loading configuration for each specimen is shown in Tab. 17. The need to submit specimens of different ages, 24h and 3d, and 7d and 28d, to the same load, arises from the availability of only two loading frames. In one of the loading frames, the analysis of the creep undergone by the specimens loaded at 24h and 3d is carried out, and in the other the specimens loaded at 3d and 28d. Young specimens (loaded at 1 and 3 days) were loaded at 265 kN (around 80% of the compressive strength at 24h and 40% at 3d), while the others (loaded at 7 and 28 days) were loaded at 353 kN (around 50% of the compressive strength at these ages). In the case of 24 h and 3d age specimens, the load was chosen to be sufficiently representative at 3d, but to be able to be supported by 24h age specimens. In the case of 7 and 28 d age specimens, a load of 50% of its compressive strength was considered adequate to see a significant evolution in the concrete.

Tab. 17. Configuration of test load.

Specimen code	Group	Loading age [d]	Test load [kN]	Test stress [MPa]
CF-1	1	1	265	15
CF-2	1	1	265	15
CF-3	2	3	265	15
CF-4	2	3	265	15
CF-5	3	7	353	20
CF-6	3	7	353	20
CF-7	4	28	353	20
CF-8	4	28	353	20

Modulus of elasticity

During the loading and unloading of the specimens arranged on each load frame, the following physical magnitudes were monitored: (a) the stress applied by tensioning the diwydag bars (b) the deformation experienced by the fibre-reinforced concrete specimens. The stress/strain curve of the specimens obtained during their loading and unloading made it possible to obtain the initial and residual modulus of elasticity of FRC for the different ages of loading analysed.

Delayed elastic strain

Once the creep test was completed and the load applied to the FRC specimens removed, the evolution over time of the strain undergone by the specimens is monitored. This monitoring makes it possible to evaluate the delayed elastic strain undergone by the specimens after the creep test.

Microscopic analysis

Microscopic images using a Scanning Electron Microscope (SEM) were obtained of the concrete with fibres used for this study.

Although the scanning electron microscope was used to obtain images at high magnifications of almost all materials, it could also be used in combination with an energy dispersive spectrometer (EDX), which also allows us to know the elements present in specific sections of a sample. For this, a Carl Zeiss EVO MA15 SEM was used, fitted with an Oxford Instruments X-ray detector.

3.3. Results and discussion

3.3.1. Compressive strength

As starting data for the analysis of the creep undergone by the fibre-reinforced concrete specimens, the compressive strength of the concrete was obtained at the different loading ages. Fig. 5 shows the evolution curve of the compressive strength of FRC over time.

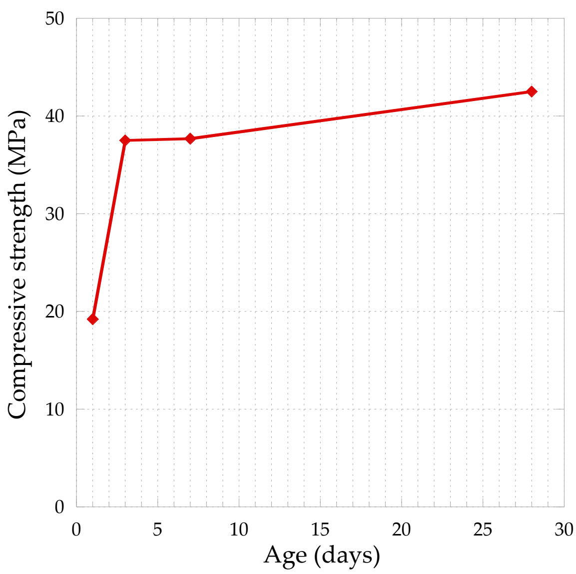

Fig. 42. Evolution of the compressive strength of FRC.

Between 3 and 28 days of age of the FRC, it is observed that there is no significant difference, with the greatest evolution occurring in the first 72 h of age.

3.3.2. *Creep test*

Fig. 43 shows the evolution of creep deformation over time, differentiating between specimens that were subjected to a load of 15MPa (24h and 3d of age) and those that were subjected to a load of 20MPa (7d and 28d of age). In the following figures, the joint results of each age rage are shown as the average evolution experienced by the two test specimens.

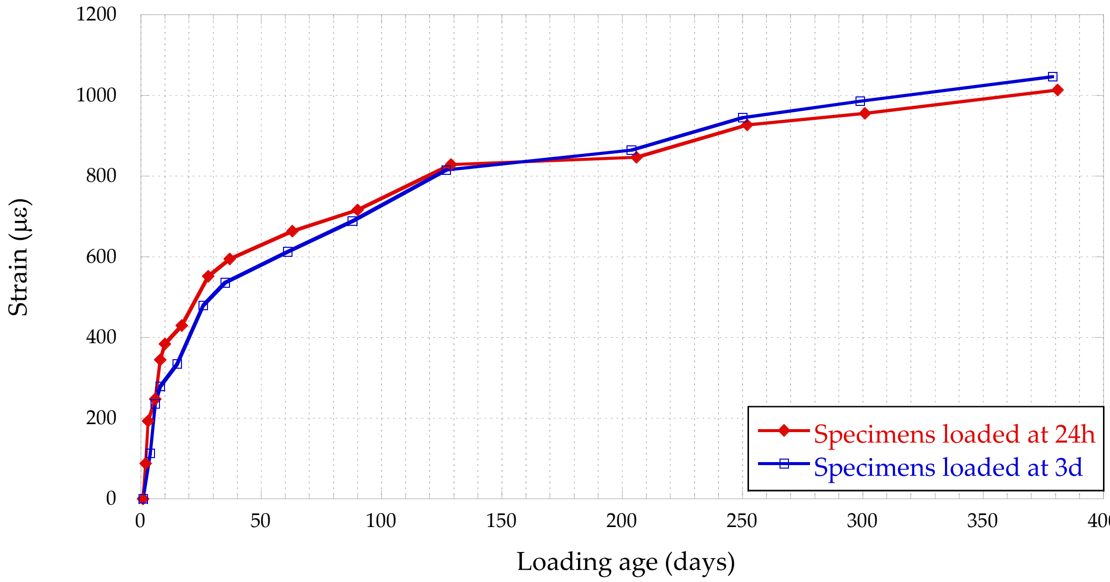

(a)

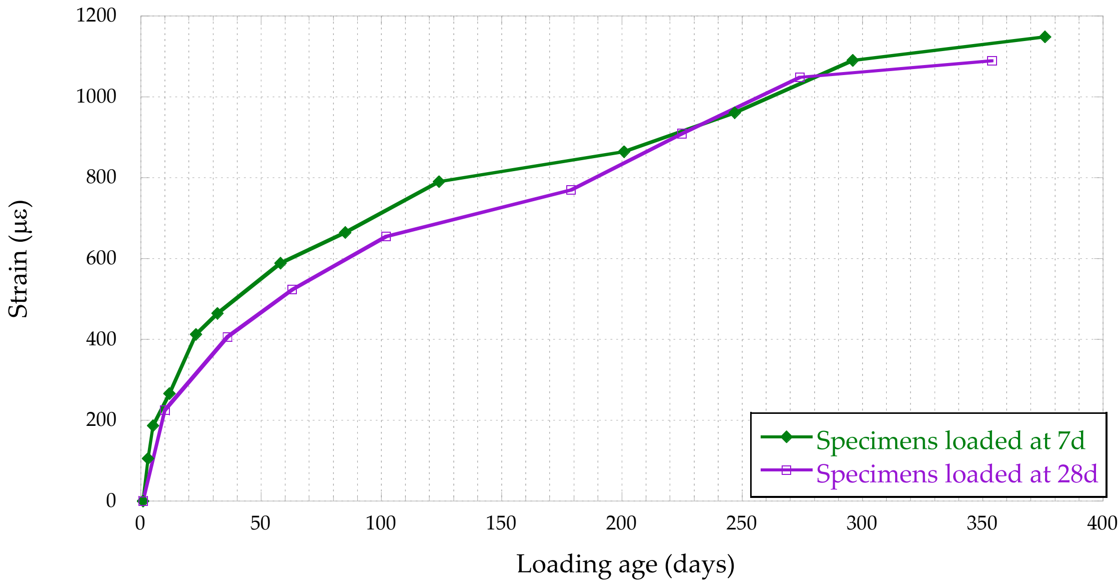

(b)

Fig. 43. Evolution of creep deformation undergone by FRC: (a) specimens loaded at 15 MPa; (b) specimens loaded at 20 MPa.

Analysing the evolution of the deformation of the FRC due to the creep episode to which it was subjected during the test, differences in strain rates are observed according to the age in the specimens loaded at 15 and 20 MPa. As can be seen in Fig. 43, in the first stage of the creep episode, the deformation of the specimens loaded at a younger age is greater. This is because the cement in the younger specimens has not hydrated sufficiently and deforms more in the first days of loading, in agreement with other authors [118].

However, for a loading age of 150 days in the specimens loaded at 15 MPa, and for a loading age of 200 days in the specimens loaded at 20 MPa, there is an inflection point from which the deformations of the specimens loaded at different ages are equalized. This is because from high ages onwards, the age of loading is not so relevant because in the long term they are similar. In other words, the effect of the load does not penalise the hydration of the cement in the long term. This tendency of creep evolution to stabilise at high loading ages has been corroborated by other authors [4]. It also coincides with the conclusion reached by other studies that greater creep evolution occurs in the first hours of aging of the reinforced concrete [119].

Proposed creep formulation

Comparing the evolution of the creep deformation of the FRC with the theoretical curve reflected in the EHE-08 standard [115], an important divergence is observed. The evolution of creep deformation undergone by FRC specimens loaded 24h after their manufacture is the one that deviates the most from the theoretical curve defined in the EHE-08 standard. For the rest of the test specimens, loaded at the ages of three, seven and twenty-eight days, there is still a divergence between their experimental behaviour and that predicted by the EHE-08 standard, but this divergence is much smaller. The maximum divergence between experimental and theoretical creep deformation is recorded for the first stage of the creep process to which the FRC specimens have been subjected during the test. Equation 6 shows the formulation proposed by the EHE-08 standard for estimating creep deformation in concrete.

$$\varepsilon_{c\sigma}(t,t_0) = \frac{\sigma(to)}{E_{c,to}} + \frac{\sigma(to)\cdot\varphi_{HR}\cdot\beta(f_{cm})\cdot\beta(to)\cdot\beta_c(t-to)}{E_{c,28}} \qquad \textbf{Equation 7}$$

$$\beta(t_0)^{\gamma} = \frac{1}{0{,}1 + {t_0}^{\alpha(t_0)}} \qquad \textbf{Equation 8}$$

$$\beta_c(t-t_0)^{\gamma} = \left(\frac{(t-t_0)}{\beta_H + (t-t_0)}\right)^{\alpha(t-t_0)} \qquad \textbf{Equation 9}$$

Where:

- σ(to) is stress on specimens during creep test.
- $E_{c,to}$ is the initial modulus of elasticity in specimens.
- $E_{c,28}$ is the modulus of elasticity of the specimens at 28 days.
- $\phi\Phi_{HR}$ is the coefficient of influence of relative humidity [115].
- $\beta(f_{cm})$ is the coefficient of influence of concrete strength [115].
- $\alpha(t_0)$ is the coefficient associated with the loading age proposed by the authors;
- $\alpha(t-t_0)$ is the coefficient associated with the evolution of creep with time proposed by the authors.

Fig. 44 represents the evolution of the error of the model proposed by the authors with the variation of the value of the coefficients "α (t0)" and "α (t-t0)", while Fig. 45 shows the range of optimal coefficients of the model proposed by the authors to minimize the deviation of the predictive model compared with the experimental results obtained in the laboratory.

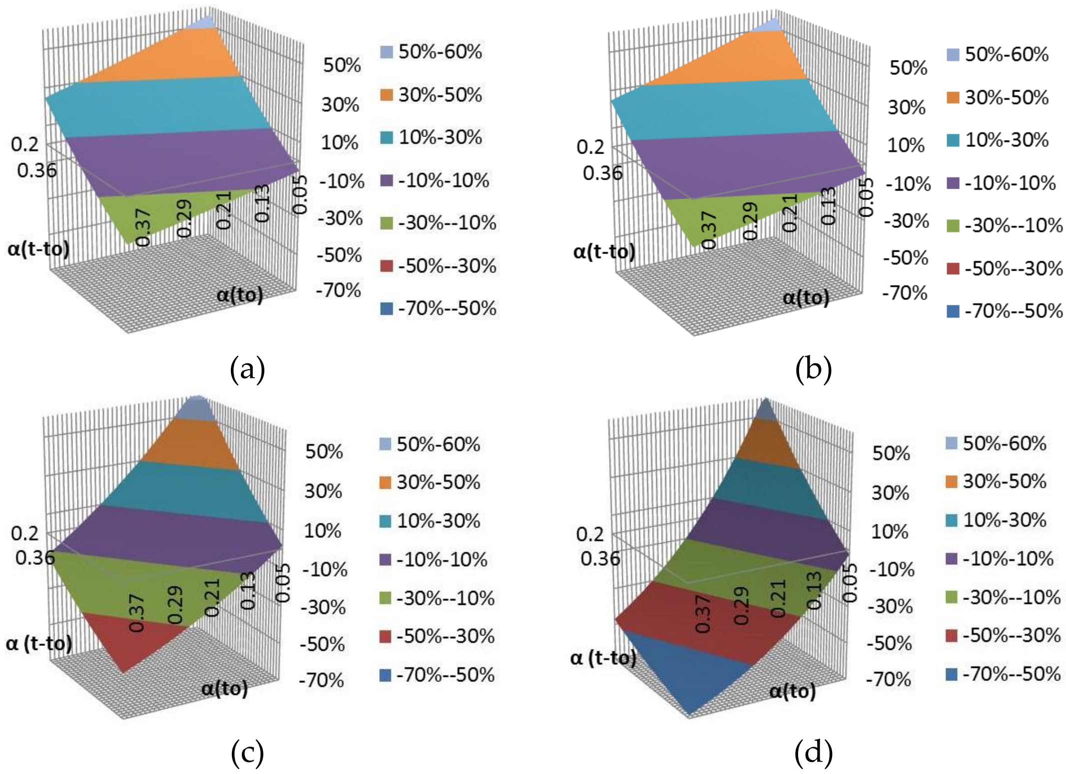

Fig. 44. Analysis of the error induced by the variation of the exponent of the creep coefficients β (t_0) and β ($t-t_0$) in the model proposed by the authors to determine the creep strain undergone by FRC: (a) FRC specimens loaded at 24h (a); at 3d (b); at 7d (c); at 28 d (d).

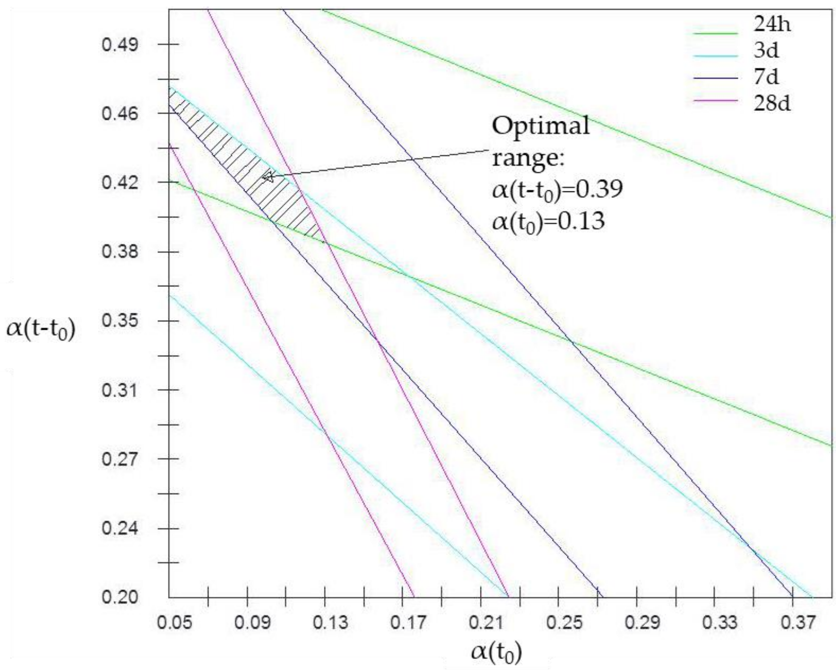

Fig. 45. Optimization of the coefficients "α (t_0)" and "α (t-t_0)" of the model proposed by the authors for calculating the creep strain of FRC.

To determine the optimal creep coefficients, the authors have scanned all possible combinations of values of these coefficients and have obtained the error of the final proposed formulation for each load age analysed in the study. Fig. 45 represents the traces of the interval corresponding to a maximum deviation of 5% for the different ages of FRC loading: (a) green trace for FRC loaded at 24h; (b) cyan trace for FRC loaded at 3d; (c) blue trace for FRC loaded at 7d; (d) pink trace for FRC loaded at 28 days. The optimal interval is taken as the area in which the divergence intervals of less than 5% converge for all the load ages analysed in the creep test. The authors propose the following values for the coefficients associated with the loading age and the evolution of creep with time: $\alpha(t_0)=0.13$; α $(t-t_0)=0.39$.

<u>*Verification of creep formulation*</u>

Fig. 46 represents the evolution of the deferred creep strain over time. The values obtained in the laboratory ("Experimental results") are compared with the predictive model of the EHE-08 ("Normative prediction") and the predictive model proposed by the authors ("Proposed model").

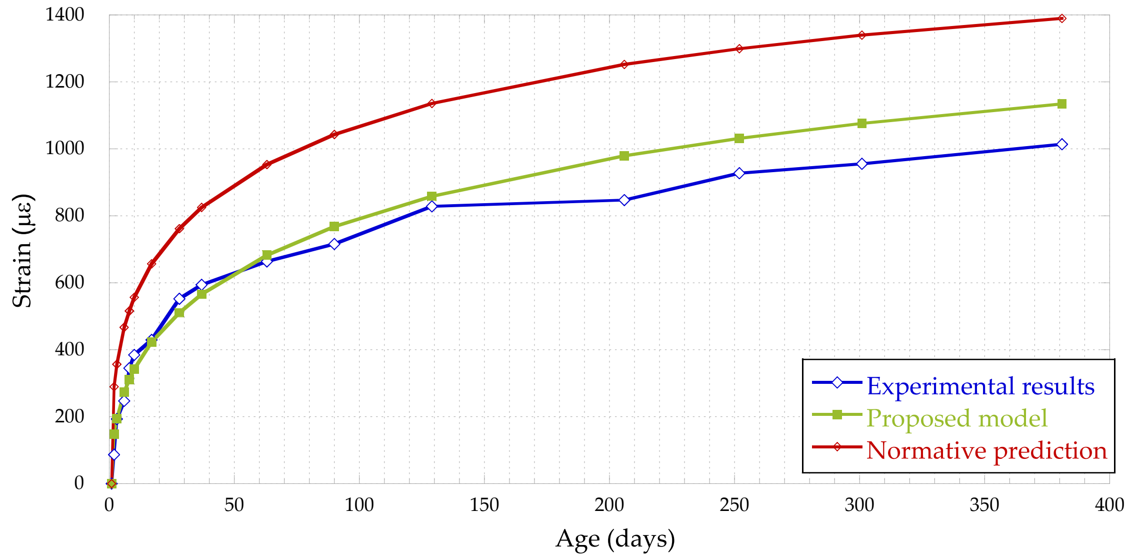
1400
1200
1000
800
600
400
200
0
Strain (με)
0
50
100
150
200
250
300
350
400
Age (days)
Experimental results
Proposed model
Normative prediction

(a)

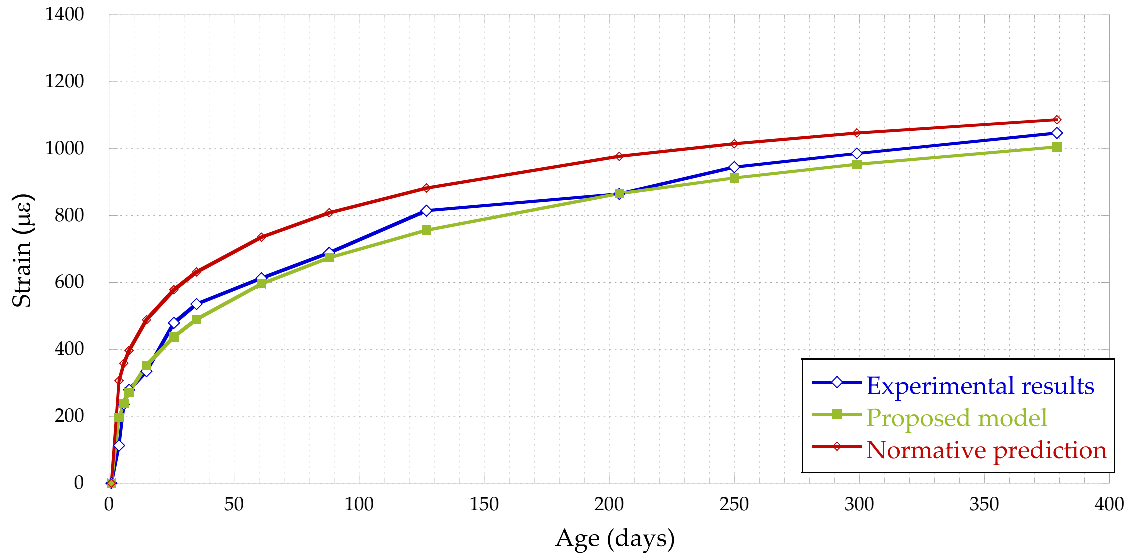
1400
1200
1000
800
600
400
200
0
Strain (με)
0
50
100
150
200
250
300
350
400
Age (days)
Experimental results
Proposed model
Normative prediction

(b)

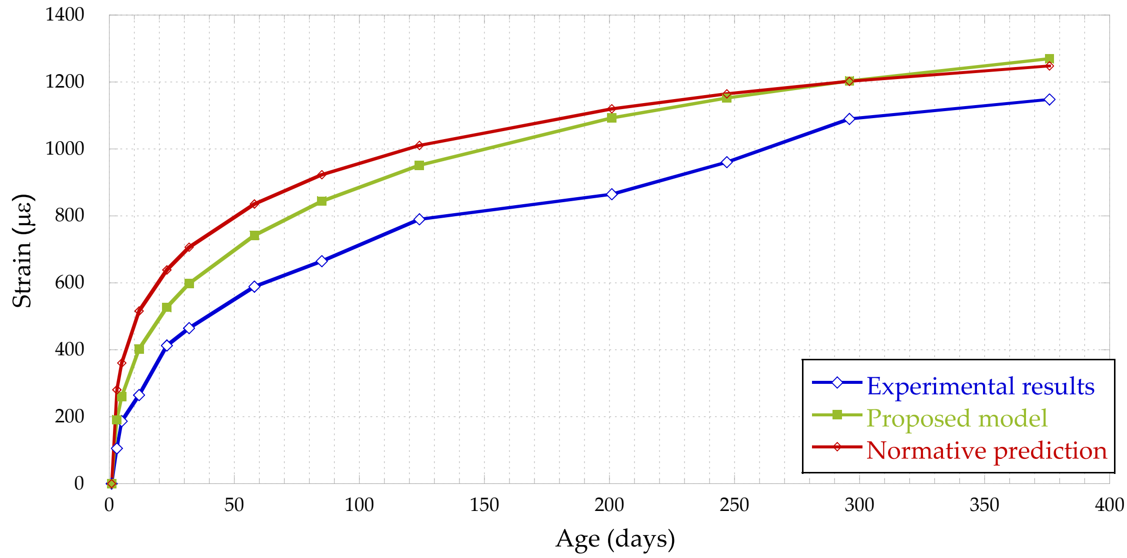
1400
1200
1000
800
600
400
200
0
Strain (με)
0
50
100
150
200
250
300
350
400
Age (days)
Experimental results
Proposed model
Normative prediction

(c)

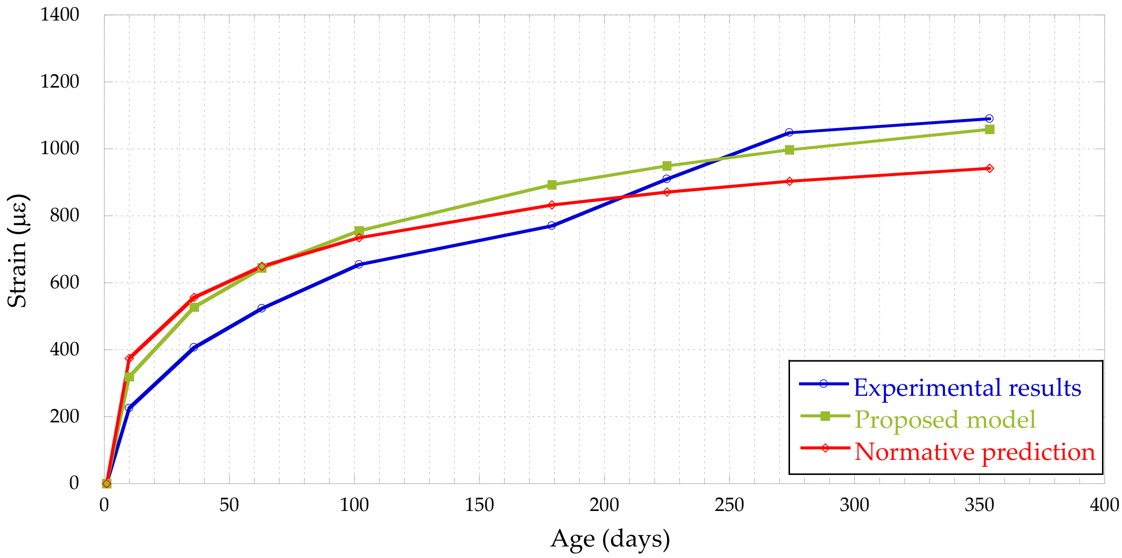

(d)

Fig. 46. Creep deformation undergone by FRC specimens: FRC loaded at 24h(a); (b) 3d; (c) 7d; (d) 28d.

The normative prediction fits relatively well with the experimental results in FRC loaded at 28d of age. However, the standard does not accurately reproduce the experimental results at early loading ages of the FRC, especially at 24h of age. Other authors have already detected discrepancies between standards and experimental creep results [118], [120].

3.3.3. *Modulus of elasticity*

The specimens loaded 24 h after their manufacture were subjected to a tension equivalent to 78% of their compressive strength. Fig. 47 (a) shows the stress/strain curve of the FRC specimens loaded at 24 h and at 3d. As expected, for the same compression stress of 15 MPa, the deformation of the loaded specimens at 24h is much greater than that corresponding to the specimens loaded at 3d. In the case of the FRC specimens loaded at the age of seven and twenty-eight days, the stress level during the creep test was similar, equivalent to 53 and 47% of their compressive strength respectively. In Fig. 47 (b), we can see the similarity of the stress/strain curves of the specimens loaded at the age of seven and twenty-eight days.

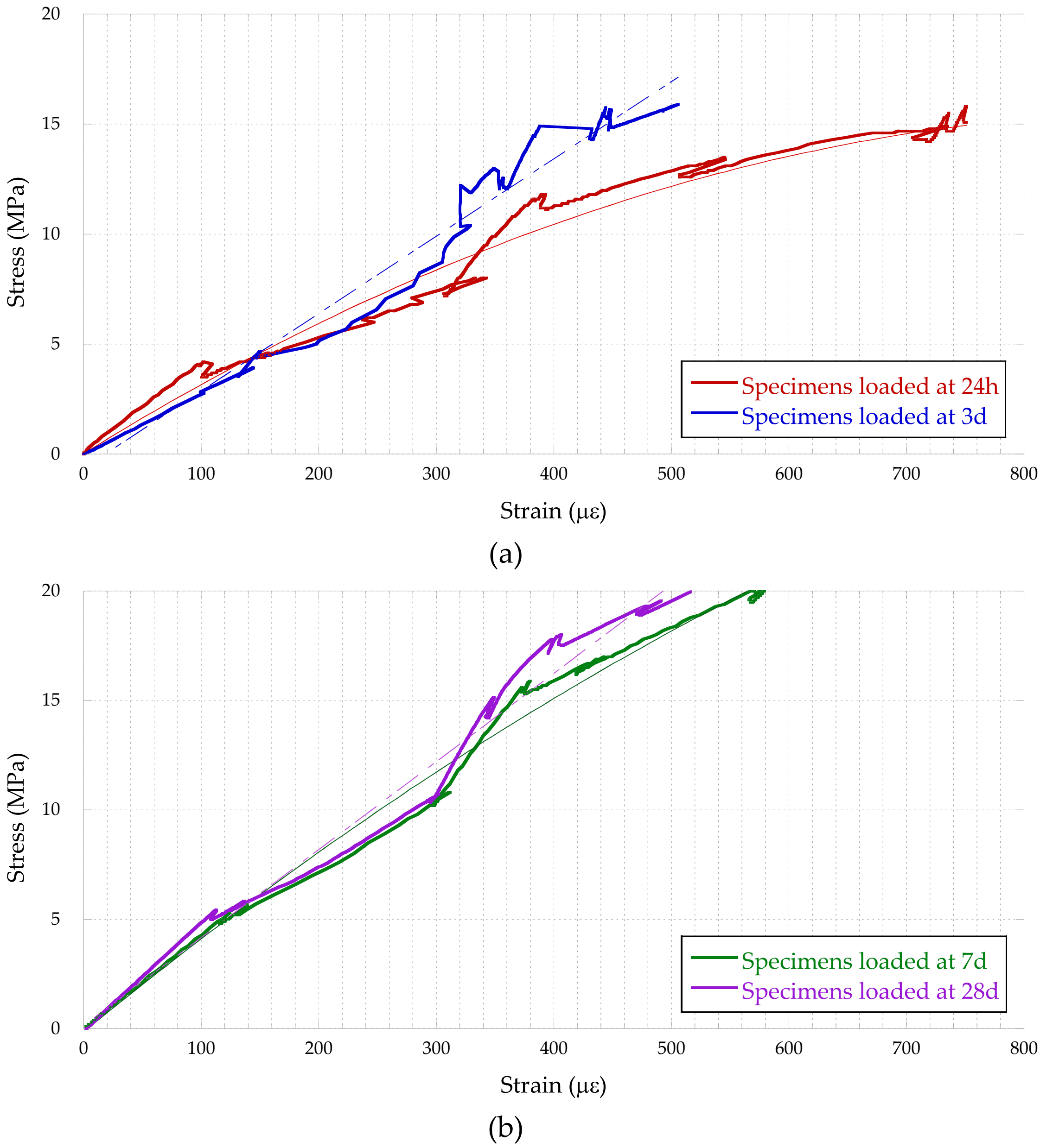

Fig. 47. Tension-deformation curve during loading of the specimens: (a) FRC specimens loaded at 15 MPa; (b) FRC specimens loaded at 20 MPa.

From the analysis of the stress/strain curves of the specimens during their loading, the modulus of elasticity of the FRC is obtained at the time corresponding to the start of the creep test. As expected, and according to the values obtained for the compressive strength of concrete, the value of the modulus of elasticity increases with the age of the concrete, as reflected in Fig. 48.

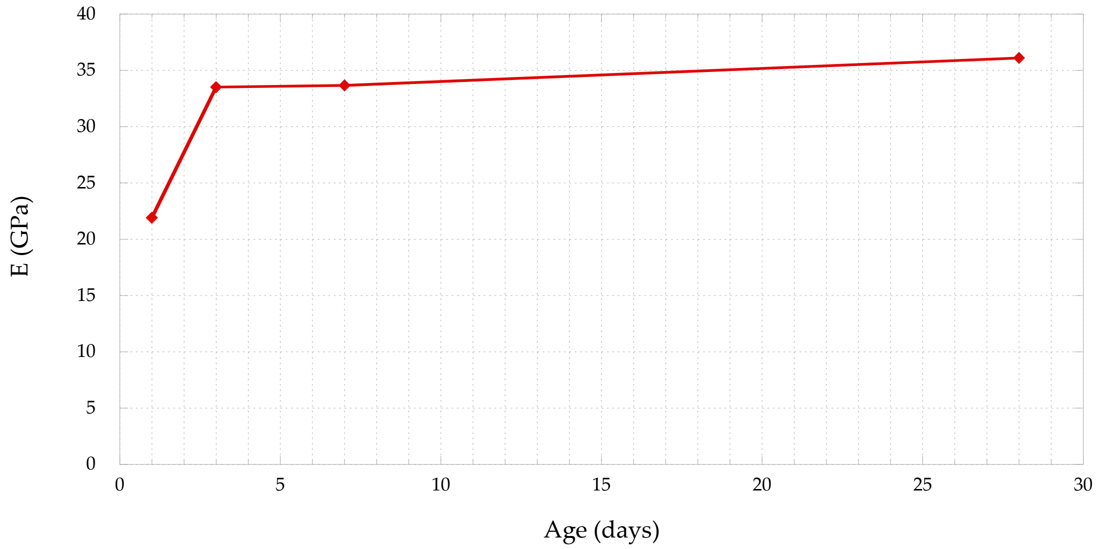

Fig. 48. Evolution of the modulus of elasticity of FRC with age.

It can be observed that the modulus of elasticity evolves with age in a similar way to the evolution of the compressive strength (Fig. 42).

Fig. 49 shows the stress/strain curves of the specimens during their unloading.

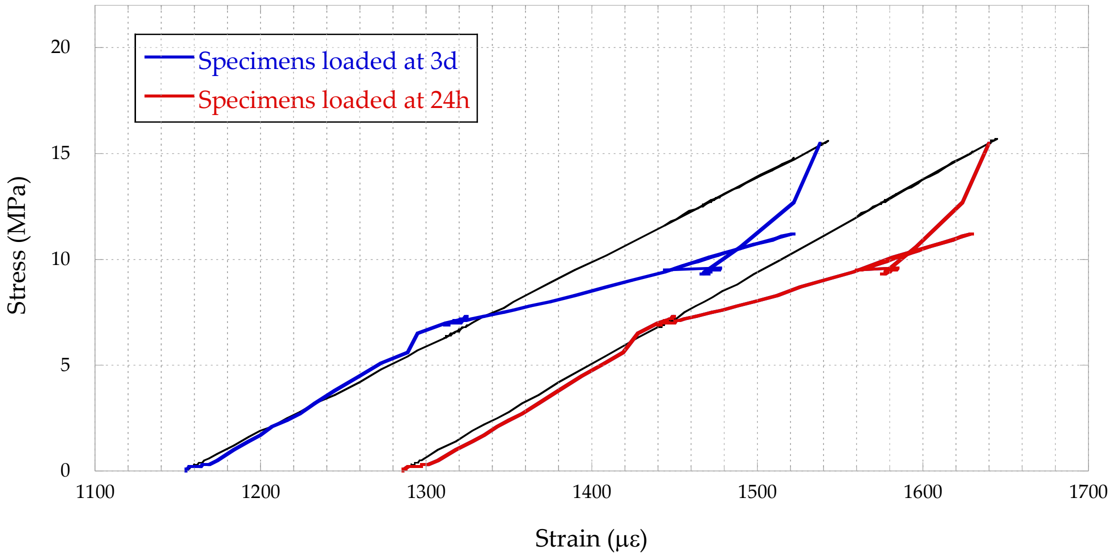

(a)

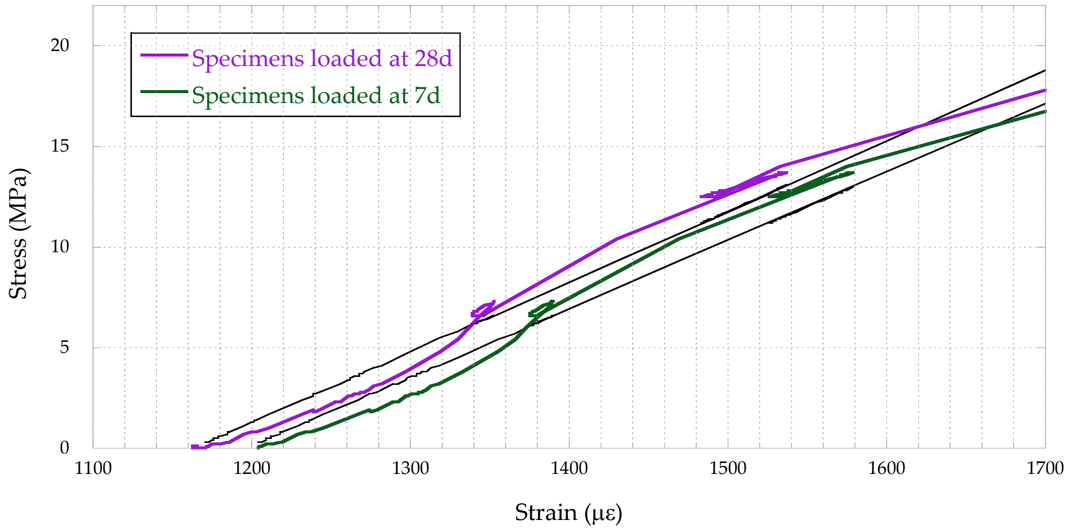

(b)

Fig. 49. Stress / strain curve during the unloading of the specimens: (a) FRC specimens loaded at 15 MPa; (b) FRC specimens loaded at 20 MPa.

Once the creep test was completed, the analysis of the stress/strain curves of the specimens during their unloading (Fig. 49) makes it possible to obtain the residual modulus of elasticity of the FRC after the 384-day duration of the creep test. In the case of the residual modulus of elasticity of FRC, it is observed that its value decreases with the increase in the loading age of the concrete.

As can be seen in Fig. 50, the FRC specimens with the highest stiffness are those that were loaded 24h after their manufacture.

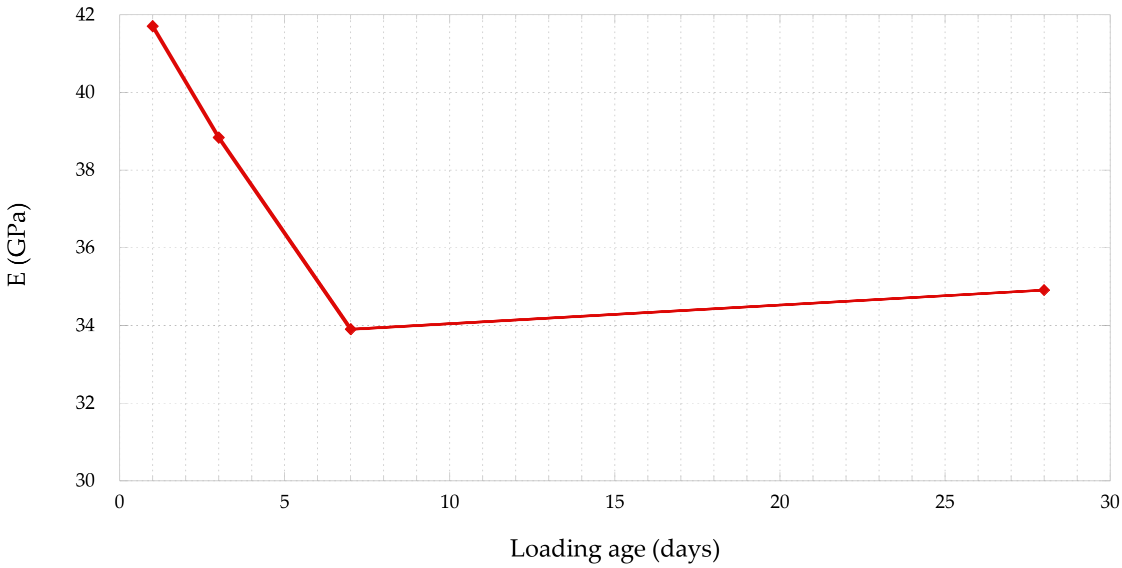

Fig. 50. Evolution of the modulus of elasticity of FRC with its loading age.

Performing a comparative analysis of the stress/strain curves of the specimens during their loading with the curves corresponding to their unloading, it can be observed that the influence of the creep of FRC on its deformation behaviour is different for concrete loaded at early age than for concrete loaded with an age greater than 3 d. Whereas in a concrete loaded at an early age, its modulus of elasticity increases after having been subjected to a creep episode, in concrete loaded at an age greater than 3d, its modulus of deformation remains unchanged (Tab. 18).

Tab. 18. Evolution of the modulus of elasticity of FRC after a creep episode. Initial "Eo" and residual "Er" modulus of elasticity

Loading Age (d)	Eo (GPa)	Er (GPa)
1	21.913	41.712
3	33.500	38.842
7	33.667	33.904
28	36.100	34.918

The difference between the initial and residual modulus of elasticity depends on the loading age. Furthermore, the two moduli of elasticity evolve in an inversely proportional way, so early loaded specimens have lower initial modulus of elasticity and higher residual modulus of elasticity.

3.3.4. *Delayed elastic strain*

Fig. 14 shows the evolution of the delayed elastic strain after the creep test. The specimens were monitored for 62d after the removal of the load.

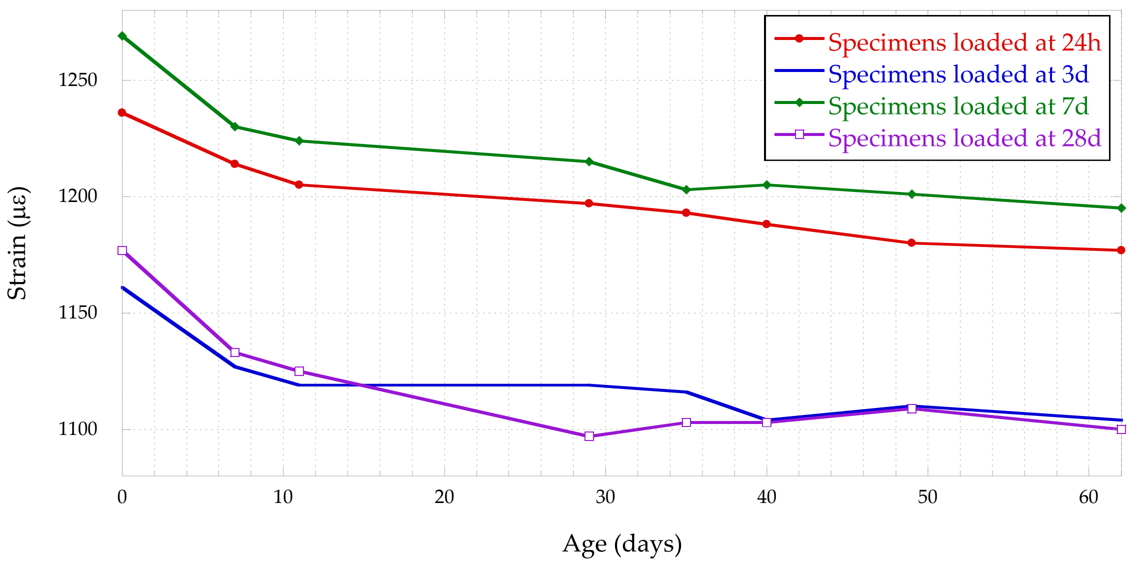

Fig. 51. Evolution of the delayed elastic strain of FRC after a creep episode.

Analysing the evolution of the delayed elastic strain after the creep test, and confirming the behaviour observed in the analysis of the instantaneous elastic strain when removing the load to which the FRC specimens were subjected, it is observed that the strain of the FRC specimens loaded at an early age is significantly less than that of samples loaded at an age greater than 3d.

After analysing the data obtained in the laboratory, the authors propose the formulation in Equation 9 to predict the delayed elastic strain of FRC after a creep episode (Fig. 52).

$$\varepsilon_e = \varepsilon_{e,i} + \varepsilon_{e,d} = \frac{\sigma}{E_{c,t_d}} \cdot \left(1 + 0.14 \cdot \left(\frac{(t - t_d)}{(1.5 \cdot (t - t_d))}\right)^{0.39}\right) \qquad \textbf{Equation 10}$$

Where:

– $\varepsilon_{e,i}$ is the instantaneous elastic strain.
– $\varepsilon_{e,d}$ is the delayed elastic strain.
– t_d is the unloading age.
– $E_{c,td}$ is the modulus of elasticity of the specimens at unloading age.

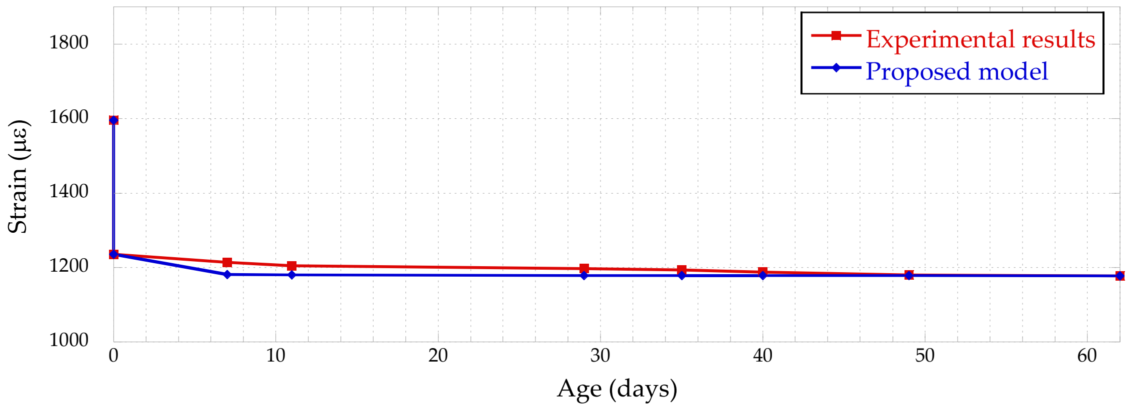
Experimental results
Proposed model
Strain (με)
1800
1600
1400
1200
1000
0
10
20
30
40
50
60
Age (days)

(a)

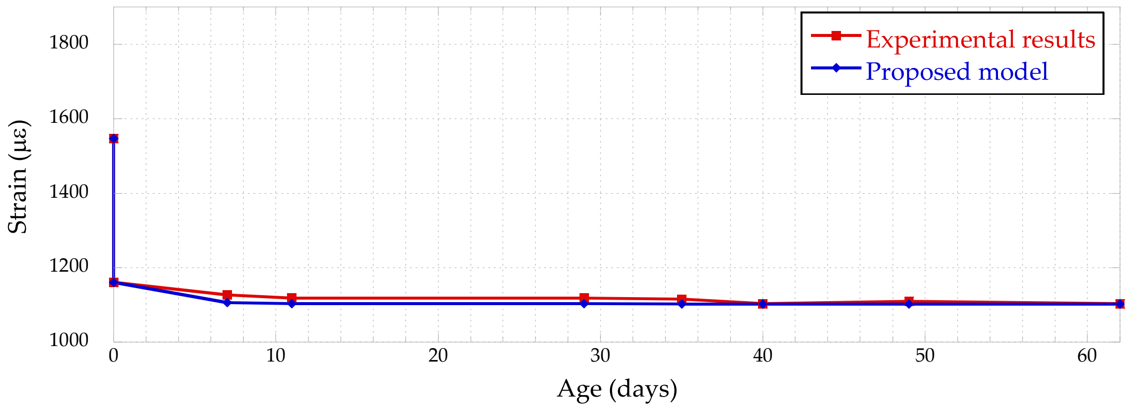
Experimental results
Proposed model
Strain (με)
1800
1600
1400
1200
1000
0
10
20
30
40
50
60
Age (days)

(b)

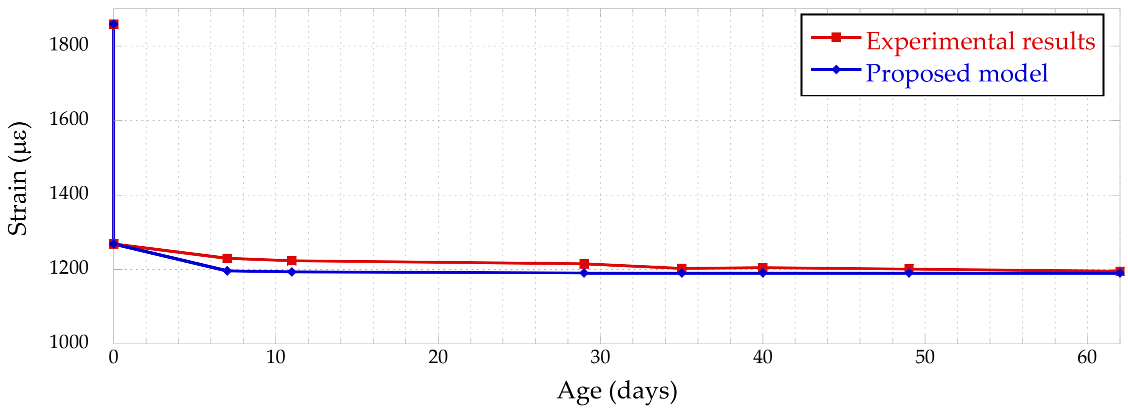
Experimental results
Proposed model
Strain (με)
1800
1600
1400
1200
1000
0
10
20
30
40
50
60
Age (days)

(c)

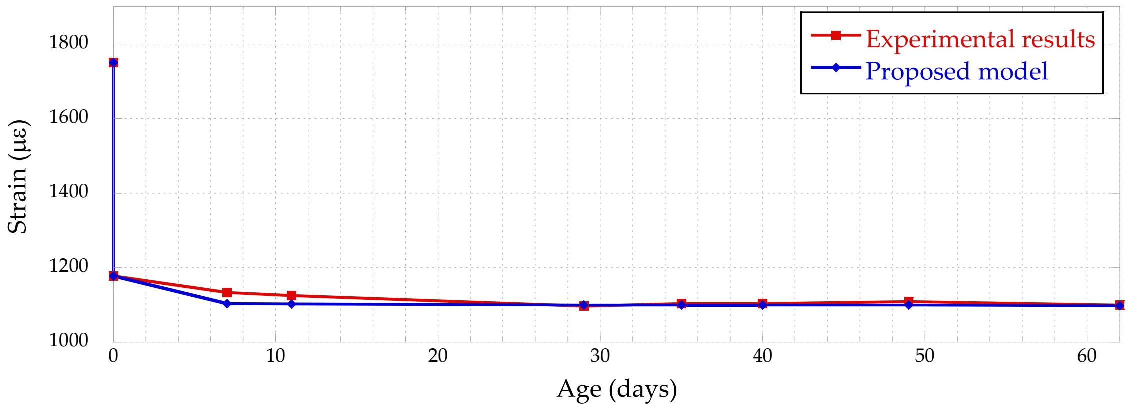

(d)

Fig. 52. Evolution of the elastic strain of FRC after a creep episode. Experimental strain versus strain predicted by the model proposed by the authors: FRC specimens loaded at (a) 24h; (b) 3d; (c) 7d; (d) 28d.

It can be observed that the instantaneous deformation is greater when the age of loading of the reinforced concrete is greater. This is due to the increase in the elastic behaviour of the concrete with age.

Furthermore, the proposed model very accurately reproduces the evolution of the deformation after removal of the load, especially the instantaneous strain and the strain produced long term.

3.3.5. *Microscopic Analysis*

In the Fig. 53-Fig. 55, the imprint of a fibre that reinforced the concrete can be seen after the mechanical tests were carried out (at different magnitudes).

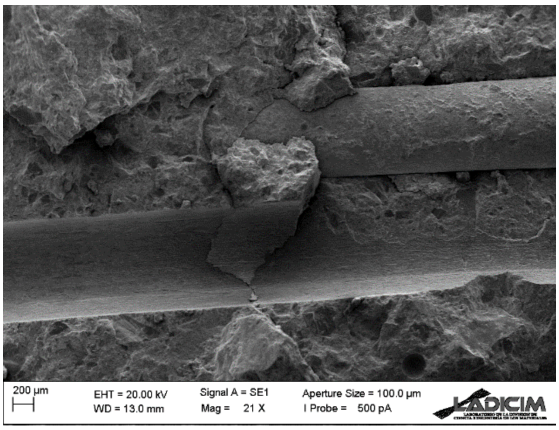

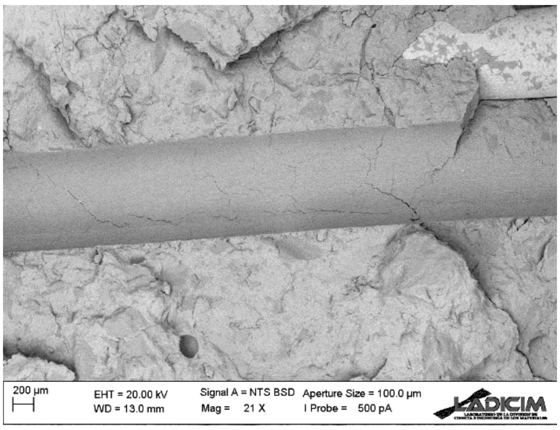

Fig. 53. Fibre (left) and "bed" fibre (right) at 21 X.

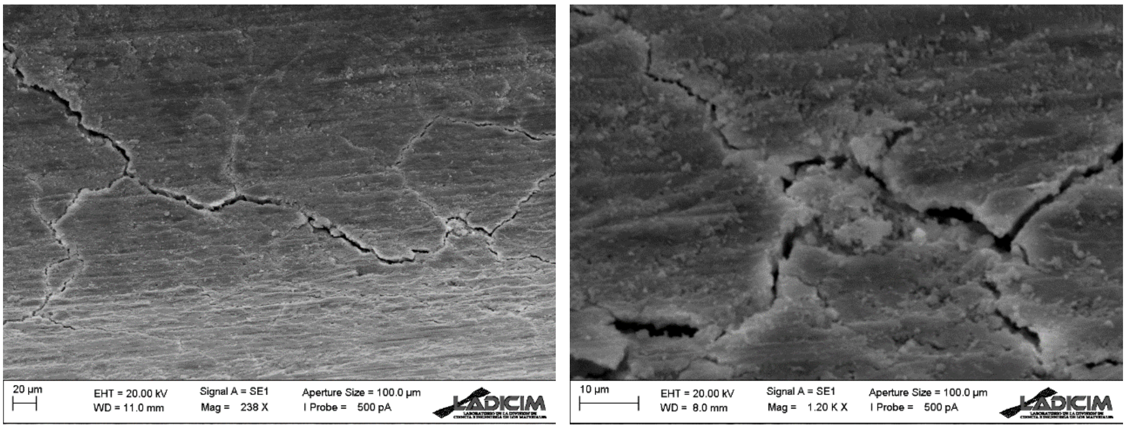

Fig. 54. Fibre "bed" at 238 X (left) and 1200 X (right).

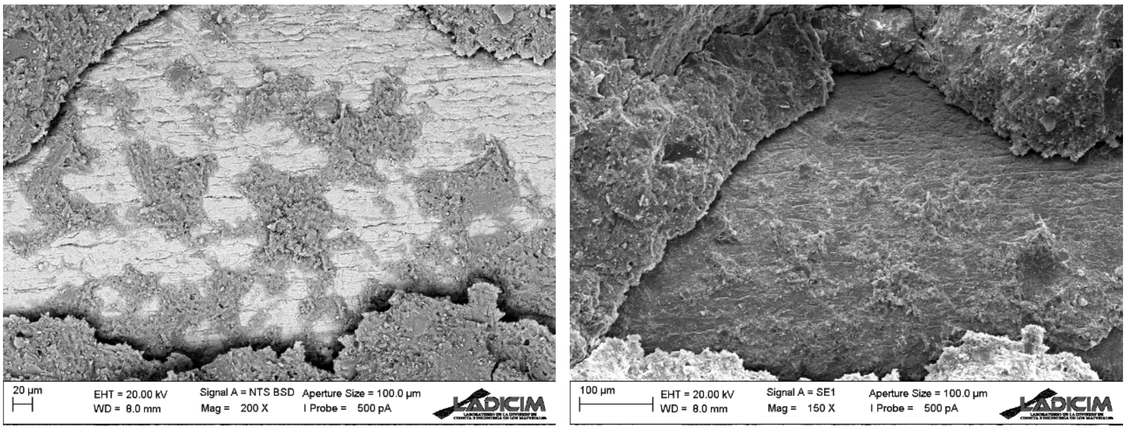

Fig. 55. Fibre "bed" at 200 X (left) and 150 X (right).

In Fig. 53, two fibres appear to penetrate the concrete. There is paste adhering to the fibres, which is a sign of good bonding between paste and fibres. On the other hand, small cracks can be seen in the microscopic images.

Microscopic images show that the mechanical tests do not cause the fibres to fissure or deform, but that the metal fibres appear detached and hardly deformed. In addition, a nodule is seen to form at the junction of several microcracks.

3.4. Conclusions

From this work, the following conclusions can be drawn:

- From the analysis of the creep strain undergone by the FRC specimens analysed during the test, two stages can be distinguished: (a) in a first stage, the creep deformation of the specimens loaded at an earlier age shows a greater strain; (b) in the second stage, the creep strain is equalized for the different loading ages.

- The strain undergone by FRC specimens loaded at an earlier age, 24 h after their manufacture, shows a much lower level than predicted by the formulation proposed by the EHE-08 standard. In the case of the specimens loaded at the ages of three, seven and twenty-eight days, the strain is also less than that foreseen in the EHE-08 standard, although the difference is not so high.
- The authors propose an adjustment of the creep coefficients proposed in the EHE-08 equation associated with the loading age β (t0) and the evolution of the creep in time βc (t-t0).
- From a comparative analysis of the stress/strain curves of the FRC specimens during their loading and unloading, it can be concluded that the FRC loaded at an earlier age stiffens after a creep episode.
- Once the results of the creep test of FRC loaded at different ages was analysed, it could be concluded that FRC had better creep behaviour than conventional concrete.
- Analysing the evolution of the delayed elastic deformation of the FRC specimens after the end of the creep test, it is concluded that, the FRC loaded at an earlier age, undergoes less deformation.
- The authors propose a formulation for the analysis of the delayed elastic deformation of FRC after a creep episode.

CAPÍTULO V

Conclusiones y perspectivas futuras

5.1. Conclusiones

La conclusión principal derivada de este trabajo es que el hormigón reforzado con fibras es una alternativa al hormigón armado convencional que podría optimizar tiempos y costes, facilitando la colocación del hormigón al eliminar total o parcialmente la armadura y, además, mejorando sus características. Por ello, se considera que es un material adecuado para fabricar torres de aerogeneradores que consigan mayores potencias al permitir llegar a alturas mayores, pudiendo suponer un gran impulso a la energía eólica. Además, los resultados que se han expuesto en la presente Tesis son extrapolables a cualquier estructura que emplee hormigón y pretenden fomentar el incremento del uso de este material, como sustituto total o parcial del hormigón armado convencional.

Del conjunto de los trabajos realizados, se derivan las siguientes conclusiones.

<u>Análisis estadístico de la influencia del método de vertido en la distribución de macrofibras metálicas en hormigón vibrado.</u>

De este análisis, expuesto en el Capítulo II, se concluye que el método de vertido del hormigón tiene escasa influencia en la carga de fisuración. Sin embargo, influencia notablemente el comportamiento del hormigón una vez fisurado. En concreto, se extraen las siguientes conclusiones:

- Existe una influencia de los muros de encofrado en la orientación de las fibras en el hormigón, de modo que las fibras tienden a alinearse con las caras mayores.
- Las resistencias residuales son mayores cuantas más fibras se encuentren perpendiculares al plano de carga. A su vez, al poder influenciar la disposición de las fibras con el método de vertido, se puede relacionar la dirección de hormigonado y posición del encofrado con el incremento de la resistencia residual del hormigón.
- Existe una correlación entre deformaciones circunferenciales, la cual es más precisa con valores mayores de apertura de fisura.
- Se detecta que en un vertido realizado por la cara mayor del encofrado existen aproximadamente el doble de fibras en la parte inferior respecto a la superior, lo cual influye a su vez en las resistencias residuales.

<u>Efecto del refuerzo de fibra de acero en el comportamiento a la fatiga por flexión del hormigón estructural entallado.</u>

No existen muchas investigaciones sobre el comportamiento a fatiga de los reforzados con fibra. Sin embargo, la importancia que este material puede tener, gracias a sus mejores prestaciones y ahorro en ejecución, hace necesario investigar sobre él. De ahí la importancia de los resultados obtenidos y presentados en el Capítulo III, abriendo la puerta a un nuevo tipo de análisis sobre el comportamiento del hormigón a fatiga por flexión.

En este trabajo, se han obtenido las siguientes conclusiones:

- Se obtuvo una curva S-N del material antes de que se agrietara. Una vez fisurado el hormigón, la cantidad y orientación de las fibras es tan importante en la respuesta del hormigón a las cargas cíclicas que da lugar a un comportamiento extremadamente heterogéneo.
- Se ha demostrado que la presencia de fibras aumenta la vida a fatiga del hormigón, incluso en ensayos realizados bajo control de carga. Esto proporciona un tiempo entre la rotura del hormigón y la rotura estructural, que puede utilizarse para tomar las medidas correctoras adecuadas.
- Se detectó una apertura de grieta crítica tras la cual se produce la fisuración del hormigón, que podría utilizarse como indicador del fallo prematuro de la probeta.
- Se observó un valor crítico de energía que indica que la probeta se romperá, por lo que podría utilizarse como parámetro para determinar la vida útil restante del hormigón. Sin embargo, hay que tener en cuenta que, al tratarse de un parámetro energético, es específico para cada geometría.

- Se ha comprobado que el mecanismo que produce el fallo del hormigón está causado por microfisuras propias del hormigón en la entalla que comienzan a crecer debido a las cargas aplicadas. La velocidad de crecimiento de las fisuras depende del rango de esfuerzos aplicados en el ensayo, existiendo una correlación entre ambos. Sin embargo, es probable que la geometría también influya.

Efecto del refuerzo de fibra en la fluencia del hormigón de edad temprana.

De la investigación realizada sobre la fluencia del hormigón reforzado con fibras, presentada en el Capítulo IV, se extraen las siguientes conclusiones principales:

- En la deformación por fluencia del hormigón estudiado, se han distinguido dos etapas diferenciadas. En la primera etapa, las probetas cargadas a corta edad tienen mayor deformación. En la segunda etapa, la deformación por fluencia se iguala para las diferentes edades de carga.
- La formulación de la normativa EHE-08 prevé deformaciones inferiores a las observadas durante los estudios experimentales. Además, esta diferencia es mayor cuanto menor es la edad de puesta en carga, siendo la deformación sufrida por las probetas cargadas a 24 h de edad muy inferior a la prevista por la formulación propuesta.
- Los autores proponen un ajuste de los coeficientes de fluencia propuestos en la ecuación de la normativa asociados a la edad de carga β (t_0) y a la evolución de la fluencia en el tiempo βc ($t-t_0$), para conseguir un mejor ajuste de la deformación bajo cargas de fluencia.
- Del análisis comparativo de las curvas de tensión/deformación durante la carga y descarga de las probetas de hormigón reforzado con fibras, puede concluirse que el cargado a una edad más temprana se rigidiza tras un episodio de fluencia.
- Analizando la evolución de la deformación elástica diferida, se concluye que un hormigón cargado a menor edad sufre una menor deformación.

5.2. Perspectivas de futuro

En esta Tesis doctoral se ha realizado una ampliación del estado del conocimiento de algunos de los esfuerzos críticos a los que están sometidas las torres de aerogeneradores. Si bien, aún es necesario ahondar en algunos puntos que optimicen y complementen las investigaciones ya realizadas.

- Las fibras empleadas en este trabajo han sido macrofibras de acero, ya que son las más comúnmente empleadas para resistir esfuerzos estructurales. Sin embargo, resulta de interés desarrollar los trabajos realizados con distintas fibras y dosificaciones, con el objetivo de extrapolar los resultados de forma óptima.

- Los resultados del programa experimental permiten afirmar que tanto el ensayo Barcelona como el inductivo son adecuados para cuantificar la cantidad de fibras dentro del hormigón, su orientación y la resistencia indirecta post-fisuración. El ensayo inductivo podría ser clave en la certificación del hormigón y se plantea como posible línea de investigación futura el establecimiento de un sistema estadístico para el control de calidad de cuantías en base al citado ensayo.
- No existen muchas investigaciones sobre el comportamiento a fatiga de los hormigones reforzados con fibra. Pese a la importancia de los resultados presentados y de los resultados obtenidos, abriendo la puerta a un nuevo tipo de análisis sobre el comportamiento del hormigón a fatiga por flexión, es importante resaltar que este estudio ha de ser complementado con futuros estudios en los que se analicen no sólo diferentes geometrías de probeta, sino también diferentes tamaños de entalla.
- El comportamiento a torsión del hormigón reforzado con fibras es uno de los aspectos menos investigados, por su dificultad en la realización de ensayos y el tiempo empleado en los mismos. Sin embargo, este es considerado un esfuerzo crítico, que debería ser ahondado en futuros trabajos.
- Se ha observado durante los ensayos de laboratorio, que el ajuste de la normativa española que relaciona el desplazamiento vertical con la apertura de fisura dista de los valores obtenidos para estadios de fisuración no avanzados y puede enmascarar errores para situaciones de servicio con anchos de fisura pequeños. Las primeras conclusiones extraídas fueron expuestas por la autora en el VIII Congreso ACHE con la ponencia "Desarrollo de la resistencia a flexión de hormigones reforzados con fibras" Se plantea como trabajo futuro estudiar esta correlación llevando a cabo simulaciones numéricas y ampliando la campaña de ensayos para afinar esta correlación en estadios pequeños de fisura, para proponer una formulación que optimice esta correlación.

ÍNDICE DE FIGURAS Y TABLAS

ÍNDICE DE FIGURAS

CAPÍTULO III

CAPÍTULO IV

ÍNDICE DE TABLAS

REFERENCIAS

[1] ONU, "Objetivo 13: Adoptar medidas urgentes para combatir el cambio climático y sus efectos." https://www.un.org/sustainabledevelopment/es/climate-change-2/.

[2] P. R. Shukla *et al.*, "Resumen para responsables de políticas," *El cambio climático y la tierra Inf. Espec. del IPCC sobre el cambio climático, la Desertif. la Degrad. las tierras, la gestión Sosten. las tierras, la Segur. Aliment. y los flujos gases Ef. invernadero en los ecos*, 2019, [Online]. Available: https://www.ipcc.ch/site/assets/uploads/sites/4/2020/06/SRCCL_SPM_es.pdf.

[3] J. Serna, "Experiencias en el uso de torres eólicas de hormigón," 2009, [Online]. Available: http://www.aeeolica.org/uploads/documents/wpe2009/Jose Serna_INNEOTORRES.pdf.

[4] N. Tosic, S. Aidarov, and A. De la Fuente, "Systematic Review on the Creep of Fiber-Reinforced Concrete," *Materials (Basel).*, vol. 13, p. 5098, Nov. 2020, doi: 10.3390/ma13225098.

[5] A. M. Brandt, "Fibre reinforced cement-based (FRC) composites after over 40 years of development in building and civil engineering," *Compos. Struct.*, vol. 86, no. 1, pp. 3–9, 2008, doi: https://doi.org/10.1016/j.compstruct.2008.03.006.

[6] M. di Prisco, G. Plizzari, and L. Vandewalle, “Fibre reinforced concrete: new design perspectives,” *Mater. Struct.*, vol. 42, no. 9, pp. 1261–1281, 2009, doi: 10.1617/s11527-009-9529-4.

[7] J. C. Walraven, “High performance fiber reinforced concrete: progress in knowledge and design codes,” *Mater. Struct.*, vol. 42, no. 9, p. 1247, 2009, doi: 10.1617/s11527-009-9538-3.

[8] J. Bairán, N. Tosic, and A. De la Fuente, “Reliability-based assessment of the partial factor for shear design of fibre reinforced concrete members without shear reinforcement,” *Mater. Struct.*, vol. 54, p. 185, Sep. 2021, doi: 10.1617/s11527-021-01773-z.

[9] J. A. Ortiz-Lozano, F. Mena-Sebastia, I. Segura, A. de la Fuente, and A. Aguado, “Structural use of Fiber-Reinforced Self-Compacting Concrete with Recycled Aggregates: Case Study of a Foundation Wall in Spain,” *Case Stud. Constr. Mater.*, p. e01334, 2022, doi: https://doi.org/10.1016/j.cscm.2022.e01334.

[10] A. Blanco, P. Pujadas, A. de la Fuente, S. H. P. Cavalaro, and A. Aguado, “Assessment of the fibre orientation factor in SFRC slabs,” *Compos. Part B Eng.*, vol. 68, pp. 343–354, 2015, doi: https://doi.org/10.1016/j.compositesb.2014.09.001.

[11] P. Juan-García, J. M. Torrents, R. López, and S. H. Pialarissi Cavalaro, “Influence of fiber properties on the inductive method for the steel-fiber-reinforced concrete characterization,” *IEEE Trans. Instrum. Meas.*, vol. 65, no. 8, pp. 1937–1944, 2016, doi: 10.1109/TIM.2016.2549678.

[12] A. de la Fuente, P. Pujadas, A. Blanco, and A. Aguado, “Experiences in Barcelona with the use of fibres in segmental linings,” *Tunn. Undergr. Sp. Technol.*, vol. 27, no. 1, pp. 60–71, 2012, doi: https://doi.org/10.1016/j.tust.2011.07.001.

[13] R. P. Dhakal, “Post-peak response analysis of SFRC columns including spalling and buckling,” *Struct. Eng. Mech.*, vol. 22, no. 3, pp. 311–330, 2006, doi: 10.12989/sem.2006.22.3.311.

[14] L. R. Betterman, C. Ouyang, and S. P. Shah, “Fiber-matrix interaction in microfiber-reinforced mortar,” *Adv. Cem. Based Mater.*, vol. 2, no. 2, pp. 53–61, 1995, doi: https://doi.org/10.1016/1065-7355(95)90025-X.

[15] K. Holschemacher, T. Müller, and Y. Ribakov, “Effect of steel fibres on mechanical properties of high-strength concrete,” *Mater. Des.*, vol. 31, pp. 2604–2615, May 2010, doi: 10.1016/j.matdes.2009.11.025.

[16] J. Błyszko, “Comparative Analysis of Creep in Standard and Fibre Reinforced Concretes under different Load Conditions,” *Procedia Eng.*, vol.

193, pp. 478–485, 2017, doi: https://doi.org/10.1016/j.proeng.2017.06.240.

[17] J. Sainz-Aja *et al.*, "Effect of Steel Fibre Reinforcement on Flexural Fatigue Behaviour of Notched Structural Concrete," *Mater. (Basel, Switzerland)*, vol. 14, Oct. 2021, doi: 10.3390/ma14195854.

[18] M. Pająk and T. Ponikiewski, "Flexural behavior of self-compacting concrete reinforced with different types of steel fibers," *Constr. Build. Mater.*, vol. 47, pp. 397–408, 2013, doi: https://doi.org/10.1016/j.conbuildmat.2013.05.072.

[19] D.-Y. Yoo, S.-T. Kang, and Y.-S. Yoon, "Effect of fiber length and placement method on flexural behavior, tension-softening curve, and fiber distribution characteristics of UHPFRC," *Constr. Build. Mater.*, vol. 64, pp. 67–81, 2014, doi: 10.1016/j.conbuildmat.2014.04.007.

[20] D. A. Fanella and A. E. Naaman, "STRESS-STRAIN PROPERTIES OF FIBER REINFORCED MORTAR IN COMPRESSION.," *J. Am. Concr. Inst.*, vol. 82, no. 4, pp. 475–483, 1985, [Online]. Available: https://www.scopus.com/inward/record.uri?eid=2-s2.0-0022094254&partnerID=40&md5=58c8282941cbcb5093461f3077c9ca68.

[21] D. M. Carlesso, S. Cavalaro, and A. de la Fuente, "Flexural fatigue of pre-cracked plastic fibre reinforced concrete: Experimental study and numerical modeling," *Cem. Concr. Compos.*, vol. 115, p. 103850, 2021, doi: https://doi.org/10.1016/j.cemconcomp.2020.103850.

[22] D. M. Carlesso, A. de la Fuente, and S. H. P. Cavalaro, "Fatigue of cracked high performance fiber reinforced concrete subjected to bending," *Constr. Build. Mater.*, vol. 220, pp. 444–455, 2019, doi: https://doi.org/10.1016/j.conbuildmat.2019.06.038.

[23] W.-K. Chin, H.-T. Liu, and Y.-D. Lee, "Effects of fiber length and orientation distribution on the elastic modulus of short fiber reinforced thermoplastics," *Polym. Compos.*, vol. 9, no. 1, pp. 27–35, Feb. 1988, doi: https://doi.org/10.1002/pc.750090105.

[24] M. Haghgoo, R. Ansari, and M. K. Hassanzadeh-Aghdam, "Prediction of electrical conductivity of carbon fiber-carbon nanotube-reinforced polymer hybrid composites," *Compos. Part B Eng.*, vol. 167, pp. 728–735, 2019, doi: https://doi.org/10.1016/j.compositesb.2019.03.046.

[25] R. Byron Pipes, R. L. McCullough, and D. G. Taggart, "Behavior of discontinuous fiber composites: Fiber orientation," *Polym. Compos.*, vol. 3, no. 1, pp. 34–39, Jan. 1982, doi: https://doi.org/10.1002/pc.750030107.

[26] F. Laranjeira, S. Grünewald, J. Walraven, C. Blom, C. Molins, and A. Aguado, "Characterization of the orientation profile of steel fiber

reinforced concrete," *Mater. Struct.*, vol. 44, no. 6, pp. 1093–1111, 2011, doi: 10.1617/s11527-010-9686-5.

[27] Y. Zhao *et al.*, "Numerical simulation of the casting process of steel fiber reinforced self-compacting concrete: Influence of material and casting parameters on fiber orientation and distribution," *Constr. Build. Mater.*, vol. 312, p. 125337, 2021, doi: https://doi.org/10.1016/j.conbuildmat.2021.125337.

[28] S. T. Kang, B. Y. Lee, J.-K. Kim, and Y. Y. Kim, "The effect of fibre distribution characteristics on the flexural strength of steel fibre-reinforced ultra high strength concrete," *Constr. Build. Mater.*, vol. 25, no. 5, pp. 2450–2457, 2011, doi: https://doi.org/10.1016/j.conbuildmat.2010.11.057.

[29] L. Segura-Castillo, S. Cavalaro, C. Goodier, A. Aguado, and S. Austin, "Fibre distribution and tensile response anisotropy in sprayed fibre reinforced concrete," *Mater. Struct.*, vol. 51, Feb. 2018, doi: 10.1617/s11527-018-1156-5.

[30] T. Zhang, Y. Zhang, H. Zhu, and Z. Yan, "Characterizing the thermal properties of hybrid polypropylene-steel fiber reinforced concrete under heat exposure: Insights into fiber geometry and orientation distribution," *Compos. Struct.*, vol. 275, p. 114457, 2021, doi: https://doi.org/10.1016/j.compstruct.2021.114457.

[31] P. Martinelli, M. Colombo, P. Pujadas, A. de la Fuente, S. Cavalaro, and M. di Prisco, "Characterization tests for predicting the mechanical performance of SFRC floors: identification of fibre distribution and orientation effects," *Mater. Struct.*, vol. 54, no. 1, p. 3, 2021, doi: 10.1617/s11527-020-01593-7.

[32] F. Laranjeira, S. Grünewald, J. Walraven, C. Blom, C. Molins, and A. Aguado, "Characterization of the orientation profile of steel fiber reinforced concrete," *Mater. Struct.*, vol. 44, no. 6, pp. 1093–1111, 2011, doi: 10.1617/s11527-010-9686-5.

[33] A. M. Zeyad, "Effect of fibers types on fresh properties and flexural toughness of self-compacting concrete," *J. Mater. Res. Technol.*, vol. 9, no. 3, pp. 4147–4158, 2020, doi: https://doi.org/10.1016/j.jmrt.2020.02.042.

[34] M. Zhao, J. Li, and Y. M. Xie, "Effect of vibration time on steel fibre distribution and flexural behaviours of steel fibre reinforced concrete with different flowability," *Case Stud. Constr. Mater.*, vol. 16, p. e01114, 2022, doi: https://doi.org/10.1016/j.cscm.2022.e01114.

[35] D. Dupont and L. Vandewalle, "Distribution of steel fibres in rectangular sections," *Cem. Concr. Compos.*, vol. 27, no. 3, pp. 391–398, 2005, doi:

https://doi.org/10.1016/j.cemconcomp.2004.03.005.

[36] S. Cavalaro, R. López Carreño, J. Torrents, A. Aguado, and P. Juan-García, "Assessment of fibre content and 3D profile in cylindrical SFRC specimens," *Mater. Struct.*, vol. 49, Jan. 2016, doi: 10.1617/s11527-014-0521-2.

[37] F. Laranjeira, A. Aguado, C. Molins, S. Grünewald, J. Walraven, and S. Cavalaro, "Framework to predict the orientation of fibers in FRC: A novel philosophy," *Cem. Concr. Res.*, vol. 42, no. 6, pp. 752–768, 2012, doi: https://doi.org/10.1016/j.cemconres.2012.02.013.

[38] L. F. Maya and B. Graybeal, "Fiber orientation distribution and tensile mechanical response in UHPFRC," *Mater. Struct.*, vol. 50, Feb. 2017, doi: 10.1617/s11527-016-0914-5.

[39] L. Martinie and N. Roussel, "Simple tools for fiber orientation prediction in industrial practice," *Cem. Concr. Res.*, vol. 41, no. 10, pp. 993–1000, 2011, doi: https://doi.org/10.1016/j.cemconres.2011.05.008.

[40] L. González, Á. Gaute, J. Rico, and C. Thomas, "Effect of Fibre Reinforcement on Creep in Early Age Concrete," *Appl. Sci.*, vol. 12, no. 1, 2022, doi: 10.3390/app12010257.

[41] CEN, "EN 197-1 Cement Part 1: Composition, Specifications and Conformity Criteria for Common Cements," 2011.

[42] CEN, "EN 80103:2013 Test methods of cements. Physical analysis. Actual density determination," 2013.

[43] CEN, "EN-933-1 Tests for geometrical properties of aggregates - Part 1: Determination of particle size distribution - Sieving method," 2012.

[44] CEN, "EN 83507 Concrete with fibres. Testing in compression." 2004.

[45] AENOR, "UNE-EN 12390-2. Testing hardened concrete. Part 2: Making and curing specimens for strength tests." 2022.

[46] AENOR, "UNE-EN 14651:2007. Test method for metallic fibre concrete - Measuring the flexural tensile strength (limit of proportionality (LOP), residual)." 2007.

[47] J. M. Torrents, A. Blanco, P. Pujadas, A. Aguado, P. Juan-García, and M. Á. Sánchez-Moragues, "Inductive method for assessing the amount and orientation of steel fibers in concrete," *Mater. Struct.*, vol. 45, no. 10, pp. 1577–1592, Oct. 2012, doi: 10.1617/s11527-012-9858-6.

[48] S. H. P. Cavalaro, R. López, J. M. Torrents, and A. Aguado, "Improved assessment of fibre content and orientation with inductive method in

SFRC," *Mater. Struct.*, vol. 48, pp. 1859–1873, 2015.

[49] P. Pujadas, A. Blanco, S. Cavalaro, A. De la Fuente, and A. Aguado, "Multidirectional double punch test to assess the post-cracking behaviour and fibre orientation of FRC," *Constr. Build. Mater.*, vol. 58, pp. 214–224, May 2014, doi: 10.1016/j.conbuildmat.2014.02.023.

[50] P. Pujadas, A. Blanco, S. H. Pialarissi Cavalaro, A. de la Fuente, and A. Aguado, "New analytical model to generalize the Barcelona Test using axial displacement," *J. Civ. Eng. Manag.*, vol. 19, no. 2, pp. 259–271, 2013, doi: 10.3846/13923730.2012.756425.

[51] R. Gettu, D. Gardner, H. Saldívar, and B. Barragán, "Study of the distribution and orientation of fibers in SFRC specimens," *Mater. Struct.*, vol. 38, pp. 31–37, Jan. 2005, doi: 10.1007/BF02480572.

[52] R. A. Raju, S. Lim, M. Akiyama, and T. Kageyama, "Effects of concrete flow on the distribution and orientation of fibers and flexural behavior of steel fiber-reinforced self-compacting concrete beams," *Constr. Build. Mater.*, vol. 262, p. 119963, 2020, doi: https://doi.org/10.1016/j.conbuildmat.2020.119963.

[53] Q. Cao, J. Tao, Z. Wu, and Z. J. Ma, "Behavior of FRP-Steel Confined Concrete Tubular Columns Made of Expansive Self-Consolidating Concrete under Axial Compression," *J. Compos. Constr.*, vol. 21, no. 5, 2017, doi: 10.1061/(ASCE)CC.1943-5614.0000818.

[54] Y. Tang, S. Fang, J. Chen, L. Ma, L. Li, and X. Wu, "Axial compression behavior of recycled-aggregate-concrete-filled GFRP–steel composite tube columns," *Eng. Struct.*, vol. 216, p. 110676, 2020, doi: https://doi.org/10.1016/j.engstruct.2020.110676.

[55] S. Fang, F. Liu, Z. Xiong, J. Fang, and L. Li, "Seismic performance of recycled aggregate concrete-filled glass fibre-reinforced polymer-steel composite tube columns," *Constr. Build. Mater.*, vol. 225, pp. 997–1010, 2019, doi: 10.1016/j.conbuildmat.2019.07.238.

[56] Code EHE-08, "Code on Structural Concrete EHE-08," *R. Decree 1247/2008 - Bol. Of. del Estado N° 203 - Spanish*, 2008.

[57] "REVISTA TRIMESTRAL DE LA ASOCIACIÓN CIENTÍFICO-TÉCNICA DEL HORMIGÓN ESTRUCTURAL," *Hormigón y Acero*, vol. 61-nº256, pp. 83–101, 2010.

[58] C. M. Wong, "Use of Short Fibres in Structural Concrete to Enhance Mechanical Properties," 2004, [Online]. Available: https://core.ac.uk/display/11034540.

[59] F. Altun and T. Haktanir, "A comparative experimental study of steel fibre-additive reinforced concrete beams," *Mater. construcción*, vol. 54, no. 276, pp. 5–15, 2004.

[60] R. S. Olivito and F. A. Zuccarello, "An experimental study on the tensile strength of steel fiber reinforced concrete," *Compos. Part B Eng.*, vol. 41, no. 3, pp. 246–255, Apr. 2010, doi: 10.1016/J.COMPOSITESB.2009.12.003.

[61] J. Gao, W. Sun, and K. Morino, "Mechanical properties of steel fiber-reinforced, high-strength, lightweight concrete," *Cem. Concr. Compos.*, vol. 19, no. 4, pp. 307–313, Jan. 1997, doi: 10.1016/S0958-9465(97)00023-1.

[62] E. A. Samer and B. P. N., "Normal- and High-Strength Fiber-Reinforced Concrete under Compression," *J. Mater. Civ. Eng.*, vol. 4, no. 4, pp. 415–429, Nov. 1992, doi: 10.1061/(ASCE)0899-1561(1992)4:4(415).

[63] S. H. Park, D. J. Kim, G. S. Ryu, and K. T. Koh, "Tensile behavior of Ultra High Performance Hybrid Fiber Reinforced Concrete," *Cem. Concr. Compos.*, vol. 34, no. 2, pp. 172–184, Feb. 2012, doi: 10.1016/J.CEMCONCOMP.2011.09.009.

[64] T. Job and R. Ananth, "Mechanical Properties of Steel Fiber-Reinforced Concrete," *J. Mater. Civ. Eng.*, vol. 19, no. 5, pp. 385–392, May 2007, doi: 10.1061/(ASCE)0899-1561(2007)19:5(385).

[65] S.-T. Kang, Y. Lee, Y.-D. Park, and J.-K. Kim, "Tensile fracture properties of an Ultra High Performance Fiber Reinforced Concrete (UHPFRC) with steel fiber," *Compos. Struct.*, vol. 92, no. 1, pp. 61–71, Jan. 2010, doi: 10.1016/J.COMPSTRUCT.2009.06.012.

[66] H. Huang, X. Gao, L. Li, and H. Wang, "Improvement effect of steel fiber orientation control on mechanical performance of UHPC," *Constr. Build. Mater.*, vol. 188, Nov. 2018, doi: 10.1016/j.conbuildmat.2018.08.146.

[67] M. C. Nataraja, N. Dhang, and A. P. Gupta, "Stress–strain curves for steel-fiber reinforced concrete under compression," *Cem. Concr. Compos.*, vol. 21, no. 5–6, pp. 383–390, Dec. 1999, doi: 10.1016/S0958-9465(99)00021-9.

[68] K. Wille, D. J. Kim, and A. E. Naaman, "Strain-hardening UHP-FRC with low fiber contents," *Mater. Struct.*, vol. 44, no. 3, pp. 583–598, 2011, doi: 10.1617/s11527-010-9650-4.

[69] A. A. Jhatial, G. W. Inn, N. Mohamad, U. Johnson Alengaram, K. Hung Mo, and R. Abdullah, "Influence of polypropylene fibres on the tensile strength and thermal properties of various densities of foamed concrete," *IOP Conf. Ser. Mater. Sci. Eng.*, vol. 271, p. 12058, 2017, doi: 10.1088/1757-899x/271/1/012058.

[70] A. A. Jhatial, W. I. Goh, N. Mohamad, U. J. Alengaram, and K. H. Mo, “Effect of Polypropylene Fibres on the Thermal Conductivity of Lightweight Foamed Concrete,” *MATEC Web Conf.*, vol. 150, 2018, [Online]. Available: https://doi.org/10.1051/matecconf/201815003008.

[71] Z. Wu, K. H. Khayat, and C. Shi, “How do fiber shape and matrix composition affect fiber pullout behavior and flexural properties of UHPC?,” *Cem. Concr. Compos.*, vol. 90, pp. 193–201, Jul. 2018, doi: 10.1016/J.CEMCONCOMP.2018.03.021.

[72] J. Sainz-Aja, C. Thomas, J. A. Polanco, and I. Carrascal, “High-Frequency Fatigue Testing of Recycled Aggregate Concrete,” *Appl. Sci.*, vol. 10, no. 1, p. 10, Dec. 2019, doi: 10.3390/app10010010.

[73] J. Xiao, H. Li, and Z. Yang, “Fatigue behavior of recycled aggregate concrete under compression and bending cyclic loadings,” *Constr. Build. Mater.*, vol. 38, pp. 681–688, Mar. 2013, doi: 10.1016/j.conbuildmat.2012.09.024.

[74] A. Alliche, “Damage model for fatigue loading of concrete,” *Int. J. Fatigue*, vol. 26, no. 9, pp. 915–921, Sep. 2004, doi: 10.1016/J.IJFATIGUE.2004.02.006.

[75] Ł. Skarżyński, I. Marzec, and J. Tejchman, “Fracture evolution in concrete compressive fatigue experiments based on X-ray micro-CT images,” *Int. J. Fatigue*, vol. 122, pp. 256–272, Mar. 2019, doi: 10.1016/j.ijfatigue.2019.02.002.

[76] C. Thomas, J. Sainz-Aja, J. Setien, A. Cimentada, and J. Polanco, “Resonance fatigue testing on high-strength self-compacting concrete,” *J. Build. Eng.*, 2021.

[77] J. Sainz-aja, C. Thomas, I. Carrascal, J. A. Polanco, and J. De Brito, “Fast fatigue method for self-compacting recycled aggregate concrete characterization,” *J. Clean. Prod.*, p. 123263, 2020, doi: 10.1016/j.jclepro.2020.123263.

[78] D. Ferreño *et al.*, “Experimental and finite element fatigue assessment of the spring clip of the SKL-1 railway fastening system,” *Eng. Struct.*, vol. 188, pp. 553–563, Jun. 2019, doi: 10.1016/j.engstruct.2019.03.053.

[79] British Standards Institution, “Eurocode 2 — Design of concrete structures,” *Part 1-1 Gen. rules rules Build.*, 2015, doi: 10.7773/cm.v27i4.501.

[80] N. K. Banjara and K. Ramanjaneyulu, “Experimental and numerical study on behaviour of HSFRC overlay strip strengthened flexural deficient RC beams,” *Eng. Struct.*, vol. 198, p. 109561, 2019, doi: https://doi.org/10.1016/j.engstruct.2019.109561.

[81] K. Holschemacher, T. Mueller, and Y. Ribakov, “Effect of steel fibres on mechanical properties of high-strength concrete,” *Mater. Des.*, vol. 31, no.

5, pp. 2604–2615, May 2010, doi: 10.1016/J.MATDES.2009.11.025.

[82] K. Neocleous, H. Angelakopoulos, K. Pilakoutas, and M. Guadagnini, “Fibre-reinforced roller-compacted concrete transport pavements,” *Proc. Inst. Civ. Eng. - Transp.*, vol. 164, no. 2, pp. 97–109, Mar. 2011, doi: 10.1680/tran.9.00043.

[83] W. Chao, Z. Yamei, and M. Aibin, “Investigation into the Fatigue Damage Process of Rubberized Concrete and Plain Concrete by AE Analysis,” *J. Mater. Civ. Eng.*, vol. 23, no. 7, pp. 953–960, Mar. 2011, doi: 10.1061/(ASCE)MT.1943-5533.0000257.

[84] Y. Ma, J. Gu, Y. Li, and Y. Li, “The bending fatigue performance of cement-stabilized aggregate reinforced with polypropylene filament fiber,” *Constr. Build. Mater.*, vol. 83, pp. 230–236, Mar. 2015, doi: 10.1016/j.conbuildmat.2015.02.073.

[85] N. Saoudi and B. Bezzazi, “Flexural fatigue failure of concrete reinforced with smooth and mixing hooked-end steel fibers,” *Cogent Eng.*, vol. 6, no. 1, Mar. 2019, doi: 10.1080/23311916.2019.1594508.

[86] D. Valencia and M. León-Neira, “Study of fatigue performance of a concrete mix for pavements reinforced with steel fibers,” *Rev. Ing. Constr.*, vol. 32, pp. 45–58, Aug. 2017.

[87] Z. J. and H. Stang, “Fatigue Performance in Flexure of Fiber Reinforced Concrete,” *ACI Mater. J.*, vol. 95, no. 1, doi: 10.14359/351.

[88] S. J. Stephen and R. Gettu, “Fatigue fracture of fibre reinforced concrete in flexure,” *Mater. Struct.*, vol. 53, no. 3, p. 56, 2020, doi: 10.1617/s11527-020-01488-7.

[89] C. D. J. and R. W. Zemp, “Flexural Fatigue Performance of Steel Fiber Reinforced Concrete--Influence of Fiber Content, Aspect Ratio, and Type,” *ACI Mater. J.*, vol. 88, no. 4, doi: 10.14359/1875.

[90] S. Goel, S. P. Singh, and P. Singh, “Flexural fatigue strength and failure probability of Self Compacting Fibre Reinforced Concrete beams,” *Eng. Struct.*, vol. 40, pp. 131–140, 2012, doi: https://doi.org/10.1016/j.engstruct.2012.02.035.

[91] J. Zhang, H. Stang, and V. C. Li, “Fatigue life prediction of fiber reinforced concrete under flexural load,” *Int. J. Fatigue*, vol. 21, no. 10, pp. 1033–1049, 1999, doi: https://doi.org/10.1016/S0142-1123(99)00093-6.

[92] C. Thomas, I. Sosa, J. Setién, J. A. Polanco, and A. I. Cimentada, “Evaluation of the fatigue behavior of recycled aggregate concrete,” *J. Clean. Prod.*, vol. 65, pp. 397–405, Feb. 2014, doi: 10.1016/J.JCLEPRO.2013.09.036.

[93] C. Thomas, J. Setién, J. A. A. Polanco, I. Lombillo, and A. Cimentada, “Fatigue limit of recycled aggregate concrete,” *Constr. Build. Mater.*, vol. 52, pp. 146–154, Feb. 2014, doi: 10.1016/J.CONBUILDMAT.2013.11.032.

[94] AENOR, “UNE-EN 14651:2007. Método de ensayo para hormigón con fibras metálicas. Determinación de la resistencia a tracción por flexión (límite de proporcionalidad (LOP), resistencia residual). UNE-EN 14651:2007+A1.” .

[95] J. A. Sainz-Aja *et al.*, “Dynamic Calibration of Slab Track Models for Railway Applications using Full- Scale Testing,” *Comput. Struct.*, vol. Inpress.

[96] Mathworks, “Fourier Serie.” .

[97] J. D. Ríos and H. Cifuentes, “Probabilistic fatigue analysis of ultra-high-performance fibre-reinforced concrete under thermal effects,” in *MATEC Web of Conferences*, 2018, vol. 165, doi: 10.1051/matecconf/201816512001.

[98] J. D. Ríos, H. Cifuentes, S. Blasón, M. López-Aenlle, and A. Martínez-De La Concha, “Flexural fatigue behaviour of a heated ultra-high-performance fibre-reinforced concrete,” *Constr. Build. Mater.*, vol. 276, p. 122209, 2021, doi: https://doi.org/10.1016/j.conbuildmat.2020.122209.

[99] R. S. Atea, “A Case Study On Concrete Column Strength Improvement with Different steel fibers and polypropylene fibers,” *J. Mater. Res. Technol.*, vol. 8, no. 6, pp. 6106–6114, 2019, doi: https://doi.org/10.1016/j.jmrt.2019.10.005.

[100] A. M. Saba *et al.*, “Strength and flexural behavior of steel fiber and silica fume incorporated self-compacting concrete,” *J. Mater. Res. Technol.*, vol. 12, pp. 1380–1390, 2021, doi: https://doi.org/10.1016/j.jmrt.2021.03.066.

[101] J. Norambuena-Contreras, C. Thomas, R. Borinaga-Treviño, and I. Lombillo, “Influence of recycled carbon powder waste addition on the physical and mechanical properties of cement pastes,” *Mater. Struct.*, vol. 49, no. 12, pp. 5147–5159, 2016, doi: 10.1617/s11527-016-0850-4.

[102] JING-XIAN SHI ;ZHI-HONG RAN, “Calculation of Creep Effect of Extradosed Cable-stayed bridge based on Midas Civil,” 2018, doi: 10.1088/1757-899X/423/1/012113.

[103] Z. Bazant, H. Asce, Q. Yu, and G.-H. Li, “Excessive Long-Time Deflections of Prestressed Box Girders. I: Record-Span Bridge in Palau and Other Paradigms,” *J. Struct. Eng.*, vol. 138, Jun. 2012, doi: 10.1061/(ASCE)ST.1943-541X.0000487.

[104] P. S. Mangat and M. M. Azari, “Compression creep behaviour of steel fibre reinforced cement composites,” *Mater. Struct.*, vol. 19, no. 5, pp. 361–370,

1986, doi: 10.1007/BF02472126.

[105] D. Nakov and P. Mark, "Experimental and Analytical Analysis of Creep of Steel Fibre Reinforced Concrete," *Period. Polytech. Civ. Eng.*, vol. 62, Sep. 2017, doi: 10.3311/PPci.11184.

[106] J. Zhang, "Modeling of the influence of fibers on creep of fiber reinforced cementitious composite," *Compos. Sci. Technol.*, vol. 63, no. 13, pp. 1877–1884, 2003, doi: https://doi.org/10.1016/S0266-3538(03)00160-X.

[107] Q. Zhao, J. Yu, G. Geng, J. Jiang, and X. Liu, "Effect of fiber types on creep behavior of concrete," *Constr. Build. Mater.*, vol. 105, pp. 416–422, 2016, doi: https://doi.org/10.1016/j.conbuildmat.2015.12.149.

[108] E. Lira Madureira and B. Fontes, "Temperature influence on creep of reinforced concrete," *Rev. IBRACON Estruturas e Mater.*, vol. 13, Jan. 2020, doi: 10.1590/s1983-41952020000600001.

[109] S.-S. Jin, S.-L. Cha, and H.-J. Jung, "Improvement of concrete creep prediction with probabilistic forecasting method under model uncertainty," *Constr. Build. Mater.*, vol. 184, pp. 617–633, 2018, doi: https://doi.org/10.1016/j.conbuildmat.2018.06.238.

[110] D. Harinadha Reddy and A. Ramaswamy, "Experimental and numerical modeling of creep in different types of concrete," *Heliyon*, vol. 4, no. 7, p. e00698, 2018, doi: https://doi.org/10.1016/j.heliyon.2018.e00698.

[111] R. Liu, H. Ye, Y. Liu, H. Zhao, J. A. F. O. Correia, and H. Xin, "Numerical simulation of concrete creep behaviour using integral creep algorithm with alternating stresses," *Structures*, vol. 29, pp. 1979–1987, 2021, doi: https://doi.org/10.1016/j.istruc.2020.11.081.

[112] P. Havlásek, V. Šmilauer, L. Dohnalová, and R. Sovják, "Shrinkage-induced deformations and creep of structural concrete: 1-year measurements and numerical prediction," *Cem. Concr. Res.*, vol. 144, p. 106402, 2021, doi: https://doi.org/10.1016/j.cemconres.2021.106402.

[113] AASHTO, "A.A.o.S.H.a.T. Officials, AASHTO LRFD bridge design specifications." Washington, DC, 2012.

[114] A. C. Institute, "ACI Committee 209. Creep and Shrinkage. Guide for modeling and calculating shrinkage and creep in hardened concrete." Farmington Hills, MI, 2008.

[115] Ministerio de Fomento. Gobierno de España, *EHE-08. Instrucción de Homigón Estructural.* 2008.

[116] E. N. 933-1:2012, "Tests for geometrical properties of aggregates - Part 1: Determination of particle size distribution - Sieving method," 2012.

[117] W. F. James W. Dally & Riley, *Experimental Stress Analysis*. New York McGraw-Hill Book Company, 1978.

[118] B. Delsaute, J.-M. Torrenti, and S. Staquet, "Modeling basic creep of concrete since setting time," *Cem. Concr. Compos.*, vol. 83, pp. 239–250, 2017, doi: https://doi.org/10.1016/j.cemconcomp.2017.07.023.

[119] S. Altoubat, "Early age stresses and creep-shrinkage interaction of restrained concrete," Sep. 2000.

[120] G. A. Landsberger and J. Gomez, "Evaluación de las deformaciones por fluencia del hormigón autocompactante," 2008.